ROMA TRE UNIVERSITY
Department of Science

Doctoral School in
Material Sciences, Nanotechnologies and Complex Systems
XXXII Cycle

Selective Oxidation of Alcohols by Supported Palladium Nanocatalysts

S. Sepehr Moeini

Tutor: Prof. Daniela Tofani

Rome, 2020

To my wife, family,
teachers and Friends

Acknowledgements

I would like to express my deepest gratitude to my Ph.D. tutor ***Prof. Daniela Tofani,*** for her heartwarming guidance, cooperation, care and love. Working with her has been a unique opportunity for me.

My sincere thanks and regards to ***Dr. Simonetta Tuti*** and ***Dr. Igor Luisetto*** for their kind and unsparing advices, support and collaboration with me.

A special gratitude to ***Dr. Tecla Gaspari*** for her great support and attention to me during my research.

I acknowledge ***Prof. Chiara Battocchio*** for her kind scientific support for the XPS analysis.

I would like to express my gratefulness to ***Dr. Sergio Lo Mastro*** for his valuable support for XRD analysis and to ***Dr. Stefano Casciardi*** (INAIL, Rome, Italy) for his great cooperation with acquiring TEM images of the catalysts.

I would like to extend my gratitude to ***Dr. Marina Grandinetti, Dr. Guido Infante***, and to ***Dr. Paolo Lupattelli*** who helped me in various aspects during my Ph.D.

Finally, I would like to express my gratitude and love to my parents, ***Hossein*** and ***Nahid*** for their limitless love and sacrifice, and to my uncle, ***Hashem,*** for being an admirable role model for me; and to my beloved wife, ***Zara***, who is a continuing source of inspiration to me.

List of Abbreviations

AA	Alfa Aesar
Acetonitrile	AcCN
BE	Binding Energy
BET	Brunauer–Emmet–Teller
BnOH	Benzyl alcohol
DCM	Dichloromethane
DMF	Dimethylformamide
DMSO	Dimethyl sulfoxide
EDG	Electron-donating Groups
EWG	Electron-withdrawing Groups
EtOAc	Ethyl acetate
EtOH	Ethanol
FID	Flame Ionization Detector
FWHM	Full Width at Half Maxima
GC	Gas Chromatography
GC-MS	Gas Chromatography-Mass Spectrometry
HR-TEM	High Resolution Transmission Electron Microscope
JCPDS	Joint Committee on Powder Diffraction Standards
MeOH	Methanol
MFC	Mass Flow Controller

NR	Nanorod
NP	Nanoparticle
PhCHO	Benzaldehyde
PhCOOH	Benzoic acid
PSD	Pore-size Distribution
RF	Radio Frequency
SA	Sigma Aldrich
SEM	Scanning Electron Microscope
TBHP	Tert-butyl hydroperoxide
TCD	Thermal Conductivity Detector
TEM	Transmission Electron Microscope
THF	Tetrahydrofuran
TOF	Turn Over Frequency
TON	Turnover Number
TPR	Temperature-programmed Reduction
XRD	X-ray Diffraction
XPS	X-ray Photoelectron Spectroscopy

List of Tables

List of Schemes

List of Figures

Abstract

Selective oxidation of alcohols is a crucial reaction in either petroleum refinery or biorefinery and biomass processing, because it represents an elegant class of atom-efficient molecular transformations for chemical valorization. This reaction can be catalyzed by a range of platinum-group and other noble and/or transition metals. The alcohol oxidation products such as aldehyde, ketone, ester and acid products are valuable intermediates for the fine chemical, pharmaceutical and agrochemical sectors. In addition, alcohols such as benzyl alcohol (**BnOH**) derivatives are used to design catalytic systems for lignin depolymerization. Lignin is the most important renewable source of aromatics on the planet, and depolymerizing the lignin can result in valuable aromatic compounds currently produced from petroleum.

In the present study, the catalytic activity of palladium supported on ceria nanorod and mesoporous silica for the aerobic oxidation of BnOH derivatives and 4-(benzyloxy)phenol is investigated. Different Pd/ceria catalysts were prepared, varying the oxidation state of palladium by changing the preparation method and palladium precursor. A selected number of samples were studied by X-ray diffraction (**XRD**), temperature-programmed reduction (**TPR**), transmission electron microscopy (**TEM**), nitrogen adsorption-desorption analysis, and X-ray photoelectron spectroscopy (**XPS**) techniques.

Catalytic activity of palladium oxide supported on ceria nanorod (**PdO_x/CeO_2-NR**) for aerobic selective oxidation of BnOH to benzaldehyde (**PhCHO**) was evaluated. The ceria nanorod was synthesized hydrothermally and the $Pd(NO_3)_2$ was deposited by a wet impregnation method, followed by calcination to acquire PdO_x/CeO_2-NR. In addition, PdO_x/CeO_2-NR was reduced

(**PdO_x/CeO_2-NR-Red**) by H_2 using TPR equipment, and tested for BnOH oxidation to assess the effect of palladium oxidation state on the catalytic activity. Furthermore, the effects of solvent and temperature on the catalytic activity of aforementioned catalysts were studied. The PdO_x/CeO_2-NR showed remarkable activity in ethanol (**EtOH**): 93% BnOH conversion along with 96% PhCHO selectivity. A mechanistic hypothesis for BnOH oxidation with PdO_x/CeO_2-NR in EtOH is presented.

Pd/ceria catalysts with different preparation methods or different palladium precursor were prepared and tested for selective BnOH oxidation. The results showed that for all the reduced samples, using toluene as solvent for BnOH oxidation resulted in higher conversions compared to utilizing EtOH. In addition, changing the palladium precursor enormously influenced the catalytic activity, and probably changed the mechanism of the reaction.

Furthermore, solvent-free aerobic oxidation of BnOH derivatives was performed using palladium oxide supported on ceria nanorod (2 wt.% Pd), leading to 34% BnOH conversion, with 99% PhCHO selectivity. The solvent-free oxidation on BnOH derivatives showed that when electron-donating groups (**EDG**) were substituted on BnOH (e.g. 4-methoxybenzyl alcohol) the conversion increased, but decrease in selectivity occurred; while electron-withdrawing groups (**EWG**) eliminated the catalytic activity to zero conversion (e.g. for 4-nitrobenzyl alcohol).

Pd-P alloy supported on functionalized mesoporous silica was tested for BnOH to compare the effect of support on the catalytic activity. This catalyst was almost inactive in EtOH, but active in toluene. Unlike other tested catalysts, utilizing supported Pd-P at temperatures above 100 °C led to decrease in selectivity of PhCHO.

Chapter 1.

Introduction

Opening Discussion

Selective oxidation reactions are considered to be one of the most crucial groups of transformations in organic chemistry. The catalytic oxidation of alcohols is of utmost importance for either petroleum refinery or biorefinery, and biomass processing, because it represents an elegant class of atom-efficient molecular transformations for chemical valorization, that are catalyzed under mild conditions by a range of platinum-group and other noble and/or transition metals. The alcohol oxidation products such as aldehyde, ketone, ester and acid products are valuable intermediates for the fine chemical, pharmaceutical and agrochemical sectors, with allylic aldehydes be particularly high-value compounds, widely applicable in numerous industries such as perfume and flavorings [1-3].

In addition to importance from chemical and industrial points of view, selective catalytic oxidation of alcohols plays a significant role in green chemistry, since in many cases it can be an environmentally friendly alternative for toxic chemical reactions. For example, benzaldehyde **(PhCHO)**, a critical fine and intermediate chemical in many industries as pharmaceutical, dyestuff, agrochemical and perfumery [4], is conventionally produced by oxidation of toluene or hydrolysis of benzal chloride, but in the former, the selectivity is low, and the latter leads to undesirable chlorine contamination [5]. PhCHO can be produced from selective catalytic oxidation of benzyl alcohol **(BnOH)** as well. Although expensive and toxic chromium and manganese salts can be used as stoichiometric oxidants, but they might be replaceable by cheaper and more ecofriendly oxidants like oxygen and air [6]. The major part of the present PhD thesis

is dedicated to selective and aerobic catalytic oxidation of BnOH to PhCHO over supported palladium catalysts.

For an oxidation process to be ideally green, it is essential to design a highly active and selective recyclable catalyst, capable of working at atmospheric pressure in the presence of oxygen and the absence of solvents and bases. Stoichiometric oxidations catalyzed by transition metal compounds or sulfoxides are still commonly used, despite the formation of a large amount of undesirable products. Several homogeneous noble metal-based catalysts are able to perform the selective oxidation of alcohols, but, besides the difficulty to isolate the catalyst from the reaction mixture, reusability of expensive noble metal and purification of products, they require the use of organic solvents or high oxygen pressure. Therefore, considering easier catalyst recycling and products separation, noble metal heterogeneous catalysts might be an advantageous alternative [7].

Even though the feasibility of omitting the solvent from catalytic oxidations might lead to a greener reaction and a cheaper process, studying the behavior of a catalyst in solvents with different natures is still necessary. This is particularly valid for catalytic oxidation of benzylic alcohols, because this reaction is a basic model for oxidative depolymerization of lignin , a process in which, solvents might play a critical role [8-10]. Lignin, the most important renewable source of aromatics on the planet, is a complex three-dimensional amorphous phenylpropanoid polymer. Lignin valorization is the name of different processes leading to depolymerization of lignin into valuable aromatic compounds that, currently is obtained from petroleum resources [11-13].

In general, selective oxidation of BnOH and its derivatives not only is important from industrial and economic point of view due to precious produced compounds, but also is a key step of developing catalysts for one of most important processes of green chemistry, i.e., valorization of lignin.

1.1. Catalysis

As a simple definition, "catalyst" is a substance that facilitates a chemical reaction. It might seem that catalysts accelerate chemical reactions; but in fact, catalysts open up new routes to equilibrium. In other words, catalysts deal with the kinetics, not the thermodynamics of chemical reactions. Svante August Arrhenius, formalized the relation among reaction rate constant, k (mol L^{-1} s^{-1}) for zero order reactions and s^{-1} for first order reactions), and the absolute temperature, T (K), based on empirical observations (*Equation 1.1*). In this equation, A, represents the pre-exponential factor which is a constant for each chemical reaction; R is the universal gas constant (~2 cal mol^{-1} K^{-1}), and E_a is the reaction activation energy (cal mol^{-1}). Decrease in E_a leads to increase of k, and this how a catalyst works [7].

$$k = Ae^{-\frac{Ea}{RT}} \qquad \textbf{Equation 1.1}$$

Catalysis has been a key element for development of chemical industry and became the base of the large-scale production of chemicals. Catalysis contributed to preservation of resources as well as diminishing the industrial pollutions [14,15] which are both, crucial concepts of green chemistry. In other words, "catalysis is the key to sustainability" [16].

1.1.1. E Factor, Atom Economy and Environmental Quotient

When it comes to quantifying the "greenness" of a chemical process, certain measures are defined, from which E factor and atom economy are among the basics. For a chemical reaction, E factor is defined as below:

$$E = \frac{kg\ of\ waste}{kg\ of\ product} \qquad \textbf{Equation 1.2}$$

where waste is everything produced except desired product. Water, gases as carbon dioxide or NO_x, inorganic salts, heavy metal salts, and/or organic compounds are examples of most common "waste" of chemical reactions. The factor of "atom economy" considers the number and identity of the atoms of reactants in a chemical reaction that are incorporated into the desirable product/products. As an example, the stoichiometric oxidation of 1-Phenylethanol to the corresponding ketone, with chromium trioxide in sulfuric acid and catalytic oxidation with O_2 are reported in *Scheme 1.1a*. and *Scheme 1.1b* respectively. The atom efficiency of the stoichiometric oxidation is 42% while the atom efficiency of the catalytic oxidation with molecular oxygen is 87%, assuming 100% conversion of substrate to the desirable product (acetophenone).

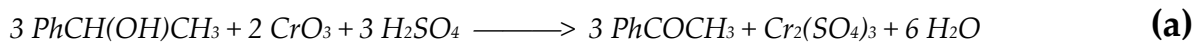

(a)

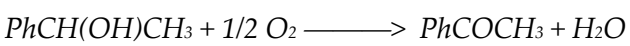

(b)

Scheme 1.1. Stoichiometric (**a**) and catalytic (**b**) oxidation of 1-Phenylethanol.

E factor and atom economy exclude the nature of wastes in chemical reactions. For example, in the reaction showed in *Scheme 1.1b*, water is considered as waste, and its production decreased the atom economy of the reaction. But from environmental point of view, $Cr_2(SO_4)_3$ waste of the stoichiometric oxidation (*Scheme 1.1a*) is far more important than H_2O waste. Therefore, a third factor, "environmental quotient" (EQ), is defined as bellow:

$$EQ = E \times Q \qquad \textbf{Equation 1.3}$$

where E is the E factor and Q is an arbitrarily assigned unfriendliness quotient whose value depends on toxicity, ease and efficiency of recyclability, etc., of each chemical compound or element [7,16,17].

In general, the atom economy plays an important role in green chemistry. Ideally, every atom participating in a process should be converted to product. Classic organic synthesis protocols often use stoichiometric reagents many of those are toxic, containing atoms that are not incorporated in the products and must be gotten rid of. This is disadvantageous not only for the environment, but also from economic point of view, because the lost is twice: once paying for the additional reagents, and once spending for waste disposal and product separation. Shifting from stoichiometric to catalytic reactions might be beneficial for the environment as well as for the economy of chemical industries. However, it is not guaranteed because many alternative catalytic reactions, are still costly and/or lead to toxic waste, either due to price/nature of the uncollectable catalyst, or production of undesirable products because of low yield of the favorable product.

1.1.2. Efficiency of Catalytic Reactions and Catalysts

One of common methods of measuring the efficiency of a chemical reaction, is to assess three key factors, namely reactant conversion, product selectivity and product yield (*Equation 1.4 - 1.6*). By definition, reactant conversion is the fraction of reactant that is converted during the chemical reaction. The product selectivity is the fraction of a certain product out of all the produced materials. The product yield calculated the fraction of production of a specific reaction product, compared to the ideal production, i.e., 100% reactant conversion and 100% product selectivity.

$$substrate\ conversion\ (\%) = \frac{moles\ of\ reacted\ substrate}{initial\ moles\ of\ substrate} \times 100 \qquad \textbf{Equation 1.4}$$

$$product\ selectivity\ (\%) = \frac{moles\ of\ product}{moles\ of\ reacted\ substrate} \times 100 \qquad \textbf{Equation 1.5}$$

$$product\ yield\ (\%) = \frac{substrate\ convertion\ \times\ product\ selectivity}{100} \qquad \textbf{Equation 1.6}$$

While conversion, selectivity and yield refer to the efficiency and results of chemical reactions, turnover number (**TON**) and turnover frequency (**TOF**) are common means to measure the efficiency of a catalyst. TON is the average number of substrate moles that each mole of catalyst converted to a product, during the course of reaction. TOF counts the same value as TON, but per unit of time. TON and TOF for a homogeneous catalysis is given in *Equation 1.7* and *Equation 1.8*.

$$TON = \frac{moles\ of\ reacted\ substrate}{moles\ of\ catalyst} \times 100 \qquad \textbf{Equation 1.7}$$

$$TOF\ (h^{-1}) = \frac{TON}{Time} \qquad \textbf{Equation 1.8}$$

In case of heterogeneous catalysis, number of active sites should be used for calculating TON and TOF. But since extracting this number in many cases is difficult, mass of catalyst is used alternatively.

1.1.3. Catalysts Categorization

Catalysts can be categorized according to a variety of properties; but, perhaps the most common classification is *homogeneous*, *heterogeneous* and *biocatalysts*.

In homogeneous catalysis, the reactants, products and the catalyst are all in the same phase. The most regular form of homogeneous catalysis is the condition in which, all the materials present in a solution. For instance, liquid-phase oxidation of ethylbenzene to acetophenone over cobalt ions as catalyst, in acetic acid as solvent, by H_2O_2 as oxidizing agent [18], (*Scheme 1.2*). On the other hand, in heterogeneous catalysis, the catalyst and substrate are in different phases; for example, in methanation of CO_2 (*Scheme 1.3*) over supported nickel catalyst, the substrate is in gaseous and the catalyst is in solid phase [19]. Biocatalysts are often complex proteins called enzymes that catalyze reactions in living cells. It is noteworthy that the catalytic activity of biocatalysts is not limited to living cell. As an example, in a previous research work of the author,

a commercial mixture of Cellulase and β-Glucosidase showed activity for enzymatic hydrolysis of cellulose in Calotropisgigantea fiber to glucose [20] (*Scheme 1.4*).

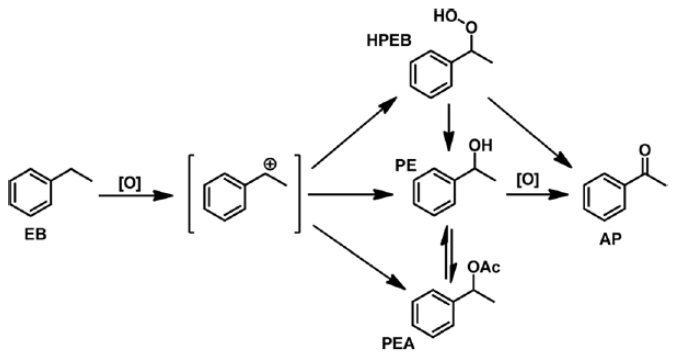

Scheme 1.2. Liquid-phase oxidation of ethylbenzene to acetophenone over cobalt ions as catalyst, in acetic acid as solvent, by H_2O_2 as oxidizing agent. Reaction conditions: ethylbenzene (EB) with 35% aq. H_2O_2, 10% $CoBr_2$ in AcOH at 80 °C. HPEB: (1-hydroperoxyethyl) benzene, AP: acetophenone, PE: phenylethanol, PEA: 1-phenylethyl acetate.

$$CO_2 + 4H_2 \longrightarrow CH_4 + 2H_2O$$

Scheme 1.3. Methanation of carbon dioxide.

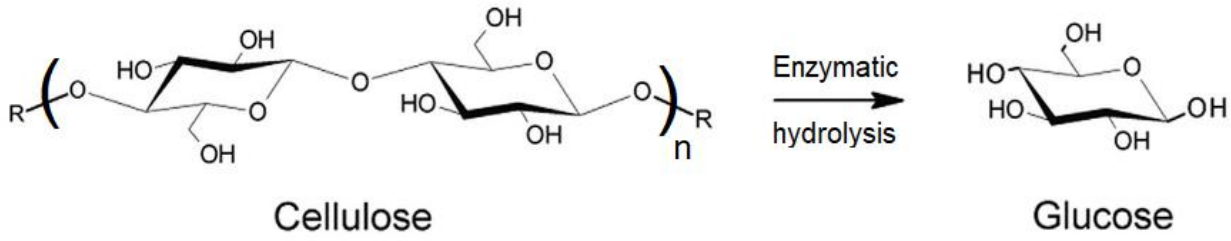

Scheme 1.4. Enzymatic hydrolysis of cellulose to glucose via Cellulase and β-Glucosidase.

Homogeneous catalysis offers high catalytic performance, in many cases, better than the heterogeneous catalytic systems; but, it only accounts for 10% of the global industrial catalytic processes. The main reason probably is that collecting and recovering the catalyst after

homogeneous catalytic reactions is a problematic task, making the whole process economically and environmentally unbeneficial. On one hand, the price of the catalyst is usually way higher than the value of the reactants thus, if possible, shouldn't be lost, and on the other hand, remaining some parts of the catalyst in the product can be extremely unfavorable, aside from environmental threat poses by industrial waste polluted with chemical catalysts. Furthermore, being in form of metal-ligand, many homogeneous catalysts are thermally sensitive due to weak resistance of the ligand against temperature. However, heterogeneous catalysis suffers from its own disadvantages, namely, low reaction yield in some cases, leaching of catalyst from the support material, mass transfer between multiphases, and catalyst deactivation due to reasons as sintering or thermal degradation (that happens at elevated temperatures) [7,21,22].

1.1.4. Nanocatalysis

As discussed in previous section, conventional homogeneous and heterogeneous catalysts each suffers from certain drawbacks. Homogeneous catalysts offer high catalytic activity and product yield; but, they are difficult/impossible to recover and reuse after the catalytic reaction. Heterogeneous catalysts are easier to recollect and recycle, while resulting lower catalytic activity, partly because of less surface area of the catalyst that is accessible for the substrate.

The inclusion of nanoscience into the science of catalysis has become a widely accepted approach to design new catalysts with high selectivity [23]. Supported or unsupported noble metals have shown a close relationship between their size and/or shape and their catalytic activity [19,24,25]. In the case of supported particles, their catalytic performance is strictly dependent on the type of chosen support, being those with higher surface areas the best ones for preparing

nanoparticles (**NPs**) directly on the support. High dispersion and low leaching can be achieved if a strong affinity between support and particles occurs. The support can also effect the electronic structure of the supported metal and/or modify the catalytic reaction by itself [26-28]. NPs of noble metals supported on different materials such as oxides have been largely applied for catalyzing chemical reactions aiming at energy conversion, environmental remediation, and chemical industry, because of their exceptional activity [29]. Oxidation of alcohols is one of reactions in which, homogeneous or heterogeneous noble metal catalysts have been extensively utilized; however, heterogeneous systems are preferred due to recoverability of the expensive catalyst [30-33].

1.2. Catalytic Oxidation of Alcohols

Carbonyl compounds such as aldehydes, acids and ketones are widely utilized as starting precursor or intermediate for the synthesis and design of high-value chemicals in numerous industrial fields such as pharmaceutical, perfumery, agrochemical, and dyestuff [32,34-37]. In industry, many of these compounds are majorly produced by inefficient and/or unsustainable conventional methods, even though they can be produced by selective oxidation of primary or secondary alcohols (*Scheme 1.5a*, and *1.5b* respectively); therefore, selective oxidation of alcohols is considered utterly important in both academic studies and industrial production [38-42]. In this regard, several aspects of this reaction has been focused on by researchers, aiming at improving the reaction from economic and environmental points of view, for example, high efficiency of the reaction, i.e., substrate conversion and product selectivity, mild reaction conditions (temperature,

pressure, pH), omitting the use of solvent or using greener and/or cheaper solvents, environmentally-friendliness of oxidizing agent, efficiency and eco-friendliness of the utilized catalyst, etc. An ideally economic and green alcohol oxidation requires a highly active and selective recyclable catalyst that works in atmospheric pressure of air or molecular oxygen and room temperature, without any solvent or base. [3,37,43,44].

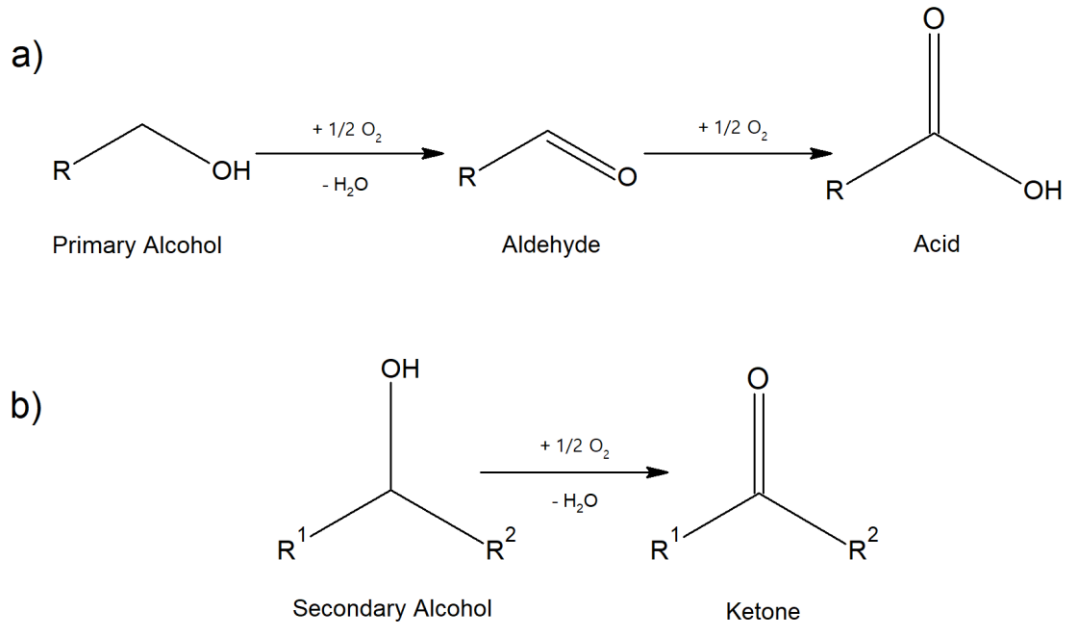

Scheme 1.5. Oxidation of (**a**) primary alcohols to aldehyde and acid, and (**b**) secondary alcohols to ketone.

1.2.1. Examples of catalytic alcohol oxidation

In 1977, palladium catalyzed oxidation of alcohols by molecular oxygen was performed for the first time by Blackburn and Schwartz using $PdCl_2$ with sodium acetate ligand [45]. Since then, many studies have been focused on catalytic activity of palladium for selective oxidation of alcohols by air or O_2. Many homogeneous palladium catalysts have been reported. Palladium (II) acetate for instance showed high activity and selectivity for oxidation of a variety of primary and secondary alcohols by O_2 in presence of a base and organic solvents [46,47] as well as water

[48,49]. *Table 1.1* shows some of the reactions performed in abovementioned research works. Although the alcohol conversion and the product selectivity of the oxidation reactions were high in many of the experiments, but the necessity of utilizing base and irrecoverableness of the catalyst pose serious disadvantages to these reactions.

Schultz et al. compared three catalyst systems developed by their group [50]. In this report, a Pd-N-heterocyclic carbene catalyst was used for aerobic oxidation of alcohols at room temperature using 1 mol% catalyst. The activity of this catalyst was compared with the previously reported $Pd(OAc)_2$/TEA (a mixture of palladium(II) acetate and triethylamine) [51] and $Pd(IiPr)(OAc)_2$ [52] catalyst systems. The new system ($Pd(IiPr)$-$(OPiv)_2$) was similar to $Pd(IiPr)(OAc)_2$, but in the new system, acetate was replaced by pivalate (PivO, tert-Butylformate), because they had realized that more basic anionic ligands improved the oxidation rates. Although $Pd(IiPr)$-$(OPiv)_2$ system represented a mild oxidation, the scope was limited to the primary aliphatic alcohols, and sterically encumbered alcohols were not oxidized well. They also evaluated the substrate scope of the three catalytic systems for more complex alcohols such as 1,2- and 1,3-mono-protected diols as well as amino alcohols. The authors demonstrated that both the $Pd(IiPr)$-$(OPiv)_2$ and $Pd(IiPr)(OAc)_2$ systems were more efficient in terms of catalyst loading and oxygen concentration. $Pd(IiPr)(OAc)_2$ showed the greatest ability to be modulated through changing temperature.

Table 1.1. Oxidation of primary and secondary alcohols by homogeneous palladium catalysts and O_2 in basic conditions. [a] dimethyl sulfoxide. [b] PhenS*: bathophenanthroline disulfonate.

Substrate	Product	catalyst	Solvent	Yield (%)	Ref
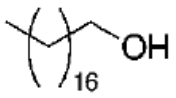	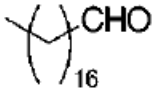	$Pd(OAc)_2$	Toluene	95	30
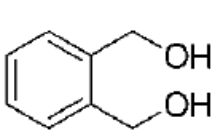	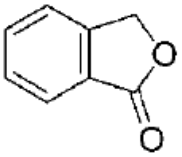	$Pd(OAc)_2$	Toluene	85	30
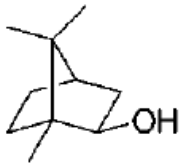	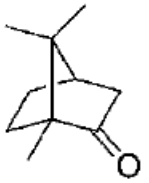	$Pd(OAc)_2$	Toluene	93	30
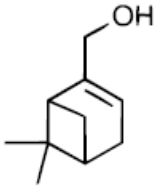	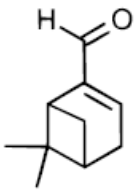	$Pd(OAc)_2$	DMSO[a]	50	31
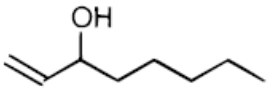	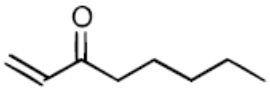	$Pd(OAc)_2$	DMSO	53	31
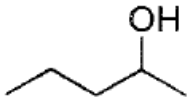	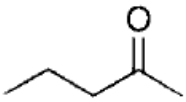	PhenS*Pd(OAc)$_2$[b]	Water	90	32
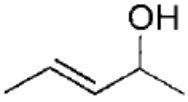	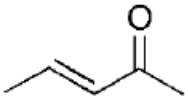	PhenS*Pd(OAc)$_2$	Water	79	32
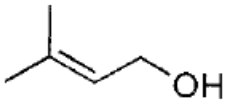	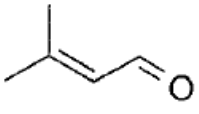	PhenS*Pd(OAc)$_2$	Water	88	32
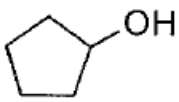	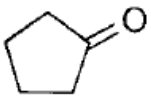	PhenS*Pd(OAc)$_2$	Water	90	32

As noted earlier, difficulty to isolate the catalyst from the reaction mixture, reusability of expensive noble metals and purification of products remain a complex task. Therefore, a valid alternative due to the more convenient catalyst recycling and products separation is noble metal heterogeneous catalysts [7,53,54]

Hackett et al. showed that Pd dispersed on high surface area, mesoporous alumina (350 m^2g^{-1} surface area; 3 nm pore diameter) offered exceptional activity for selective aerobic allylic alcohol oxidation in toluene. Palladium was deposited by wetness impregnation with tetraamine palladium(II) nitrate solution, on an alumina support which was prepared by modified surfactant-templated route through hydrolysis of aluminum sec-butoxide and subsequent aging in the presence of lauric acid following by calcination at 500 °C [55]. After palladium deposition, the catalyst was first calcined and then reduced under H_2. Schematic depiction of the prepared catalyst is given in *Figure 1.1*. They found out that the yield of aldehyde production (crotonaldehyde and cinnamaldehyde) were enhanced up to 10-fold over that had been achieved in their previous research [56] using a conventional amorphous alumina support with smaller surface area (180 m^2g^{-1}) for the aerobic oxidation of croton alcohol and cinnamyl alcohol (see *Scheme 1.6* for the oxidized alcohols and produced aldehydes' chemical structures). This was attributed to the greater dispersion achievable over the higher alumina area, and its ability to stabilize single-site Pd^{2+} catalytic centers. They observed that high palladium loading resulted in bigger clusters and metallic palladium, while for lower metal loadings, palladium tended more to stabilize on the support in oxidized isolated form (see *Table 1.2*) [55]. In case of conventional alumina support, it was observed that increase in palladium loading up to 0.84 wt.% improved the conversion of cinnamyl alcohol, while further increase in Pd loading to 2.02 wt.% diminished

the conversion (*Figure 1.2*), due to adverse effect of high Pd loading on particle size and dispersion of metal on the support.

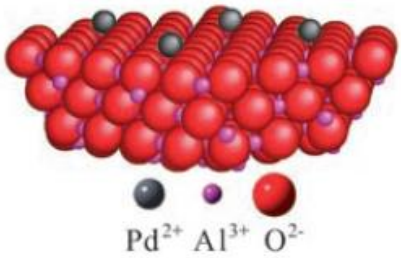

Figure 1.1. Schematic depiction of palladium on alumina surface, prepared by Hackett et al. [55].

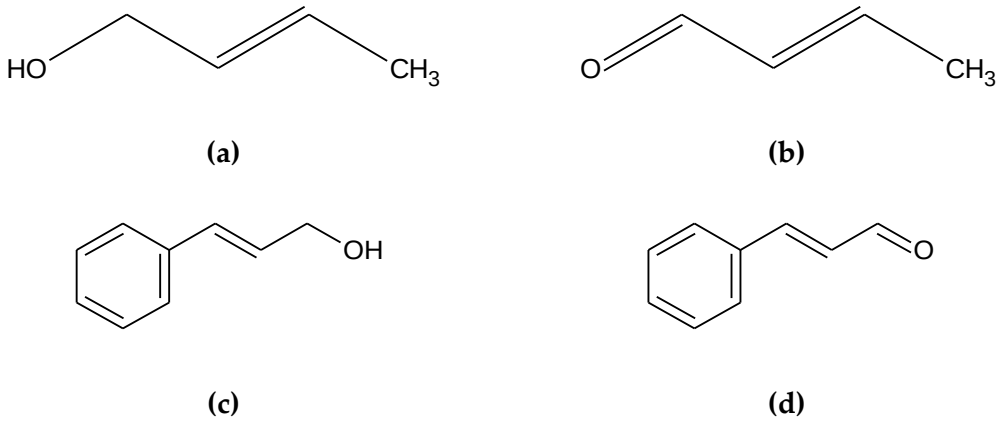

Scheme 1.6. Chemical structure of (**a**) croton alcohol, (**b**) crotonaldehyde, (**c**) cinnamyl alcohol, and (**d**) cinnamaldehyde.

Table 1.2. Structural and catalytic properties of Pd/mesoAl_2O_3 [55] in the aerobic oxidation of croton alcohol and cinammyl alcohol to corresponding aldehydes.

Pd loading (wt.%)	Particle size (nm)	Total Pd^{2+} (%)	Crotonaldehyde Yield (mmol h^{-1} $g_{cat.}^{-1}$)	Cinnamaldehyde Yield (mmol h^{-1} $g_{cat.}^{-1}$)
0.03	0.13	85	3.1	1.9
0.06	0.8	59	5.1	1.8
1.03	1.3	43.4	29.9	9.0
2.37	2.0	23.6	24.8	8.2
4.70	4.4	17.8	17.1	7.2

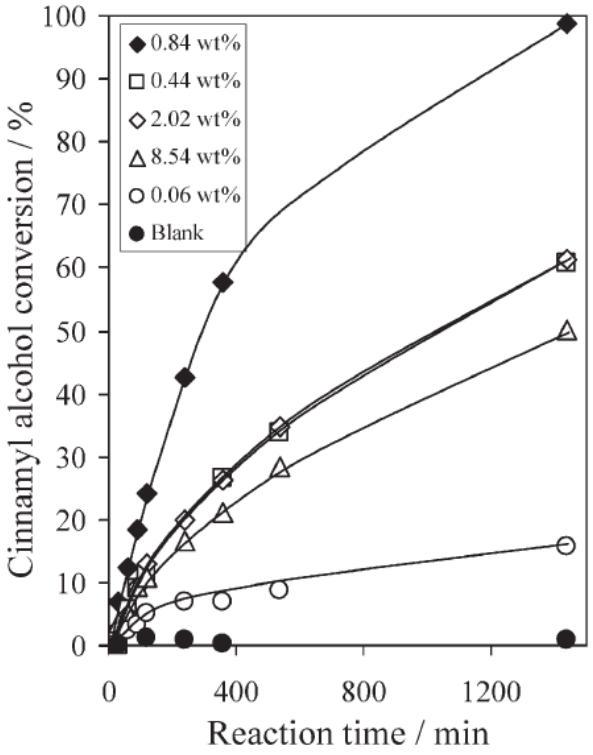

Figure 1.2. Reaction properties for cinnamyl alcohol selective aerobic oxidation over Pd supported on conventional amorphous alumina [56].

Wada et al. prepared catalysts included palladium oxide NPs of 1.5–3.0 nm diameter, located on the surface of TiO_2 crystalline particles and covered by an ultrathin microporous silica layer [57]. The catalysts showed excellent catalytic activities towards the aerobic oxidation of BnOH in water, and mild activity in toluene; but, the catalysts were not active for the oxidation of a bulkier alcohol, 2-naphthylmethanol, suggesting the size selectivity of the catalysts due to the microporous thin silica layer on its surface. The ultrathin microporous silica layer was reported to be responsible for the suppression of the growth of PdO particles during the calcination, given that the preparation of catalysts was finalized by controlled calcination process.

The NPs of many transition/noble metals are reported to be effective for selective oxidation of alcohols. Copper-manganese oxide on carbon system has been proven to be efficient for

selective oxidation of different alcohols to the corresponding aldehydes or ketones with molecular oxygen at 80 °C [58]. Anderson et al. showed that Pt supported on Al_2O_3 and Ru supported on carbon are active in aerobic oxidation of 2-octanol to the corresponding ketone in water as solvent. However, they reported that utilizing H_2O_2 as oxidant led to better catalytic activity compared to air [59]. Yamaguchi and Mizuno tested Ru supported on alumina for solvent-free selective oxidation of a range of primary and secondary alcohols with molecular oxygen, resulted in high alcohol conversion and selectivity towards the corresponding aldehyde or ketone [60]. Performing the same reactions in organic solvents was studied by the same group [61]. Utilizing a polar solvent, i.e., acetonitrile (**AcCN**) led to significant decrease in alcohol conversion compared to non-polar toluene or less polar ethyl acetate (**EtOAc**) solvents; but the selectivity of aldehyde remained constant. A 4-step mechanism is proposed for the aerobic oxidation of alcohols over prepared Ru/alumina catalyst (see *Scheme 1.7*) including formation of Ru^{n+}-alcoholate species through the ligand exchange between Ru^{n+}-hydroxide and the alcohol, β-hydride elimination of the alcoholate species to the corresponding carbonyl compound and the Run+-hydride species, and re-oxidation of Ru^{n+}-hybrid through insertion of molecular oxygen into Ru^{n+}-hybrid [61].

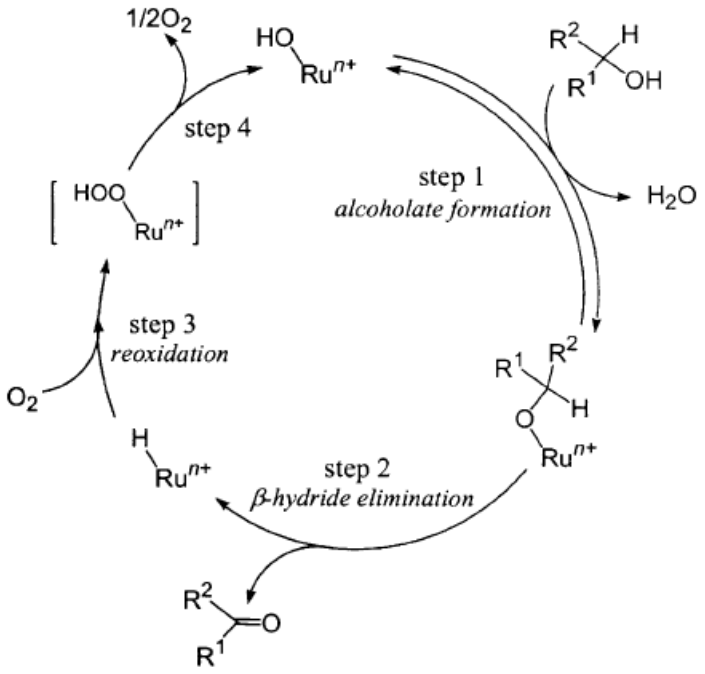

Scheme 1.7. Mechanism of Ru/alumina catalyzed aerobic oxidation of alcohols, proposed by Yamaguchi and Mizuno [61].

Abad et al. prepared gold NPs supported on nano cerium oxide, and tested the catalytic activity on a range of allylic alcohols, and compared the results with those achieved by Pd/Au bimetallic catalysts supported on TiO_2, for the same oxidation reactions [62]. They observed that the mono metallic gold catalyst led to extensively higher selectivity towards unsaturated carbonylic compounds; for example, in case of oxidation of 1-Octen-3-ol, 99% yield of unsaturated carbonylic products was achieved by Au/CeO_2, while 26% yield was obtained by the bimetallic $Au\text{-}Pd/TiO_2$ catalyst. *Scheme 1.8* shows the possible competing chemical processes during gold or palladium catalyzed aerobic allylic alcohols oxidation. The percentage of each product (if produced during the reaction) is partly dependent on the alcohol substrate [62].

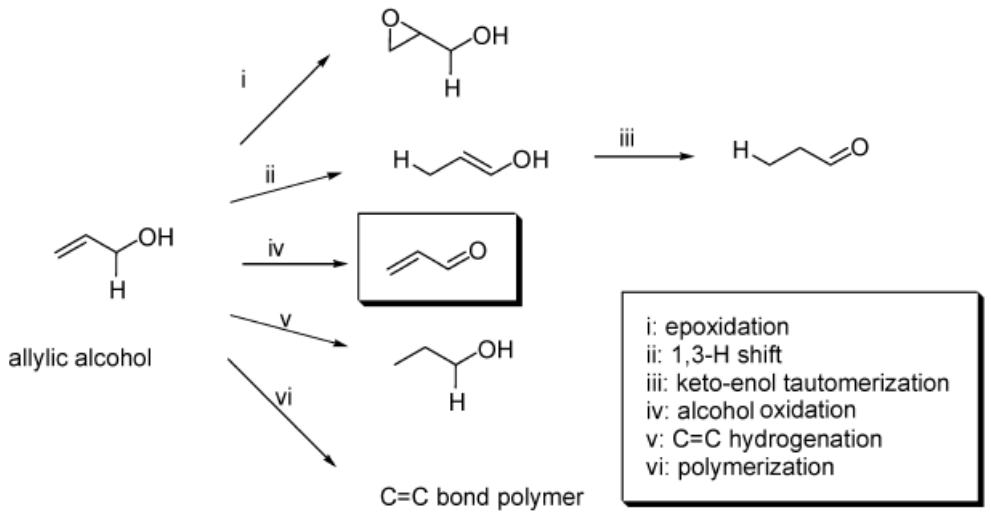

Scheme 1.8. Six possible chemical processes competing during aerobic oxidation of allylic alcohols catalyzed by gold or palladium [62].

1.3. Benzyl alcohol

Oxidation of benzyl alcohol (BnOH) is of utmost importance from scientific research, industrial, and environmental points of view [63-66]. Products of BnOH oxidation, specially benzaldehyde (PhCHO), are key materials in many industries such as perfumery, pharmaceutical, agrochemical, and dyestuff manufacturing [67-69]. The traditional PhCHO production methods pose economic and environmental disadvantages; therefore, if being performed efficiently and environmentally friendly, BnOH catalytic oxidation can be a proper alternative [70-72]. In this regard, many factors should be considered such as activity, selectivity, recyclability and toxicity of the catalyst, price and eco-friendliness of the oxidizing agent, and of the reaction solvent (if used), required temperature and pressure, etc. [3,7,73].

Because of economic and environmental issues, it is an advantage if a designed catalytic system works well in solvent-free conditions, or in cheaper and greener solvents; however, in

case of BnOH and other benzylic alcohols, it can be important for a catalyst to show high performance in presence of solvents too. The reason is that benzylic alcohols are basic "model compounds" for lignin oxidative depolymerization [74], which will be shortly discussed in Section 1.4.

BnOH can be oxidized to PhCHO by a range of metal catalysts. But the oxidation might continue to produce benzoic acid (**PhCOOH**). The reaction is depicted in Scheme 1.9. Therefore, it's extremely important for a catalyst to be selective towards the favorable product, i.e., PhCHO, or corresponding aldehydes of other benzylic alcohols.

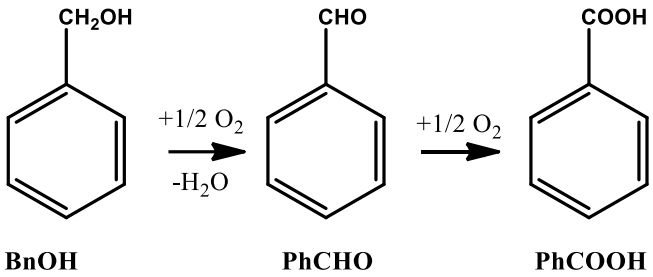

Scheme 1.9. Oxidation of benzyl alcohol (**BnOH**) to benzaldehyde (**PhCHO**) and final benzoic acid (**PhCOOH**).

Hydrogen peroxide and tert-butyl hydroperoxide (**TBHP**) have been used as oxidant in some studies; for instance, ferric tridodecanesulfonate [75] and $CoFe_2O_4$ NPs [76] with H_2O_2, or Mg-Al hydrotalcite [77] and Vanadium hydrophosphate with TBHP [78] have been applied to perform the oxidation of BnOH. But it would be preferred if the reaction can be oxidized by oxygen, or even better, by air at atmospheric pressure.

Utilizing noble metals to catalyze aerobic oxidation of BnOH to PhCHO is widely investigated. For instance, Ruthenium is proved successful in catalyzing this oxidation reaction, using air or molecular oxygen. Ruthenium is applied in form of tetrapropylammonium

perruthenate (TRAP) [79], $RuCl_2(PPh_3)_3$ in combination with 2,2′,6,6′-tetramethylpiperidine *N*-oxyl (TEMPO) [80] and supported on Al_2O_3 [60]. Many research works are dedicated to assess the catalytic behaviors of gold on BnOH oxidation reaction. Unsupported nanoporous gold showed good catalytic activity and high PhCHO selectivity in gas-phase oxidation of BnOH with molecular oxygen [81]. Gold NPs supported on Si/Ti [82], zeolite type metal-organic framework [83], mesoporous HMS silica [84] and recently BiClO [85] are also investigated and proved to be reactive for BnOH oxidation.

Palladium NPs on various supports for oxidation with air or O_2 were studied and in many cases, seemed promising due to high activity and selectivity. Considering the price of noble metals and environmental issues, recoverable and reusable heterogeneous systems are preferred. Some examples of supported palladium used for BnOH selective oxidation with air or oxygen include Pd supported on pumice [86], hydroxyapatite-supported palladium nanoclusters [87], SBA-15-supported palladium NPs [88], mesoporous alumina-supported palladium [55], Pd/COP-4 as an organic polymer-supported palladium [89], and more recently, mesoporous CN-supported Pd NPs [90], PdO/CuO NPs on zeolite-Y crystallite [91] and palladium NPs on a Cu based nanoporous metal-organic framework [92]. Furthermore, bimetallic Au/Pd NPs catalysts supported on TiO_2 [93,94], polyaniline [95], mesoporous silica SBA-15 [96] and SBA-16 [97], and Ti-NT nanotubes [98] have been investigated.

1.3.1. Mechanism of Pd-catalyzed BnOH Oxidation

The mechanism of the alcohols oxidation over Pd^0 has been investigated [3,99-101]. Oxygen is chemisorbed on palladium surface, oxygenated Pd mediates the assisted homolytic cleavage of

the O – H bond of BnOH, leading to formation of an alkoxide–palladium bond and a PdOH. Finally, a near Pd^0 cause the hydrogen abstraction, permitting the release of the PhCHO and of a molecule of water [3] (*Scheme 1.10*).

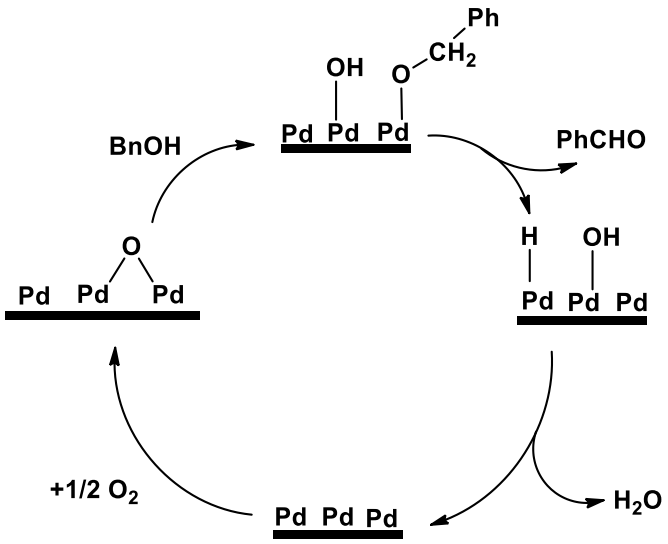

Scheme 1.10. Mechanism of BnOH oxidation catalyzed by Pd^0 supported on ceria (thick lines).

PhCHO, toluene, benzyl ether, benzene, PhCOOH and benzyl benzoate are the 6 products observed for oxidation of BnOH over Pd NPs at the temperature range close to 70–100 °C. The mechanism proposed by Savara et al. based on a microkinetic model, can justify the route to each of the 6 aforementioned products. For instance, Savara et al. postulates that the if the alkoxy, instead of losing a hydrogen, loses an oxygen, an alkylic derivative would appear. This alkyl can convert to toluene or ether, based on the conditions: the alkyl might catch a near-by hydrogen attached to the surface and produce toluene; alternatively, the alkyl might convert to ether if there is alkoxy bound to the near-by surface. The formation of acyl derivatives was justified by an intermediate which might be produced if an alkoxy interacts with a near-by oxygen on the surface

similar to toluene and ether routes, production of PhCOOH, benzyl benzoate or benzene from carbonyloxyl, depends on the conditions [3,101,102].

1.3.2. Factors in BnOH selective oxidation

Several reaction variables might influence the catalytic behavior and subsequently, the conversion of substrate and selectivity for the desirable product, namely oxidant, temperature, solvent (if applicable), concentration, etc.

1.3.2.1. Oxidant

Most of the palladium-catalyzed selective BnOH oxidation utilized molecular oxygen as oxidant [1,3,54]. However, air [103,104] and H_2O_2 [105] are studied as well. Kong et al. synthesized $PdFe_3O_4$@mCeO_2 microsphere including a magnetite core and a mesoporous CeO_2 shell [106]. The catalytic test for oxidation of BnOH was performed using O_2 flow, leading to 80.5% BnOH conversion and 94.8% selectivity for PhCHO at 100 °C. Yan et al. performed the solvent-free BnOH oxidation over palladium NPs supported on carbon nanotube, [107], by 20 mL min^{-1} O_2 flow, bubbling into a mixture of 50 mmol of BnOH (5.174 mL) and 10 mg catalyst (Pd 1 wt.%) at 160 °C. The selectivity of PhCHO have been above 90% in all experiments; but, with generally low BnOH conversion. Dell' Anna et al. compared the catalytic activity of palladium supported on porous methacrylic polymer, using air or oxygen as oxidant and water as solvent. At 100 °C, O_2 resulted in 75% and 99% conversion and selectivity, while with air, both of conversion and selectivity were lower, standing at 57% and 77% respectively [103]. Rostamnia et al., utilized air flow at 80 °C for BnOH oxidation over Pd supported on graphene oxide nanocomposite catalyst

[104], which led to 98% PhCHO yield. Increase in the reaction rate is reported for reaction over Au-Pd catalyst supported on TiO_2, at 120 °C [108], when the pressure of oxygen changed from 2 to 5 bar (*Figure 1.3*). Conversion of substrate and PhCHO selectivity grew to approximately 95% and 80% respectively at the maximum pressure, with diminish in amount of produced toluene.

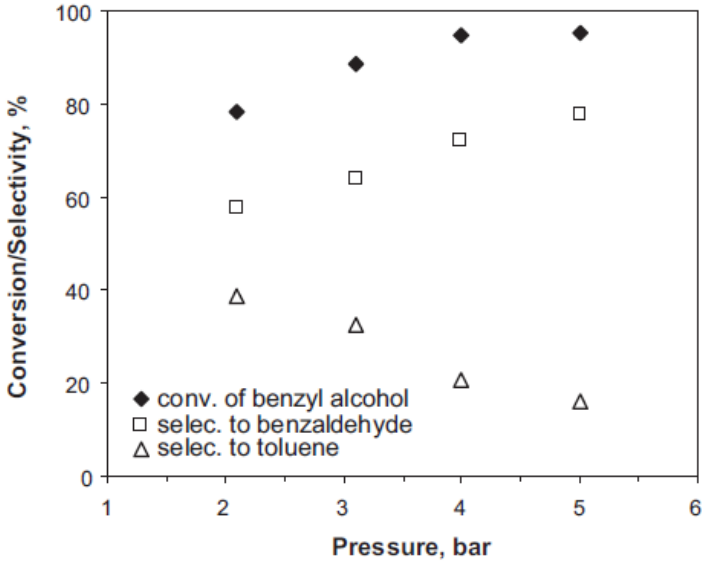

Figure 1.3. Effect of pressure on conversion and selectivity during BnOH oxidation catalyzed by Au-Pd/TiO_2 at 120 °C [108].

1.3.2.2. Temperature

Cao et al. tested the effect of temperature on catalytic activity of bimetallic Au-Pd supported on TiO_2 catalyst for BnOH oxidation to PhCHO, using O_2 [108]. The reaction was carried out at 80 - 140 °C. *Figure 1.4* shows the effect of reaction temperature on the alcohol conversion and aldehyde aldehyde/toluene selectivity. The BnOH conversion increased with the temperature from 20% at 80 °C up to 81% for the reaction at 140 °C, but the PhCHO selectivity diminished at the temperatures above 100 °C, from almost 70% at 100 °C down to 60% at 140 °C. The same

phenomenon is reported by Qi et al. for BnOH oxidation catalyzed by partially reduced palladium supported on MnO_x [109]. Increasing the temperature from 100 to 130 °C has led to rise in BnOH conversion from 50% at 100 °C, to 70% at 130 °C; but, the selectivity decreased from almost 98% to near 80% by heating the reaction up to 130 °C. Chan-Thaw et al. suggest that the reason of lower PhCHO selectivity at temperatures above 100 °C is that activation barrier for the formation of toluene through the C — O bond cleavage is higher than for the PhCHO formation [3].

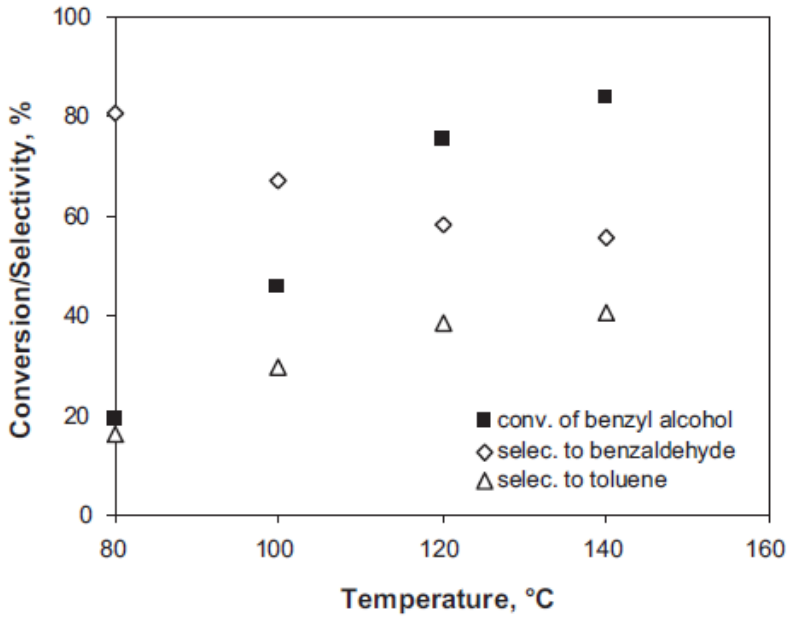

Figure 1.4. Effect of temperature on conversion and selectivity during BnOH oxidation catalyzed by Au-Pd/TiO_2 [108].

1.3.2.3. Solvent and Concentration

Many organic solvents have been utilized for BnOH catalytic oxidation by palladium catalysts. For instance, toluene [90,95], xylene [101] dimethyl sulfoxide (**DMSO**) [110,111], and AcCN [112] are investigated. Rostamnia et al. [104] explored the solvent effects on the oxidation

of BnOH catalyzed by a highly dispersive Pd supported on graphene oxide nanocomposite, using either water, ethanol **(EtOH)**, methanol **(MeOH)**, toluene, or dichloromethane **(DCM)** as solvent (*Figure 1.5*). The best PhCHO yield was achieved in nonpolar toluene (80% PhCHO yield). It was hypothesized that the reason was that the catalyst dispersed properly in toluene, consequently exhibiting a higher catalytic efficiency. The yield of PhCHO for the reactions with EtOH, MeOH, and water was ~35%, 34% and 28% respectively, following by below 5% PhCHO yield obtained using DCM. Addition of a surfactant to water resulted in significant increase of PhCHO yield, up to ~95%, due to enhanced catalyst dispersion in solvent. The authors attributed the higher yield in water/surfactant system compared to toluene, to the exclusive solubility of O_2 in water [104].

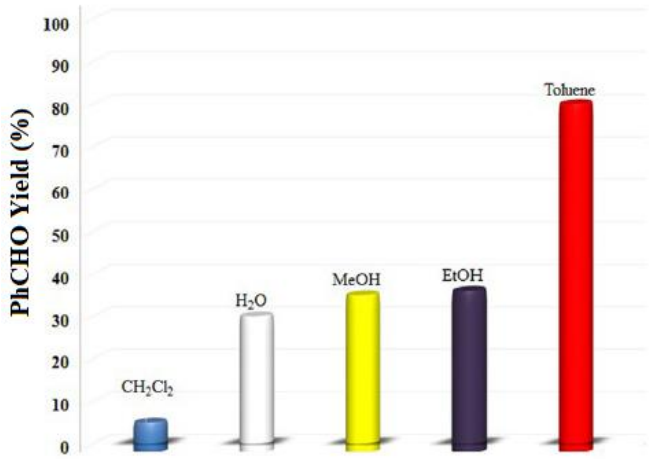

Figure 1.5. Effect of solvent on catalytic activity of 0.0096 mmol Pd-Supported graphene oxide nanocomposite in oxidation of 6 mmol BnOH at 80 °C [104].

Yang et al. studied the effect of solvent, using palladium supported on a mineral clay, palygorskite (PG) [112]. X-ray photoelectron spectroscopy (**XPS**) analysis of the supported palladium samples showed that the major palladium species was Pd^{2+}, with the Pd $3d_{5/2}$ peak at 337.3 eV BE. The best catalytic performance was observed in AcCN, leading to 100% BnOH

conversion and 99% PhCHO selectivity. The authors attributed this result to high polarity of AcCN. But the second best catalytic activity was observed in the nonpolar toluene (85% conversion) followed by 73% conversion obtained from the reaction in DCM solvent, which possesses a higher dielectric constants compared to toluene. The recyclability of the supported palladium catalyst was tested at the optimized conditions by Yang et al. (*Figure 1.6*), leading to slight decreases in BnOH conversion and preserving high PhCHO selectivity for five reaction rounds. Catalyst was separated, washed several times with EtOH and deionized water, and dried in vacuum at room temperature before being used in the next oxidation round [112].

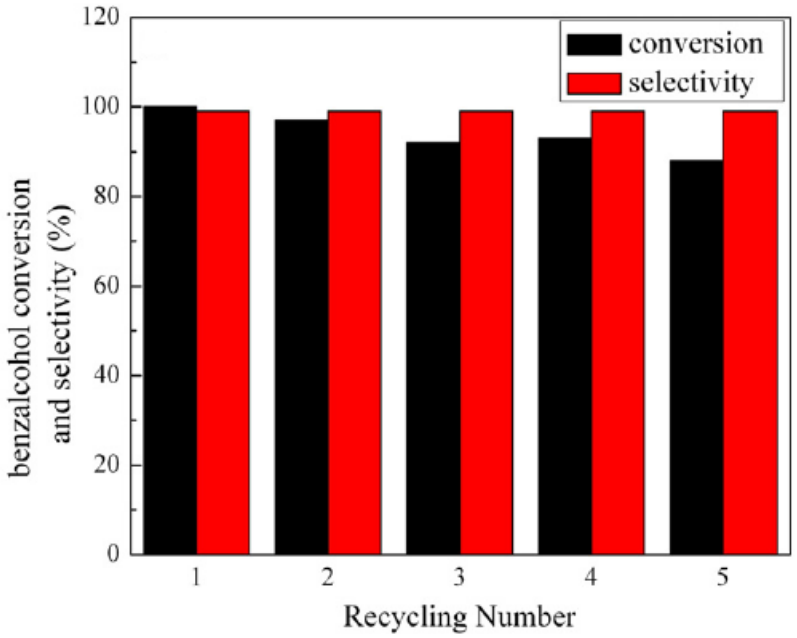

Figure 1.6. Recyclability test of Pd/PG in BnOH oxidation [112].

Dimitratos et al., compared [113] the oxidation in toluene and in water, using palladium, gold and platinum mono or bimetallic catalysts supported on activated carbon. All of the prepared

catalysts showed better activity in water. Best result was obtained by Au 73%-Pd 27% catalyst in water, resulted in 96% BnOH conversion and 94% PhCHO selectivity.

The catalytic activity of palladium NPs supported on mesoporous carbon nitride (Pd/CN) for the aerobic BnOH oxidation was studied by Xu et al. [90]. The reactions were carried out utilizing 10 mL toluene as solvent at 80 °C. As the amount of BnOH increases from 0.4 to 1.0 mL, its conversion improves from 39% to 94%, preserving 100% selectivity towards PhCHO but further addition of the substrate concentration resulted in decreases in BnOH conversion. The authors postulated that since the catalytic reaction proceeds in the presence of 10 mL toluene under the low amount of feedstock (< 0.8 mL), the solvent with high concentration might impede the adsorption of BnOH on the surface of heterogeneous catalyst, thus undermining catalytic activity [90]. The authors also tested the oxidation of other benzylic alcohols, and the substrates, products and results are presented in *Table 1.3*. They observed that the catalytic activity for each case depends on the property of substituent. Addition of electron-donating groups (**EDG**) i.e., methyl and methoxy, led to high catalytic activity (> 92%) in shorter reaction time, while substituting electron-withdrawing group (**EWG**) i.e., nitro, resulted in a significant decrease in alcohol conversion i.e., down to 54%. Xu et al. hypothesized that electron-withdrawing groups would hinder the activation of hydroxyl in the catalytic reactions [90]. As shown in *Section 1.3.1* and *Scheme 1.10* for mechanism of BnOH oxidation with Pd, the hydroxyl group should be activated on Pd to form the alkoxide, which later undergoes a dehydrogenation and then transformation into aldehyde. The EDGs are able to facilitate the formation of carbocation-type transition state, whereas, EWG would impede it [90]. However, Xu et al. reported that elongating the duration of

the oxidation of 4-nitrobenzyl alcohol up to 10 hours resulted in increase in alcohol conversion to 87% [90].

Table 1.3. Oxidation of benzylic alcohols (1 mL) by Pd/CN & O_2, at 80 °C in 10 mL toluene [90].

Substrate	Product	Reaction Time (h)	Aldehyde Yield (%)
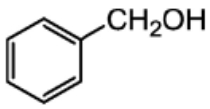	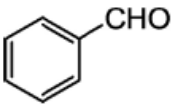	4	94
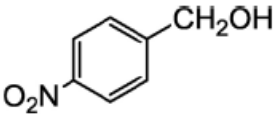	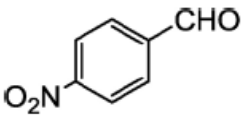	4	92
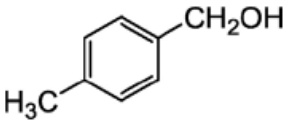	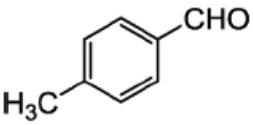	3	93
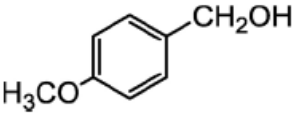	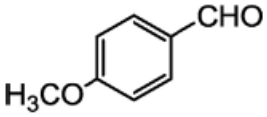	2.5	53

1.3.2.4. Effect of Catalyst properties

Zhou et al. studied the crucial role of both the size and the distribution of Pd NPs on the activity and selectivity [89]. Palladium was supported on a covalent organic polymer (COP-4). The Pd/COP-4 catalysts prepared with an impregnation method and H_2 reduction, were active for the aerobic oxidation of BnOH to PhCHO whether with or without solvent. Pd/COP-4-DH (prepared with dimethylformamide (**DMF**)) with a mean palladium size of 7.7 nm and a dispersion of 0.145 resulted in 32% BnOH conversion (*Table 1.4*). The other catalyst (Pd/COP-4-WH, prepared with water) with 9.9 nm and 0.113 dispersion led to less conversion (20.1%), showing that solvents used in the process of preparing the catalysts might influence the

interaction between the support and the metal particles and thus the distribution of the particles and the catalytic activity. DMF used in this contribution can build a bridge between the COP-4 support and the Pd particles. However, the achieved PhCHO selectivity was higher with Pd/COP-4-WH, because particle size distribution of Pd/COP-4-DH was broader [89].

Table 1.4. Catalyst properties catalytic activity of Pd supported on covalent organic polymer (COP-4), for BnOH to PhCHO aerobic solvent-free oxidation at 160 °C [89].

Catalyst	Pd Size (nm)	Pd Dispersion	Conversion (%)	Selectivity (%)
COP-4	-	-	6.2	100
Pd/COP-4-WH[a]	9.9 ± 0.2	0.113	20.1	57.1
Pd/COP-4-DH[b]	7.7 ± 1.8	0.145	32.0	89.8

[a] Catalyst prepared with water. [b] Catalyst prepared with dimethylformamide.

Crystal structure of palladium may affect the catalytic activity for BnOH oxidation. Ferri et al. studied the oxidation of BnOH catalyzed by Pd supported on alumina. [114]. They observed that in comparison with other palladium faces, Pd (111) was more likely to host the decarboxylation, leading to unfavorable benzene production; but, PhCHO production showed insignificant dependence on Pd structure, occurred on all exposed faces [114].

1.3.2.5. Effect of Support

Support may influence the catalytic activity of metal NPs, for instance, by changing the electronic and structural properties of the NPs through surface interaction with the support [3]. Metal sintering, over-oxidation, and leaching of metal can be affected by support properties; in addition, the support itself may play a role in the reaction by absorbing the reactants [3,54], or, as

shown in *Table 1.4* for COP-4 support, by directly catalyzing the reaction even without presence of metal NPs [89].

CeO_2 is a reductive oxide, efficient as support for metals such as Pd, Pt, and Au to catalyze reactions like amination of alcohols [115], and oxidation of CO [116] and alcohols [117]. The reason is the enhanced surface area and high amount of surface-active sites (oxygen vacancies) on nano ceria in comparison with other common supports [117-119]. This higher oxygen vacancy roots from the presence of Ce(III) on the ceria surface which can promote the absorption of molecular oxygen. In other words, the oxygen reserving capacity of a ceria sample depends on the Ce^{3+}/Ce^{4+} ratio, which may itself be related to ceria morphology [120]. It has been shown that CeO_2 support with different morphologies such as nanorod, nanocube, or nano-octaedron differently effected the catalytic performances, as reported for lean methane combustion over palladium supported on ceria nanorod, nanocube, or nanotube catalysts [120] and in BnOH oxidation over palladium supported on CeO_2 truncated octahedra and cubes [121].

Other metals supported on ceria have also been tested for different reactions, for instance, Cu or Ni supported on ceria nanorod (**CeO_2-NR**) led to a higher activity compared with other support morphologies; in particular, the nanorod morphology showed better activity in the CO oxidation [122], in the dry reforming of methane [123], and in the synthesis of dimethyl carbonate from methane and MeOH [124].

X-ray diffraction (**XRD**) technique is utilized in many research works to study the crystal structure of catalysts and the possible effect of metal deposition on the support structure. For instance, the XRD patterns of Pd/ceria samples (*Figure 1.7*) in Lei et al. research work [120], reported to show reflections that according to Joint Committee on Powder Diffraction Standards

(**JCPDS**), were assigned to face-centered cubic structure of CeO_2. All characteristic peaks of three Pd/ceria samples (at 28.6°, 33.1°, 47.5°, 56.3°, 59.1°, 69.4°, 76.7°, and 79.07°) were corresponded to the (1 1 1), (2 0 0), (2 2 0), (3 1 1), (2 2 2), (4 0 0), (3 3 1), and (4 2 0) planes respectively, indicative of ceria face-centered cubic structure (JCPDS No. 34-0394). Lei et al. claimed that since no peak of Pd phase was observed, Pd particle size was small and NPs were well-dispersed on the support [120]; however, this might be due to other reasons such as low metal loading (below the device detection limit) [125,126].

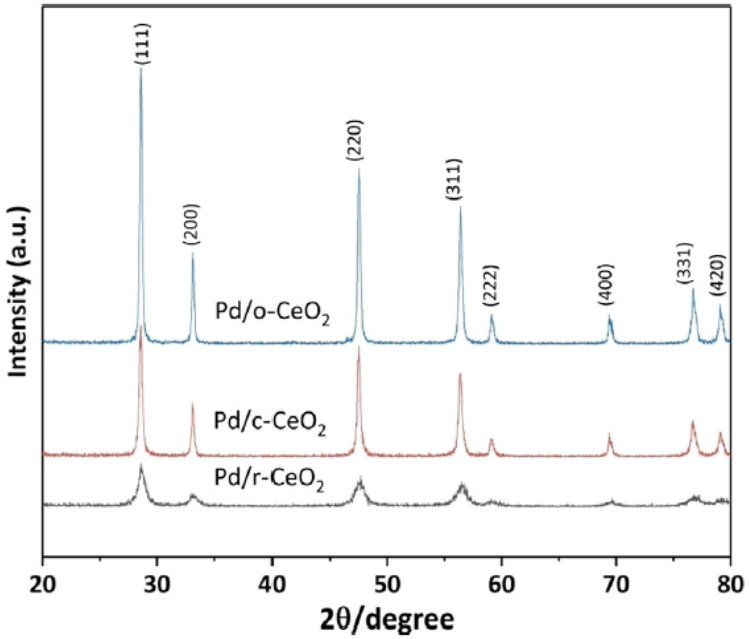

Figure 1.7. XRD patterns of Lei et al. Pd ceria samples. o-CeO_2, c- CeO_2, and r- CeO_2 represents ceria with nano-octaedron, nanocube, and nanorod morphologies respectively [120].

Zhang et al. reported that the bimetallic Au/Pd supported on CeO_2-NR showed remarkable catalytic activity and selectivity in BnOH oxidation using molecular oxygen [119]. Oxidation of BnOH catalyzed by $PdCl_2$ supported on spherical, microrods, or spindle-like CeO_2 particles was investigated by Liu et al.[117]. The scanning electron microscope (**SEM**) images are depicted in

Figure 1.8, proving the formation of targeted morphologies. The experiments were performed using molecular oxygen at 80 °C, and 1:4 molar ratios of BnOH to $PdCl_2$. Yields of PhCHO of the reactions are reported in *Table 1.5*. Among three used support morphologies, nanosphere ceria derived the best PhCHO yield and microrod-structure ceria performed the weakest.

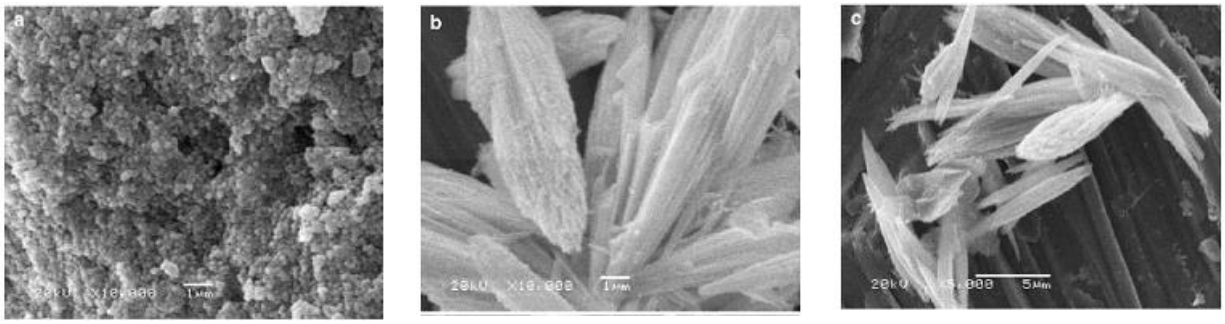

Figure 1.8. SEM images of: (**a**) nanosphere, (**b**) microrod, and (**c**) spindle-like ceria particles synthesized and acquired by Liu et al. [117].

Table 1.5. Surface area (S_{BET}) and total pore volume (V) of ceria-supported $PdCl_2$ catalysts, and results of BnOH oxidation [117].

Ceria Morphology	S_{BET} (m^2/g)	V (cm^3/g)	PhCHO Yield (%)
nanosphere	112.3	0.18	99
microrod	97.2	0.14	84
spindle-like	117.6	0.12	90

This was explained by data from the Brunauer–Emmet–Teller (**BET**) surface area acquired from nitrogen adsorption-desorption analysis (*Table 1.5*). Microrod structure showed least surface area while spindle-like ceria had the most, and nanosphere ceria was reported to be in the middle. The other important factor is total pore volume, whose amount for spherical ceria was higher than that of spindle-like and microrods ceria so it was concluded that better Pd nanoparticles dispersion over nanosphere, led to higher PhCHO production.

Zhang et al [119] compared the catalytic behavior of CeO_2-NR-supported bimetallic Au/Pd by monometallic Pd in selective BnOH oxidation using 1.0 MPa molecular oxygen. CeO_2-NRs were reported to be 10-20 nm and 50-300 nm in diameter and length respectively, and lots of metal NPs with the narrowly distributed size around 2.6 nm were evenly deposited on the ceria according to transmission electron microscope (**TEM**) images shown in *Figure 1.9a* [119]. By studying the high resolution transmission electron microscope (**HRTEM**) image (*Figure 1.9b*), Zhang et al. realized that the fringe distance for the ceria support was 0.287 nm, in good agreement with the value corresponds to (200) ceria lattice plane (*Figure 1.9b*). In addition, the 0.204 nm fringe distance measured for the metal particles was reported to be pretty close to related value of both palladium and gold (200) lattice space [119].

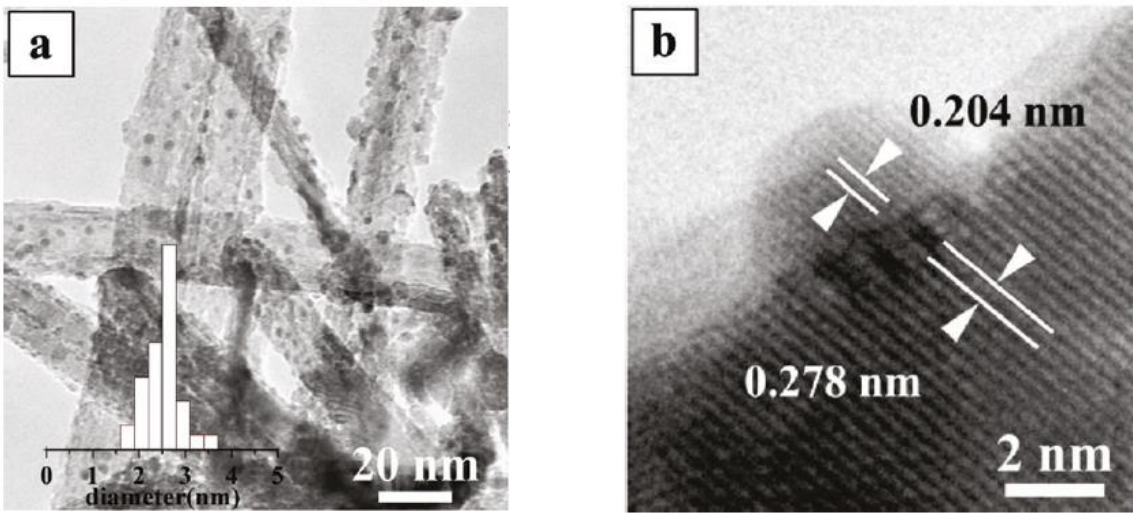

Figure 1.9. TEM (**a**) and HRTEM (**b**) images of AuPd/CeO_2 sample (Au:Pd 1:5, 1.2 wt.%) [119].

Utilizing XPS analysis, Zhang et al measured the oxidation state of palladium and gold in one of samples (*Figure 1.10*). By comparing the peak positions (Au $4f_{7/2}$ at ~83.3 nm and Pd $3d_{5/2}$ at ~334.9 nm) with reference values, it was shown that Pd and Au were in metallic state, indicating

the reduction of palladium and gold by the Ce^{3+} at room temperature. Bimetallic catalyst demonstrated better reactivity than monometallic Pd/CeO_2-NR, but slightly better PhCHO selectivity was achieved by the monometallic catalyst (Table 1.6). Higher activity of bimetallic system was attributed to electron density being pulled away from Pd by Au leading to improved interaction among Pd and BnOH atoms [119].

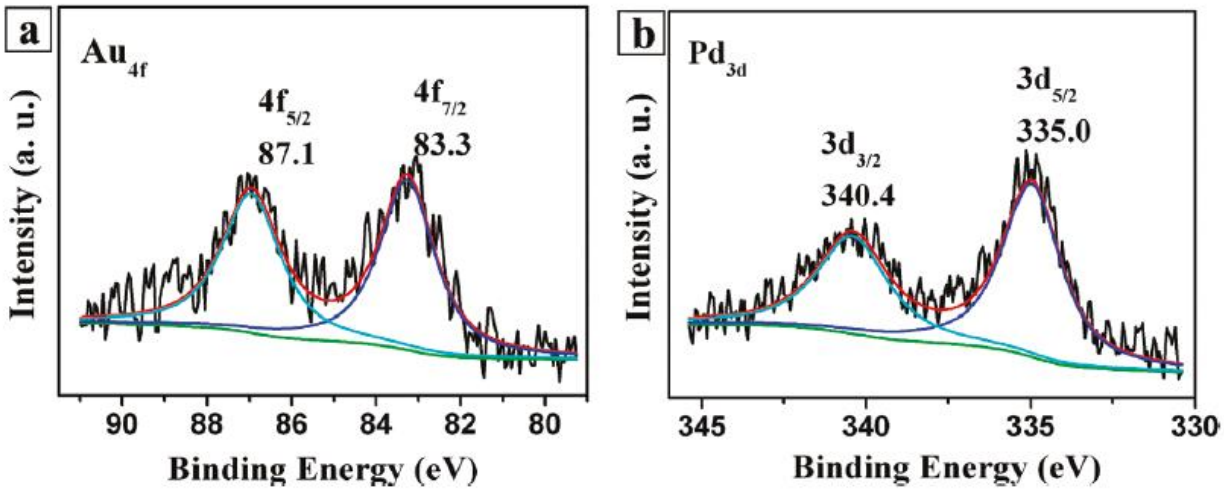

Figure 1.10. Au 4f (**a**) and Pd 3d (**b**) XPS spectra of AuPd/CeO_2 sample (Au:Pd 1:5, 1.2 wt.%) [119].

Table 1.6. Metal composition and catalytic activity of Pd/CeO_2 and some of AuPd/CeO_2 samples prepared and used in aerobic BnOH to PhCHO oxidation at 120 °C by Zhang et al. [119].

Au:Pd	Time (min)	Conversion (%)	Selectivity (%)
0:1	60	95.7	95.0
1:5	22	94.7	92.3
1:3	40	96.6	94.4

Xin et al studied the effect of CeO_2 morphology on the catalytic activity of ceria-supported palladium single atoms (**Pd_1**) as well as hexapalladium clusters (**Pd_6**) in BnOH aerobic oxidation. [127]. Pd_1 or Pd_6 were deposited on either truncated octahedron ceria (**CeO_2(T)**), ceria nanocube (**CeO_2 (C)**), or ceria nanorod (**CeO_2 (R)**). HRTEM images of CeO_2 (T) and CeO_2 (C) supports

(before metal deposition), as well as images of CeO_2 (R) sample -after Pd_1 or Pd_6 deposition are shown in *Figure 1.11* [127]. Xin et al. measured the fringe distances of ceria samples and reported that the main exposed plane in CeO_2 (C) was (100), while both CeO_2 (R) and CeO_2 (T) mainly exposed (111) plane. For instance, the measured 0.31 nm fringe distance of Pd_1/CeO_2 (R) and Pd_6/CeO_2 (R) (*Figure 1.11c* and *1.11d* respectively), were in good agreement with the d value of ceria (111). In addition, Xin et al. were unable to identify any Pd particles in the HRTEM images of Pd_1/CeO_2 (R) or Pd_6/CeO_2 (R) [127].

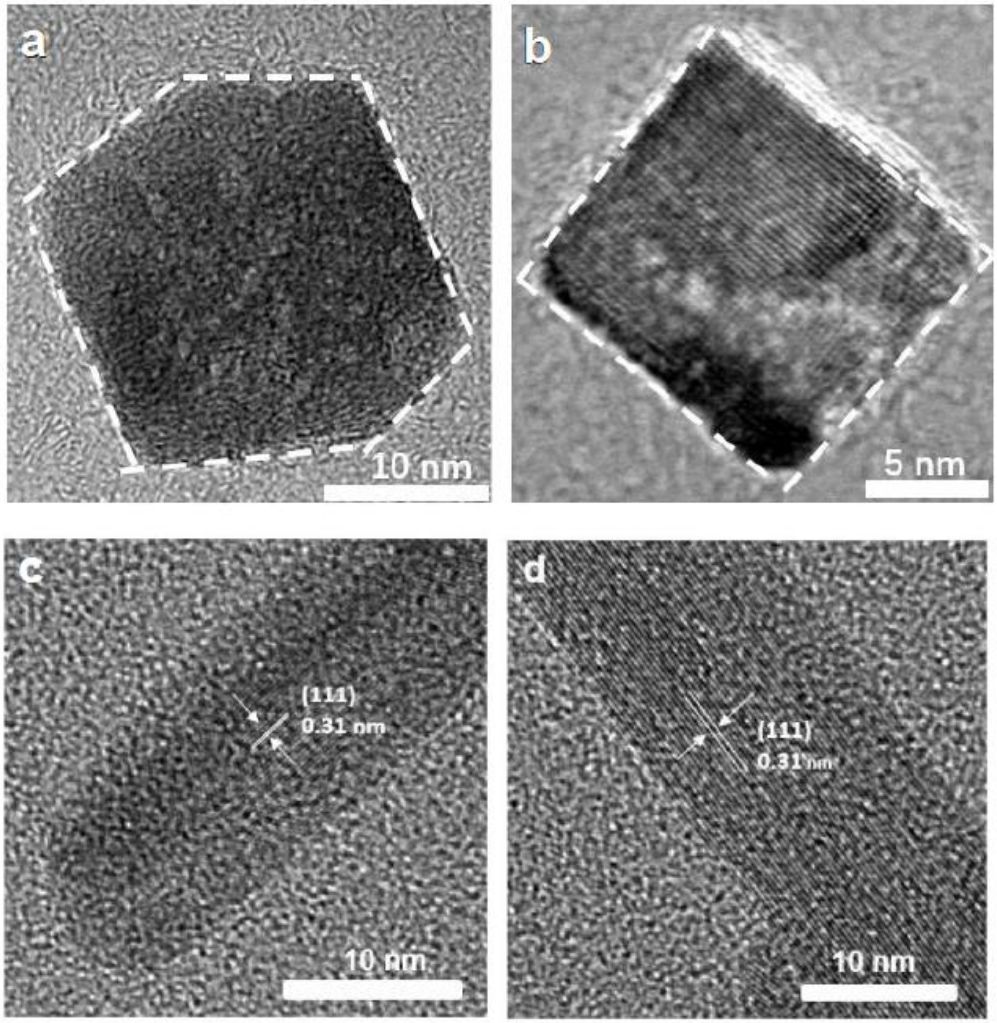

Figure 1.11. HRTEM images of (**a**) truncated octahedron ceria (CeO_2(T)), (**b**) ceria nanocube (CeO_2(C)), (**c**) ceria nanorod supported with Pd single atoms (Pd_1/CeO_2 (R), and (**d**) ceria nanorod supported with hexapalladium clusters (Pd_6/CeO_2 (R)) [127].

Xin et al. tested all the Pd/ceria samples in aerobic solvent-free BnOH oxidation (*Figure 1.12*) [127]. Regardless of the support morphology, all the samples with hexapalladium clusters, namely Pd_6/CeO_2 (R), Pd_6/CeO_2 (T), and Pd_6/CeO_2 (C) were almost inactive, while all the samples with atomically dispersed palladium, namely Pd_1/CeO_2 (R), Pd_1/CeO_2 (T), and Pd_1/CeO_2 (C) showed activity for BnOH oxidation, indicating the critical effect of metal particle size, Xin et al. claims [127]. Among the reactions catalyzed by Pd_1/ceria samples, best result was achieved using CeO_2 (R) as support, leading to ~26% BnOH conversion. This result was slightly higher than that achieved using truncated octahedral CeO_2 as support (~24% BnOH conversion), even though both CeO_2 morphologies exposed the (111) plane which has a synergy with palladium for catalyzing selective BnOH oxidation [121,127], showing the superiority of nanorod morphology in the performed experiments [127]. The catalysts were reduced at the final stage of preparation, but as shown by Tan et al., keeping palladium in metallic state on CeO_2-NR is a problematic task [128].

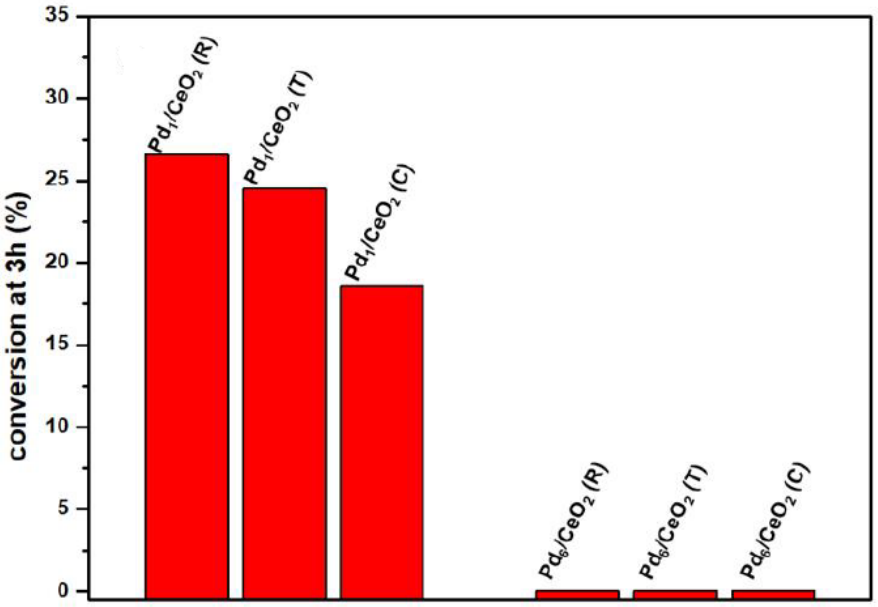

Figure 1.12. BnOH conversion by different Pd/ceria samples prepared by Xin et al. [127]. Reaction conditions: 5 mmol BnOH, 10 mg catalyst, 1 atmosphere O_2, 100 °C, 3h, solvent-free.

Furthermore, Xin et al., chose the best support morphology, i.e., CeO_2 (R), and utilized it for aerobic solvent-free oxidation of BnOH substituted with methyl, methoxy, or nitro group. The results are summarized in *Table 1.7*. It can be observed that substituting different groups, influenced the outcome of the reactions. As expected, Pd_6/CeO_2 (R) was still inactive in the oxidation of substituted benzylic alcohols [127].

Table 1.7. Solvent-free oxidation of BnOH and substituted benzylic alcohols with Pd single atoms or Pd hexamers supported on CeO_2 (R) (Pd_1/CeO_2 (R) and Pd_6/CeO_2 (R) respectively). Reaction conditions: 5 mmol BnOH, 10 mg catalyst, 1 atmosphere O_2, 100 °C, 3h [127].

Substrate	catalysts	Conversion (%)	Aldehyde selectivity (%)
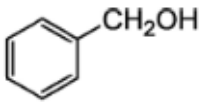	Pd_1/CeO_2 (R)	26.60	100
	Pd_6/CeO_2 (R)	0	N/A
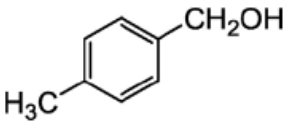	Pd_1/CeO_2 (R)	18.63	100
	Pd_6/CeO_2 (R)	0	N/A
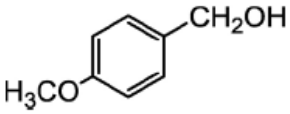	Pd_1/CeO_2 (R)	11.12	100
	Pd_6/CeO_2 (R)	0	N/A
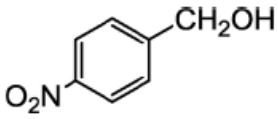	Pd_1/CeO_2 (R)	27.13	100
	Pd_6/CeO_2 (R)	0	N/A

In contrary to research work of Xu et al. [90], Xin et al. observed that placing an EDG like methyl or methoxy in the BnOH molecule decreased the conversion of benzylic alcohols, while

addition of an EWG ended up in even a slightly higher alcohol conversion compared to BnOH conversion in the same conditions [127]. This might suggest that in two abovementioned studies, the reaction mechanisms were different.

1.4. Benzylic Alcohols as Lignin Model Compounds

Lignocellulosic biomass, the most abundant and renewable natural resource on Earth, is composed of a complicated mixed structure of three natural biopolymers, namely cellulose, hemicellulose, and lignin [11,129-131]. Cellulose (*Scheme 1.11a*) is a semi-crystalline long chain polysaccharide formed by D–glucose units, linked by β–1,4 glycosidic bonds. Hemicellulose (*Scheme 1.11b*) is a complex, branched and heterogeneous amorphous polymeric network of pentoses such as xylose, and, hexoses such as mannose. Lignin (*Scheme 1.11c*) consists of an amorphous three-dimensional complex structure in which, p-hydroxyphenyl (**H**), guaiacyl (**G**) and syringyl (**S**) units are linked by C — O or C — C bonds. In the structure of plants (*Figure 1.13*) cellulose fibers are connected to lignin through hemicellulose. The role of lignin is to hold the cellulose and hemicellulose together, and to provide resistance and impermeability [11,132,133].

If separated, isolated, and chemically transformed, these three biopolymers can end up in a vast and multifunctional group of value-added biofuels, platform and intermediate chemicals, that are conventionally produced from petroleum [134-136]. For instance, bioethanol fuel can be produced from cellulose by hydrolysis to glucose (as explained in *Section 1.1.3, Scheme 1.4*) and subsequent fermentation of glucose to EtOH. This bioethanol can be potentially used as fuel either alone or in mixture with gasoline [20].

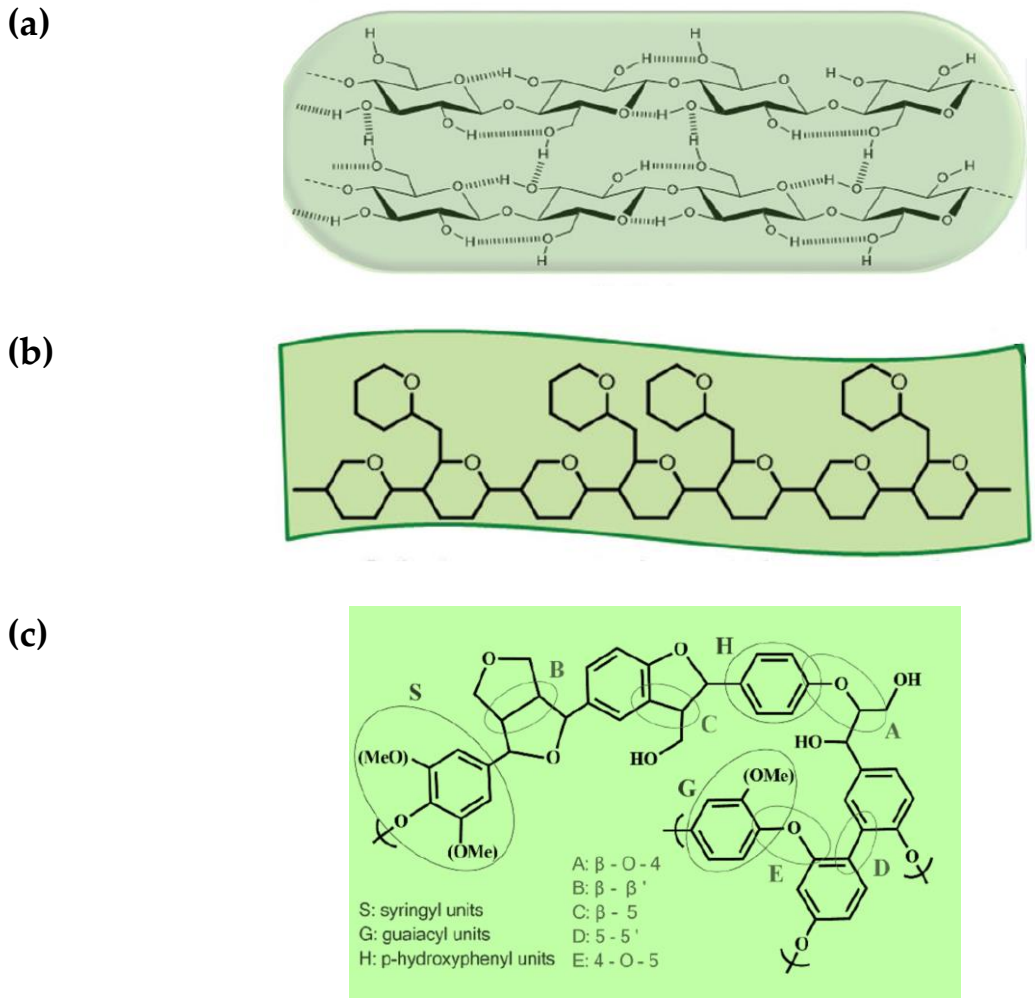

Scheme 1.11. Structure of (**a**) cellulose, (**b**) hemicellulose example, and (**c**) lignin example [132].

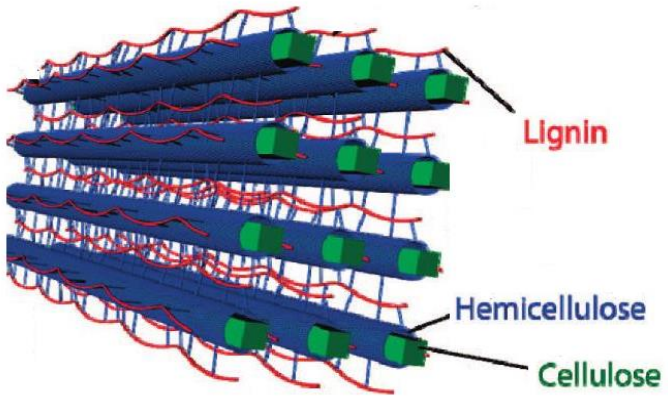

Figure. 1.13. Schematic representation of the location and structure of main components of lignocellulosic material.

Among three major components of lignocellulosic biomass, lignin is considered as a unique natural resource of numerous aromatic polymers [9,137]. Catalytic oxidative depolymerization of lignin aiming at extracting the highly valuable lignin monomers has been the title of many research works, especially during the last decade To better understand the cracking mechanism of lignin linkages, different "lignin model compounds" resembling those linkages have been employed by researchers, and numerous catalytic systems have been designed and tested in the oxidation of the linkages of the model compounds, and in oxidative depolymerization of lignin [8,138,139]. The most abundant linkages in lignin structure are β — O — 4, α — O — 4 and 4 — O — 5 (*Scheme 1.11c*) [10]. Examples of lignin model compounds, including those containing the noted linkages are shown in *Scheme 1.12*.

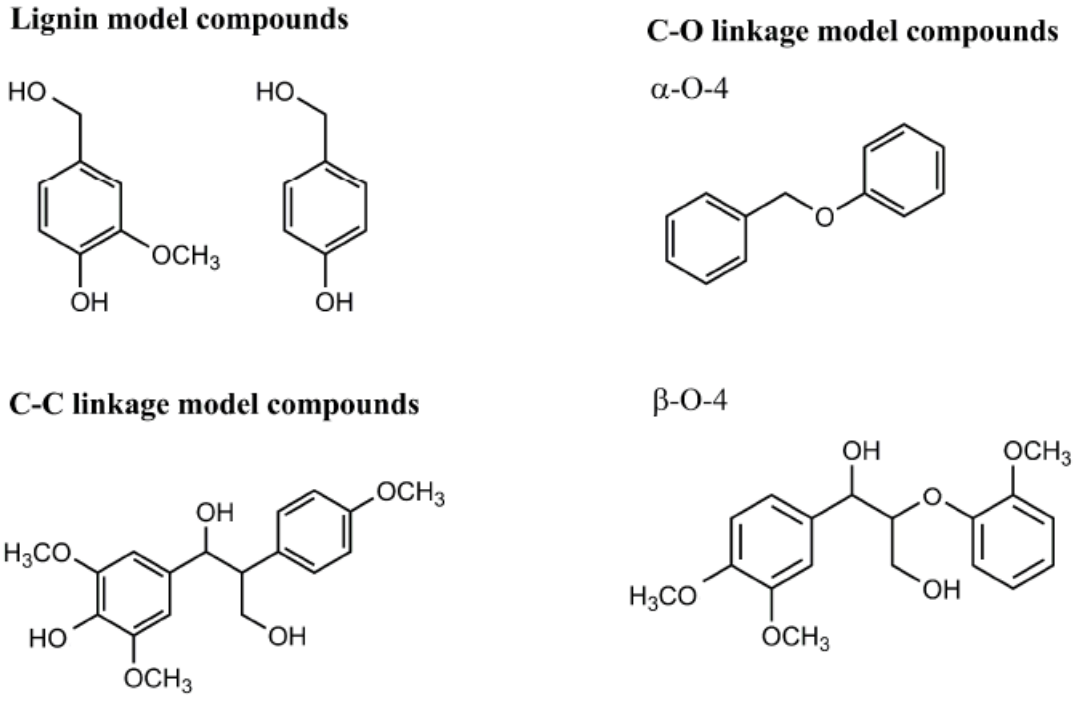

Scheme 1.12. Examples of lignin model compounds resembling the common linkages in lignin.

BnOH along with substituted benzylic alcohols are the most basic lignin model compounds. Since lignin oxidative depolymerization is regularly performed in solvents, studying the activity of a catalyst in different solvents is critical.

In this PhD research, several Pd/ceria nanorod catalysts have been synthesized and their catalytic activity in aerobic oxidation of BnOH and 4-benzyloxyphenol in different organic solvents has been studied. The catalysts were characterized by Temperature-Programmed Reduction (**TPR**) and nitrogen adsorption-desorption analysis (performed by the author), as well as XRD, TEM and XPS (conducted by technicians and colleagues of the author), and the results of analytical techniques are discussed. In addition, one of synthesized catalysts, palladium oxide supported on CeO_2–NR was tested in the aerobic solvent-free oxidation of BnOH and substituted benzylic alcohols. Furthermore, a number of palladium supported on mesoporous silica catalysts prepared by the colleagues of the author has been examined for the BnOH and 4-benzyloxyphenol in different organic solvents. Detection and quantification of the products of catalytic oxidation at different stages of the reactions were carried out by gas chromatography-mass spectrometry (**GC-MS**).

Chapter 2.

Experimental

2.1. Chemicals

$PdCl_2$; 10 wt.% $Pd(NO_3)_2$ solution in 10 wt.% nitric acid; $Ce(NO_3)_3 \cdot 6H_2O$; Oleylamine; Trioctylphosphine; (3-aminopropyl) triethoxysilane; Citric acid, 1-pentanol, K_2PdCl_4, Benzyl alcohol (**BnOH**), Benzaldehyde (**PhCHO**), 4-Methoxybenzyl alcohol and all other chemicals except those reported below are from Sigma Aldrich (Germany)

40% Pd in $Pd(NO_3)_2 \cdot 2H_2O$; Pd 10% w/w in $Pd(NO_3)_2$ solution; $NaH_2PO_2 \cdot H_2O$; and all BnOH derivatives were from Alfa Aesar.

Cyclooctanone, Celite, SiO_2, filter cel, were from Fluka.

n-Dodecane was from Merk-Schuchardt (Germany).

Mesoporous silica, SiO_2, were from STREM Chemicals.

2.2. Catalyst Preparation

2.2.1. Preparation of Pd/ceria Catalysts

Different palladium/ceria nanorod catalysts were prepared by the author, varying the palladium deposition method, palladium precursor, palladium oxidation state, and palladium wt.%. Preparation methods are described in the following.

2.2.1.1. Synthesis of Ceria Nanorod

Ceria nanorod (**CeO_2-NR**) was prepared according to previously published method [125]. 1.300 g of $Ce(NO_3)_3 \cdot 6H_2O$ were dissolved in 20.0 mL of distilled water and then added to an alkali

solution formed by dissolving 14.400 g NaOH in 40.0 mL of distilled water in a Teflon bottle (*Figure 2.1*) under intense stirring for 30 min. Afterward, to perform a hydrothermal treatment on the mixture, the Teflon bottle was placed in a stainless-steel autoclave vessel. Then the vessel was tightly sealed and put in oven at 100 °C for 24 h. Next, the obtained purple precipitate was separated by vacuum filtering over a paper filter, washed several times with distilled water and EtOH, and dried at 120 °C for 24 h. The dried solid was milled in an agate mortar and calcined at 400 °C for 5 hours.

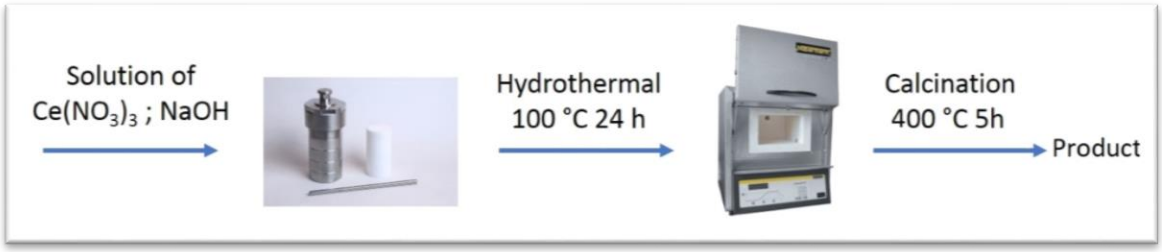

Figure 2.1. Preparation of ceria nanorod (**CeO_2-NR**).

2.2.1.2. Preparation of Palladium Oxide Supported on CeO_2-NR

Palladium oxide supported on CeO_2-NR (**PdO_x/CeO_2-NR**) was prepared by depositing palladium nitrate on CeO_2-NR via wet impregnation process, aiming at achieving CeO_2/Pd molar ratio of 95/5 (2 wt.% Pd), and a final calcination (*Figure 2.2*). A volume of 10.0 mL of 0.020 M aqueous solution of $Pd(NO_3)_2{\cdot}2H_2O$ was gradually added to 1.000 g of CeO_2-NR in a flask while stirring and heating at 60 °C for 2 h. Afterward, the water was evaporated and the solid was dried at 120 °C for 24 h in oven, followed by milling and calcination at 500 °C for 5 h to achieve PdO_x/CeO_2-NR. The utilized palladium(II) nitrate solution was prepared by dissolving the proper

amount of Alfa Aesar palladium(II) nitrate dehydrate powder in distilled water at room temperature, helped by gradual addition of tiny amounts of HNO_3.

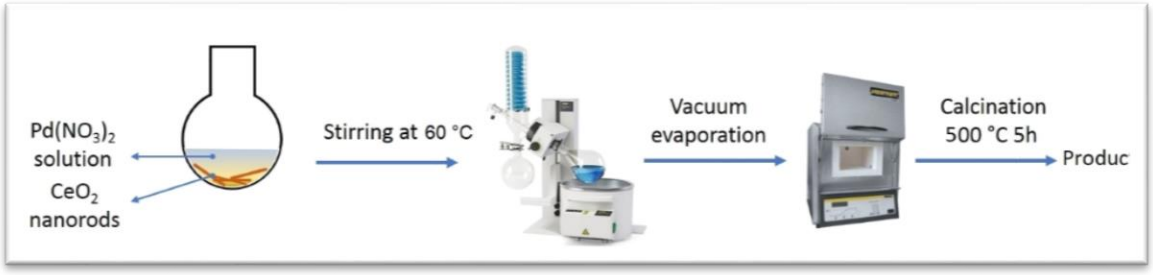

Figure 2.2. Preparation of Palladium Oxide Supported on ceria nanorod (**PdO_x/CeO_2-NR**).

2.2.1.3. Preparation of Reduced Palladium Oxide Supported on CeO_2-NR

250 mg of prepared PdO_x/CeO_2-NR was subjected to reduction by H_2-TPR (described in *Section 2.5.2.2*) and the produced sample (**PdO_x/CeO_2-NR -Red**) was subjected to catalytic testing to study the effect of Pd oxidation state on the catalytic behavior of the palladium/ceria system.

2.2.1.4. Methanol-reduced Pd/ceria

For preparation of this catalyst (**Pd/CeO_2-NR-Me-Red),** methanol (**MeOH**) was utilized as solvent to reduce palladium during wet impregnation, aiming at obtaining 2 wt.% Pd: 0.017 g $PdCl_2$ was dissolved in 30.0 mL MeOH by stirring at room temperature for 18 h. The obtained solution was gradually added to 0.500 g CeO_2-NR, which led to immediate start of darkening the color of ceria powder. Then, the temperature was increased to 50 °C, maintaining there for 5 h, while the mixture was vigorously stirred. By heating to 50 °C, the color of the solid became dark green, and ended up in greenish black after 5 hours at 50 °C. Afterwards, the liquid was removed

by centrifuge, and the solid was washed by MeOH three times, following by drying in room temperature for 24 h and milling. A part of this catalyst was utilized in aerobic BnOH oxidation, the other part of this sample was subjected to calcination (500 °C for 5 h), before being tested in catalytic oxidation of BnOH.

2.2.1.5. Hydrazine-reduced Pd/CeO_2-NR

For preparation of this catalyst (**Pd/CeO_2-NR-Hz-Red)** hydrazine was utilized to reduce palladium during wet impregnation, with the aim of achieving 2 wt.% Pd: 10 mL of 0.020 M aqueous solution of $Pd(NO_3)_2{\cdot}2H_2O$ was prepared described in *Section 2.2.1.2*. Subsequently, 1.160 g of prepared CeO_2-NR powder was added and stirred for 2 h at 60 °C. Then, an aqueous hydrazine solution (1.80 mmol) was added drop by drop to the mixture. Hydrazine and palladium molar ratio was fixed to 5:1. After 4 h, the precipitate was recovered by centrifugation, washed with plenty of water and ethanol (**EtOH**) and finally dried overnight at 65 °C.

2.2.1.6. Preparation of Palladium Oxide Supported on CeO_2-NR by Palladium Nitrate Commercial Solution

As described in *Section 2.2.1.2*, PdO_x/CeO_2-NR was prepared using solid palladium(II) nitrate dehydrate. precursor from Alfa Aesar (**AA**). Palladium oxide supported on CeO_2-NR was also prepared by palladium(II) nitrate commercial solutions. Preparation method was similar to that of PdO_x/CeO_2-NR, except that instead of dissolving palladium(II) nitrate dehydrate powder, the commercial palladium(II) nitrate solutions from AA or Sigma Aldrich (**SA**) was used. With AA

palladium(II) nitrate solution, three catalysts (2, 4 or 5.2 wt.% palladium) and with Sigma Aldrich solution, one sample (2 wt.% palladium) were prepared.

2.2.2. Preparation of Pd/silica Catalysts

In order to understand the role of the support on the catalytic activity of palladium for oxidation of alcohols, the oxidation reaction was tested using palladium/silica catalytic system. Palladium metallic as well as palladium phosphorous supported on amine-functionalized mesoporous silica was prepared by colleagues of the author, using a commercial mesoporous silica.

2.2.2.1. Functionalization of mesoporous silica Support: NH_2SiO_2

Mesoporous silica support was functionalized with 3-aminopropyltriethoxysilane (3-APTES) in order to add amine groups on the pore channels. 1.0 g of mesoporous silica, 100.0 mL of toluene and 2.5 mL of 3-APTES were put in a flask under stirring in flow of Ar for 12 hours. Then, the mesoporous silica was washed with water and EtOH for 3 cycles, using centrifuge for recovering the solid, which was finally dried at room temperature overnight.

2.2.2.2. Synthesis and loading of Pd^0 nanoparticles

0.0355g of $PdCl_2$ (2 mmol), 20.0 mL of oleylamine and 0,1 mL of trioctilphosphine were added in a flask under stirring at room temperature. The reaction was heated up to 240 °C under gentle Ar flow for 1.5 h. During the synthesis, gradual colour change from yellowish white to brown and finally to black was observed, indicating nucleation and subsequent growth of Pd^0 particles.

The Pd nanoparticles (**NPs**) were separated from the reaction mixture by adding 50 mL of isopropanol, followed by centrifugation. The Pd^0 NPs were further washed by dispersing in cyclohexane (10.0 mL). Thereafter, an amount corresponding to 2 wt.% of Pd^0 NPs was added to the functionalized mesoporous silica by dispersion in 5.0 mL of cyclohexane and ultra-sonicated for 1 h. Finally, the dispersion was centrifuged, washed with EtOH and dried overnight in air.

2.2.2.3. Synthesis of Pd-P alloy supported on NH_2 mesoporous silica by in-situ reduction

0.8052 g of citric acid, 18.0 mL of EtOH and 70.0 mL of distilled water were mixed under stirring and 0,4596 g of sodium hydroxide was added to obtain sodium citrate. Then, 0.03128 g of K_2PdCl_4 was added and completely dissolved under stirring. Then 0.5000 g of mesoporous functionalized silica, was added to the mixture which was then stirred for 2h. Finally, 0.5087 g of sodium hypophosphite monohydrate was dissolved in 50.0 mL of distilled water and dropped in the mixture, maintaining the stirring for 4 h at 80 °C. The precipitate was repeatedly centrifuged with distilled water and EtOH, and dried overnight in air at room temperature [126].

All the supported palladium catalysts, whether those prepared by the author, or the catalysts prepared by other members of our research group, are listed in *Table 2.1*. An acronym is specified to each catalyst which will be used in the text from now on.

Table 2.1. List of palladium catalysts tested in oxidation reactions.

Sample acronym	Pd wt.%	Support	Pd precursor	Description
CeO_2-NR	-	-	-	Ceria nanorod support
PdO_x/CeO_2-NR	2	CeO_2-NR	$Pd(NO_3)_2.2H_2O$	Solid precursor of Alfa Aesar
PdO_x/CeO_2-NR-Red	2			Reduced by H_2-TPR
Pd/CeO_2-NR-Me-Red	2		$PdCl_2$	Pd reduced with MeOH during the wet impregnation
Pd/CeO_2-NR-Hz-Red*	2		$Pd(NO_3)_2.2H_2O$	Pd reduced with hydrazine following the wet impregnation
PdO_x/CeO_2-NR-AA2	2		$Pd(NO_3)_2$ solution	Alfa Aesar $Pd(NO_3)_2$ solution, Pd 10% w/w
PdO_x/CeO_2-NR-AA4	4			
PdO_x/CeO_2-NR-AA5.2	5.2			
PdO_x/CeO_2-NR-SA2	2			Sigma Aldrich $Pd(NO_3)_2$ solution
Pd^0/NH_2SiO_2*	2	Functionalized mesoporous silica	$PdCl_2$	Pd^0 or palladium phosphorous supported on amine-functionalized mesoporous silica
Pd-P/NH_2SiO_2*	2		K_2PdCl_4	

* Prepared by colleagues of the author

2.3. Catalyst Testing

The catalytic activity of prepared Pd/ceria and Pd/silica samples was tested in oxidation of BnOH and BnOH derivatives, and of 4-benzyloxyphenol as a lignin model compound.

2.3.1. Oxidation of BnOH in Organic Solvents by Air/O_2

The catalytic activity of different Pd/ceria and Pd/silica catalysts for BnOH oxidation was investigated using a 25 mL round-bottom three-neck flask equipped with reflux condenser, gas inlet and thermometer. The reactions generally were tested during 5-hour reaction time, changing

several parameters: solvent, temperature, substrate concentration, catalyst/substrate ratio, and oxidant (20 mL min^{-1} air or O_2).

2.3.2. Leaching test

Leaching test of PdO_x/CeO_2-NR catalyst was conducted using 16 mg catalyst for the aerobic BnOH (0.16 mmol) oxidation in EtOH at 78 °C. After 45 min, the catalyst was removed by centrifuge (10000 rpm, 20 min) and the remaining solution was subjected to reaction conditions again, to check any possible progress in the conversion of the substrate.

2.3.3. Recyclability test

Recyclability test of PdO_x/CeO_2-NR was carried out by performing the aerobic BnOH (0.16 mmol) oxidation in EtOH at 78 °C for three rounds using. In each round, after 5 hours the catalyst was separated by centrifuge (10000 rpm, 20 min), washed 3 times with EtOH and dried at room temperature to be used in the next round. The weight of catalyst in each round of reaction was 32 mg. Parallel reactions were carried out to acquire a proper amount of catalyst after recovering.

2.3.4. Solvent-Free Aerobic Oxidation of Benzylic alcohols

Catalytic activity of PdO_x/CeO_2-NR-SA2 for solvent-free aerobic oxidation of BnOH as well as substituted benzylic alcohols was assessed in a 10 mL two-neck round bottom flask, equipped with reflux condenser and gas inlet. For each reaction, 10 mmol of substrate was added to the flask, which was then put into a pre-heated silicon oil bath. When the temperature of substrate arrived at 100 °C, it was subjected to vigorous stirring and 10 mL min^{-1} air flow, bubbled into the

liquid/melted substrate. Then, 10 mg of PdO_x/CeO_2-NR-SA2 (catalyst/substrate molar ratio approximately 1:5320) was added, and the temperature and stirring maintained for 5 hours after which, the reactants were analyzed.

2.3.5. Oxidation of 4-benzyloxyphenol in Organic Solvents

All the Prepared Pd/ceria and Pd/silica catalysts (*Table 2.1)* were tested for oxidation of 4-benzyloxyphenol. For each reaction, 10 mL of 16 mM 4-benzyloxyphenol solution (in EtOH or toluene) and 32 mg of the testing catalyst was added to a 25 mL round-bottom three-neck flask equipped with reflux condenser and gas inlet. 20 mL min^{-1} air or O_2 was bubbled into the reaction mixture, while intensely stirring. A silicon oil bath was utilized to heat the system up to boiling of the applied solvent. Furthermore, other catalytic systems, either commercial catalysts or catalysts prepared by the colleagues of the author for other projects, were tested for the oxidation of 4-benzyloxyphenol, namely, Co_3O_4, platinum supported carbon, ruthenium supported on Mg-Al alloy oxide, $BaZrO_3$, $CzZrO_3$, $SrZrO_3$, and cobalt supported on Mg-Al alloy oxide (either non-calcined, or calcined at 500 or 800 °C).

2.4. Analytical Method

2.4.1. Gas Chromatography-Mass Spectrometry

Detection and quantification of the products of catalytic oxidation at different stages of the reactions were carried out by gas chromatography-mass spectrometry (**GC-MS**), using an internal standard for calculating the substrate conversion, products' selectivity.

2.4.1.1. Background

Gas chromatography mass spectrometry is a method by which a mixture of compounds can be both separated and identified. The compounds are first separated by gas chromatography as described below and then analyzed by the mass spectrometer.

Gas chromatography (**GC**), is a common type of chromatography used in analytical chemistry for separating and analyzing compounds that can be vaporized without decomposition. In gas chromatography, the mobile phase is a carrier gas, usually an inert gas such as helium or hydrogen. The stationary phase is a thin polymeric layer liquid at the operative conditions, supported on glass or metal column. The temperature of the system can be controlled and modified during the analysis. Gas chromatography is like fractional distillation, since both processes separate the components of a mixture primarily based on boiling point (or vapor pressure) differences. Each compound being analyzed, reaches its boiling point in the heated column, starts vaporizing, interacts with the stationary phase and dilutes in it as a function of its affinity. This causes each compound to move through the column at a different rate and to be elute at a different time, known as the retention time of the compound. These properties permit to separate and recognize compounds in a mixture. The comparison of retention times is what gives GC its analytical usefulness.

Fractional distillation is typically used to separate components of a mixture on a large scale, whereas GC can be used on a much smaller scale to detect compounds in an unknown mixture (i.e. microscale).

To establish the identity of the different separated compounds flowing out from the GC column, a detector is needed. Usually a FID (flame ionization detector) detector is used to determine and quantify compounds. *Figure 2.3* shows the diagrams of a GC, a GC split injector, and a FID detector. On entering into the detector, the all carbonaceous substances are burned with air and hydrogen at the jet's tip. Radical carbocations are formed as products of the combustion and they are detected by an anode detector. (*Figure 2.4*) [140].

In Mass spectra detector the molecules eluted from the GC are ionized to form charged particles, by removal of an electron. The radical cations formed pass through a magnetic field that sort them according to their mass-to-charge ratio (m/z). Ionization is achieved in a number of ways. In an electron impact (**EI**) mass spectrometry, the sample is introduced into a high-vacuum chamber where it is bombarded with highly energetic electrons. The bombarding electrons eject an electron from a molecule to form a radical cation, called molecular ion. The molecular ion is then detected and its mass to charge recorded. Because the relative molecular masses of the molecular ion and the sample are essentially identical, the mass spectrometer determines the Mw of the sample. Normally the excess of energy in the bombarding electrons causes the molecular ion to break down to give fragment cations and fragment radicals. Identification of the fragments provides information on the structure of the molecule. The ions are separated by their mass to charge ratio using a magnetic quadrupole analyzer. The quadrupole consists of four parallel metal rods. Each opposing rod pair is connected together electrically, and a radio frequency (**RF**) voltage is applied between one pair of rods and the other. A direct current voltage is then superimposed on the RF voltage. Ions travel down the quadrupole between the rods. Only ions of a certain mass-to-charge ratio will reach the detector for a given ratio of voltages: other ions have unstable trajectories and

will collide with the rods. This permits selection of an ion with a particular m/z or allows the operator to scan for a range of m/z-values by continuously varying the applied voltage [141].

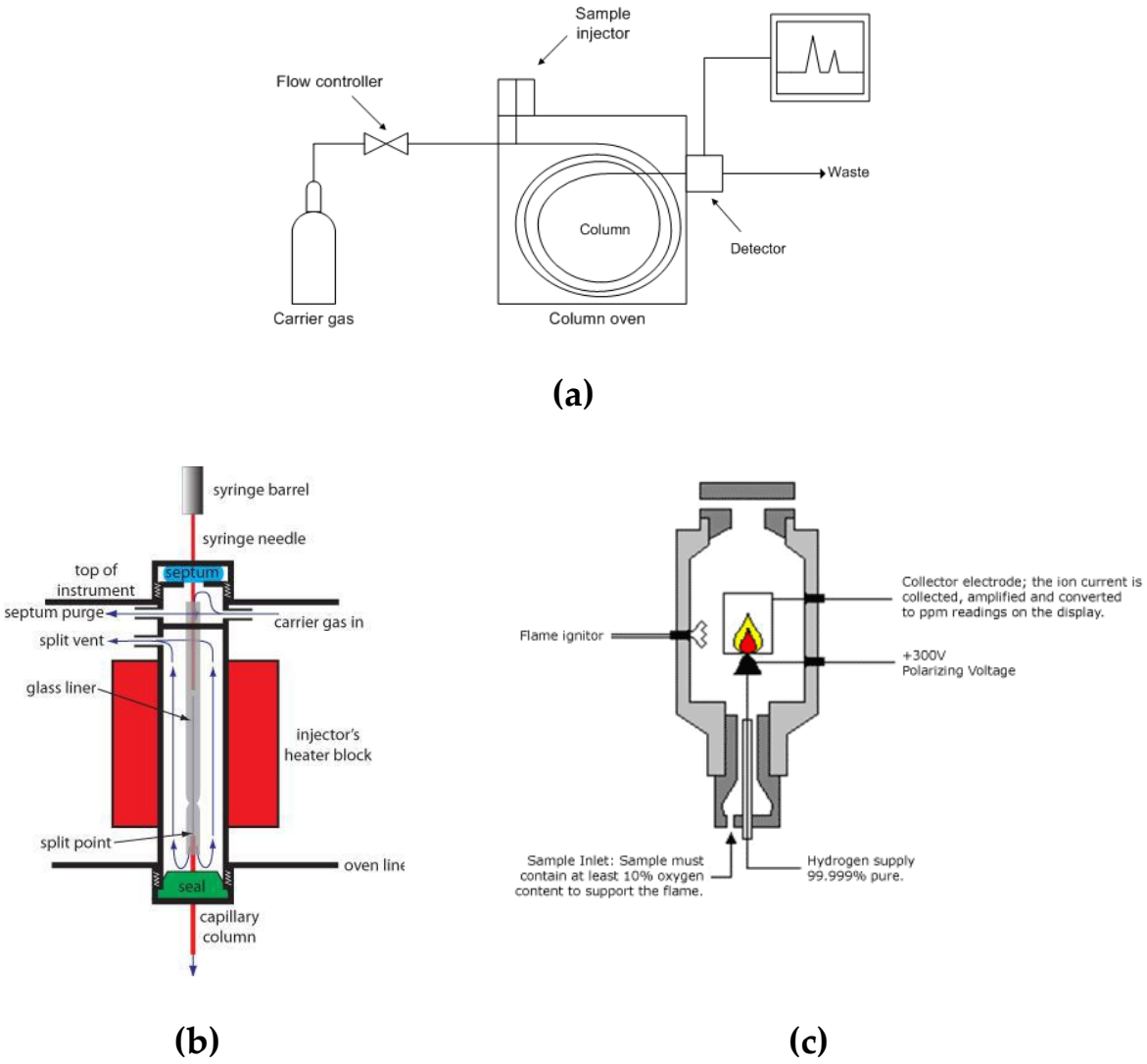

Figure 2.3. Diagram of a gas chromatograph (**a**); GC split injector diagram (**b**); flame ionization detector diagram (**c**).

The separated ions can then be quantified using a faraday cup or electron multiplier. When a beam or packet of ions hits the metal, it gains a small net charge that can then be discharged to measure a small current equivalent to the number of impinging ions. By measuring the electrical current (the number of electrons flowing through the circuit per second) in the metal part of the

circuit the number of charges being carried by the ions in the vacuum part of the circuit can be determined (*Figure 2.4a*) [142]. An electron multiplier uses this principle of secondary electrons to amplify the signal. Ions are directed onto a first dynode which causes the emission of secondary electrons which are accelerated through an electric potential so that they strike a second dynode. This process can be repeated numerous times causing an amplification of the signal up to 106 times (*Figure 2.4b*) [143].

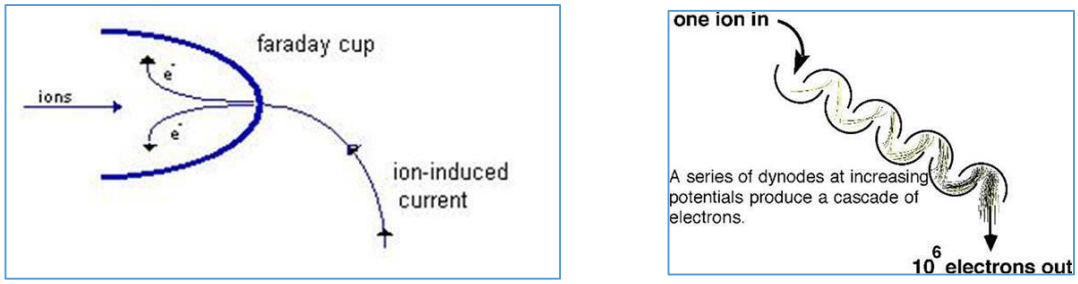

(a) **(b)**

Figure 2.4. Faraday cup diagram (**a**); electron multiplier diagram (**b**).

2.4.1.2. Experimental

Samples from the reactions were passed over a celite path entrapped between two pieces of cotton in a glass Pasteur pipet, by eluting with diethyl ether, and analyzed by GC-MS. The analyses were carried out on a Shimadzu VG 70/250S apparatus equipped with a Supelco SLB™ column (30 m, 0.25 mm and 0.25 m film thickness), using a temperature profile at 50 °C for 4 minutes followed by a 10 °C/min temperature gradient until 250 °C for 10 min. The injector temperature was 250 °C.

An internal standard compound (either cyclooctanone or n-dodecane) was utilized for calculating the conversion of substrates and the selectivity towards the products. In case of the

catalytic testing in organic solvents, the internal standard compound was added before the reaction (in the substrate solution); these reactions were analyzed hourly, by taking a 0.01 mL sample. In case of analyzing the result of solvent-free reactions, first, all the reactants were dissolved in ethyl acetate (**EtOAc**), diluted to 25 mL, then the proper amount of internal standard compound was added to this solution. Surface of reflux column as well as other internal parts of the reaction set-up were washed carefully with EtOAc to ensure collecting all the presented reactants.

2.4.2. Definitions and Calculations

The catalytic activity of the prepared catalysts was assessed by calculating the conversion of substrate and selectivity of the intended products, which are the corresponding aldehydes in case of benzylic alcohol substrates.

For the simplest conducted reaction BnOH to PhCHO, the conversion and selectivity are calculated as follows:

$$\text{BnOH conversion (\%)} = \frac{\text{moles of BnOH reacted}}{\text{initial moles of BnOH}} \times 100 \qquad \textbf{Equation 2.1}$$

$$\text{PhCHO selectivity (\%)} = \frac{\text{moles PhCHO produced}}{\text{moles of BnOH reacted}} \times 100 \qquad \textbf{Equation 2.2}$$

2.5. Catalyst Characterization

A selected number of prepared catalysts were characterized. Textural and morphological properties were studied by X-ray diffraction (**XRD**), transmission electron microscope (**TEM**) and nitrogen adsorption-desorption analysis. Redox properties and oxygen storing capacity were

investigated by Temperature-programmed reduction H_2-TPR. Electronic and chemical properties at the surface of the samples are analyzed by X-ray photoelectron spectroscopy (**XPS**).

2.5.1. X-ray Diffraction

2.5.1.1. Experimental

XRD patterns were recorded using a Scintag X1 diffractometer equipped with a Cu Kα (λ=1.5418 Å) source and the Brag-Brentano θ–θ configuration in the 2θ =10 - 80 range, with 0.05° step size and 3 s acquisition time. The phases of the metal and oxide support of the catalysts were carefully analyzed by PowderX software. Peak positions in the diffraction patterns were compared with Joint Committee on Powder Diffraction Standards (**JCPDS**) database files. The average crystallite sizes of the various catalysts were calculated by using Scherrer's equation from the predominant peaks of the corresponding element.

2.5.2. Temperature-Programmed Reduction

2.5.2.1. Background

Temperature-programmed reduction (**TPR**), is a beneficial method for characterizing supported and unsupported metal and mixed metal oxides, revealing information about redox properties of samples, identification of supported metal/metals, finding efficient reduction conditions, metal-support interaction, etc. In this technique, a reducing gas mixture (typically 5% of H_2 diluted in Ar or N_2) is flowed over the metal oxide catalyst at high temperature. A thermal conductivity detector (**TCD**) measures the changes in the thermal conductivity of the exiting gas

flow by producing TCD signals that are then converted to concentration value of reducing gas (H_2), from which, the consumed H_2 can be measured. *Figure 2.5* [25], shows the TPR profile of supported nickel in oxide and reduced states.

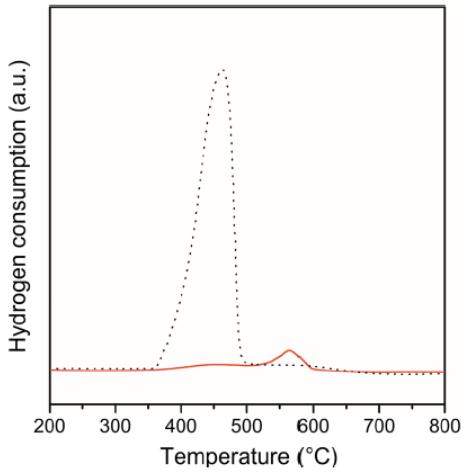

Figure 2.5. TPR profile of supported Ni, chemically reduced by hydrazine (orange line), and supported NiO (dotted black line).

2.5.2.2. Experimental

H_2-TPR experiment was performed by a Thermo Scientific TPDRO1100 flow apparatus. The PdO_x/CeO_2-NR (0.250 g) was pre-treated in a flow of 10 % O_2/He mixture (20 cm^3 min^{-1}) at 300 °C for 30 min. The H_2-TPR was conducted flowing 30 cm^3 min^{-1} of 5% H_2/Ar mixture from 50 °C up to 500 °C with a rate of 10 °C min^{-1}, maintaining the final temperature for 60 minutes. Then the sample was cooled down to 50 °C in the same mixture, followed by heating in pure Ar up to 350 °C (10 °C min^{-1}) to remove chemisorbed hydrogen, and then cooling down to room temperature. The H_2 consumption and release were measured by a TCD detector. A trap was utilized before flowing into the TCD detector to remove the generated H_2O in the reduction process.

2.5.3. Transmission Electron Microscopy

2.5.3.1. Experimental

TEM images were acquired using a FEI-Thermo Fisher Scientific Tecnai 12 G^2 Twin instrument, operating at primary electron beam energy of 120 keV, equipped with a "post-column" Gatan Biofilter electron energy filter, a Gatan 794 IF Peltier cooled charge-coupled device-based slow scan camera, equipped with EDX system. The used catalysts were dispersed in isopropyl alcohol and ultra-sonicated for 15 min. Then a drop of the suspension (~20 μL) was placed on a copper TEM grid (400 mesh), covered by an amorphous carbon film.

2.5.4. Nitrogen Adsorption-desorption Analysis

2.5.4.1. Background

Surface area and pore size distribution of a variety of solid materials such as industrial adsorbents, catalysts, pigment, etc., can be assessed by gas adsorption measurements. The nitrogen adsorption method is one of the most commonly used methods for determining the surface area of a catalyst (Brunauer-Emmet-Teller (**BET**) surface area) according to physical adsorption of nitrogen on the surface of the solid and by calculating the amount of adsorbate gas corresponding to a monomolecular layer on the surface. Relatively weak van der Waals forces between the adsorbate gas molecules and the adsorbent surface of the sample result in physical adsorption. The assessment is usually carried out at the temperature of liquid nitrogen. Measuring the amount of adsorbed either by a volumetric or continuous flow procedure.

The theory is based on the BET equation:

$$\frac{1}{\upsilon[(P^0/P)-1]} = \frac{c-1}{\upsilon_m c}\left(\frac{P}{P^0}\right) + \frac{1}{\upsilon_m c} \qquad \textbf{Equation 2.3}$$

where c is the BET constant, P is the equilibrium pressure, P° is the saturation pressure of the adsorbates at the temperature of adsorption, υ is the adsorbed gas quantity and υ_m is the adsorbed gas quantity of a monolayer [144,145].

2.5.4.2. Experimental

The surface areas of the synthesized materials were measures by N_2 adsorption isotherms at 77 K using a Micrometrics Gemini V apparatus. Before the measurement, the sample was heated at 200 °C in He for 2 h. The surface area was calculated by the BET method in equilibrium pressure range $0.05 < P/P° < 0.3$. From the desorption branch of the hysteresis loop using the BJH method, the pore size distribution was obtained, and the total pore volume was calculated from the maximum adsorption point at P/P°=0.99.

2.5.5. X-ray photoelectron spectroscopy

2.5.5.1. Experimental

XPS measurements on fresh ceria nanorod, PdO_x/CeO_2-NR, PdO_x/CeO_2-NR-Red, and Pd/ CeO_2-NR-Mt-Red were carried out at the Materials Science Beamline (**MSB**) at the Elettra synchrotron radiation source (Trieste, Italy). MSB, placed at the left end of the bending magnet 6.1, is equipped with a plane grating monochromator that provides light in the energy range of 21−1000 eV. The UHV end station, with a base pressure of 2 × 10−10 mbar, is equipped with a

SPECS PHOIBOS 150 hemispherical electron analyzer, low-energy electron diffraction optics, a dual-anode Mg/Al X-ray source, an ion gun, and a sample manipulator with a K-type thermocouple attached to the rear side of the sample. Photoelectrons emitted by C 1s, O 1s, Pd 3d and Ce 3d core levels were detected at normal emission geometry using photon energy of 630 eV impinging at 60°. Energy resolution of binding energies (**BE**) are reported after correction for charging using the aliphatic C 1s as a reference (BE 285.0 eV) [146]. Core level spectra were fitted with a Shirley background and Gaussian peak functions [147].

XPS measurements of PdO_x/CeO_2-NR used in BnOH oxidation, was performed measuring the core level spectra, using a VG Escalab MKII, equipped with a twin anode Al/Mg X-ray source (IPSE Laboratory of DTE, ENEA Casaccia, Rome, Italy). The XPS chamber is equipped with oil-free pumps to avoid carbon contaminations and the measurement were performed in a base vacuum of 3.0x10-9 mBar. The powder samples were pressed into pellets for the measurements and, a reference gold wire was placed on the pellet to account for possible sample charging. The used catalyst was previously tested in BnOH oxidation for 5 hours (conditions: 0.16 mmol substrate, 32 mg catalyst, 20 mL min^{-1} air flow, using EtOH as solvent at boiling point, i.e., 78 °C, under reflux). After the reaction, the catalyst was separated by centrifuge (10000 rpm, 20 min), washed 3 times with EtOH, and dried at room temperature. The fresh PdO_x/CeO_2-NR was also studied using abovementioned XPS facility. In addition, the XPS measurements of Pd/silica samples were carried out with the present XPS facility.

XPS measurements of PdO_x/CeO_2-NR-AA5.2 and PdO_x/CeO_2-NR-SA2 were carried out in an X-ray photoelectron spectrometer (home-made instrumentation Roma Tre University, Department of Science, Prof. Chiara Battocchio) with a dual-anode Mg/Al X-ray source, at Mg K-

alpha Photon Energy. Photoelectrons emitted by C1s, O1s, Pd3d and Ce3d core levels were detected. BEs are reported after correction for charging using the aliphatic C 1s as a reference (BE 285.0 eV) [146]. Core level spectra were fitted with a Shirley background and Gaussian peak functions [147].

2.6. Contribution of author in experimental sections

All of Pd/ceria catalysts are prepared by the author. In addition, the whole catalytic testing part (oxidation reactions, GC-MS analyses and related calculations), H_2-TPR reduction of PdO_x/CeO_2-NR, and nitrogen adsorption-desorption analysis of CeO_2-NR, PdO_x/CeO_2-NR and PdO_x/CeO_2-NR-Red are performed by the author.

Furthermore, the author participated in synthesizing of Pd/silica catalysts, as well as interpretation of the data from XRD, TPR, TEM, nitrogen adsorption-desorption analysis and XPS analysis of Pd/ceria samples, as: calculating ceria crystallite size and cell size, measuring the dimensions of CeO_2-NR, calculating the BET surface area, total pore volume and average pore diameter, of Pd/ceria samples, and finally, assigning the peaks observed in Pd/ceria samples' XPS spectra.

Chapter 3.

Results

3.1. Aerobic Oxidation of Benzyl Alcohol over PdO_x/CeO_2-NR and PdO_x/CeO_2-NR-Red

Ceria nanorod (**CeO_2-NR**) was prepared according to method described in *Section 2.2.1.1*. CeO_2-NR supported palladium oxide (**PdO_x/CeO_2-NR**) was prepared by wet impregnation method (*Section 2.2.1.2*) using palladium(II) nitrate dehydrate. This catalyst was tested in benzyl alcohol (**BnOH**) oxidation. Furthermore, PdO_x/CeO_2-NR was reduced with H_2 using Temperature-programmed reduction (**H_2-TPR**) equipment as explained in *Section 2.2.1.3*, and the reduced product (**PdO_x/CeO_2-NR-Red**) was also tested in BnOH oxidation.

3.1.1. Catalysts Characterization

3.1.1.1. XRD

The synthesized samples were studied by X-ray diffraction (**XRD**) and their patterns are shown in *Figure 3.1*. The CeO_2-NR showed the main reflections of pure cubic fluorite structure of CeO_2 (Joint Committee on Powder Diffraction Standards (**JCPDS**) card 81-0792) [148], with the average crystallite size of 23.3 nm and cubic cell size of 0.5419 nm (*Table 3.1*). The XRD pattern of the PdO_x/CeO_2-NR sample showed peaks assigned to CeO_2 having almost the same position, intensity, and full width at half maximum (**FWHM**) of CeO_2-NR, indicating no effect of Pd-loading on the particle size and on the crystal structure of CeO_2 (*Table 3.1*). No peaks of PdO phase were observed, suggesting that PdO is highly dispersed or that the PdO loading was below the detection limit of XRD. In addition, the most intense peak of PdO, expected to be very close to the

(200) reflection of CeO_2, may be hardly distinguishable. The XRD pattern of the PdO_x/CeO_2-NR-Red, reduced by H_2 up to 500 °C, was very similar to that of CeO_2, with no remarkable changes in crystal structure or particle size (*Table 3.1*), indicating that ceria was unaffected by the reduction process. No peaks of metallic palladium (Pd^0) were observed, suggesting that it was well dispersed or not detectable.[125,149].

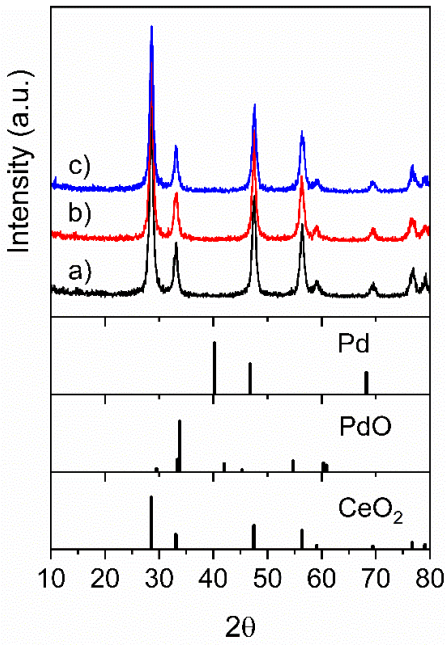

Figure 3.1. XRD patterns of: (**a**) CeO_2-NR, (**b**) PdO_x/CeO_2-NR, and (**c**) PdO_x/CeO_2-NR-Red.

Table 3.1. Textural properties and CeO_2 cell size of the samples.

Sample	Surface Area ($m^2\ g^{-1}$)	Total Pore Volume ($cm^3\ g^{-1}$)	Average Pore Diameter (nm)	CeO_2 Crystallite Size [1] (nm)	CeO_2 Cell Size, a [1] (Å)
CeO_2-NR	116	0.40	19	23.3	5.419
PdO_x/CeO_2-NR	88	0.30	16	21.8	5.419
PdO_x/CeO_2-NR-Red	93	0.32	12	22.4	5.414

[1] By XRD analysis.

3.1.1.2. H_2-TPR

A H_2-TPR experiment was performed to analyze the reducibility and the oxygen storing capacity of PdO_x/CeO_2-NR. The reduction was conducted up to 500 °C and maintained at the final temperature for 1 h, to avoid any sintering of ceria and of Pd at higher temperatures. H_2-TPR profiles of CeO_2-NR and PdO_x/CeO_2-NR are reported in *Figure 3.2*. The profile of the pure CeO_2-NR shows a broad reduction feature with onset at about 300 °C, increasing up to 500 °C, assigned to $Ce^{4+} \rightarrow Ce^{3+}$ reduction on the surface of ceria [150,151]

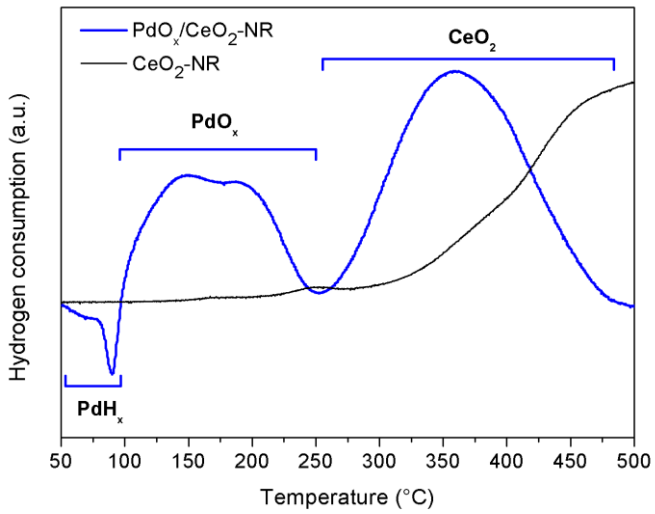

Figure 3.2. Temperature-programmed reduction (H_2-TPR) profiles of the samples: CeO_2-NR and PdO_x/CeO_2-NR.

TPR profile of PdO_x/CeO_2-NR showed several peaks: A negative peak at 90 °C, a broad peak in range 100–250 °C, with two maxima at 147 and 190 °C and a peak in temperature range 250–475 °C with a maximum at 360 °C. The negative peak at 90 °C is assigned to the hydrogen released by the decomposition of Pd hydride phase formed by the reduction of some palladium oxide at the early stage of the TPR measurement [115,152,153]; a similar negative peak was observed in previous works [152,154] and its position depended on preparation method and on the amount

of Pd supported on ceria [155]. The broad peak in the range 100–250 °C is assigned to reduction of palladium oxide to Pd^0 and is in agreement with the reduction temperature range (70–170 °C), observed on the TPR profile of a catalyst with similar Pd content [156]. The maximum at 190 °C might be due to reduction of less reducible PdO_x species in solid solution with CeO_2 lattice. The reduction peak at 360 °C is due to surface reduction of ceria that occurs at significantly lower temperature in comparison with the surface reduction observed at around 500 °C in TPR profile of pure CeO_2-NR. This shift to lower temperatures (roughly 140 °C) can be explained by the promoting effect of Pd on the surface reduction of ceria through the hydrogen spill-over [150]. The hydrogen spill-over phenomenon did not permit a correct quantitative evaluation of the extent of Pd and CeO_2 reduction from the TPR peak integration. The produced PdO_x/CeO_2-NR-Red from TPR was tested in BnOH oxidation reaction as well.

3.1.1.3. TEM

CeO_2-NR and PdO_x/CeO_2-NR were investigated by transmission electron microscope (**TEM**) and the images are shown in *Figure 3.3*. The CeO_2-NR sample showed a uniform well-developed structural anisotropy characteristic of the rod-like morphology with the average length of 110 nm and the average width of 9 nm (*Figure 3.3a*). In addition, 0.31 nm fringe distances assessed in CeO_2-NR and PdO_x/CeO_2-NR (*Figure 3.3b, d*) were in good agreement with d value of the ceria (111) plane and were the only crystalline planes observed. In some published researches, (100) and (110) exposed planes are reported for CeO_2-NR [120,125,157]. However, palladium supported on the (111) plane of CeO_2 seems to have a particular synergy with the support, showing higher activity and selectivity in methane combustion, CO oxidation, and BnOH oxidation [120,121,127].

As shown in *Figure 3.3c*, after palladium deposition, the average length of nanorod decreased up to 55 nm. The lack of evidence of palladium particles in the high-resolution transmission electron microscopy (**HRTEM**) images of PdO_x/CeO_2-NR, might be attributable to the high dispersion of palladium oxide species on the surface of the support, in agreement with XRD analysis.

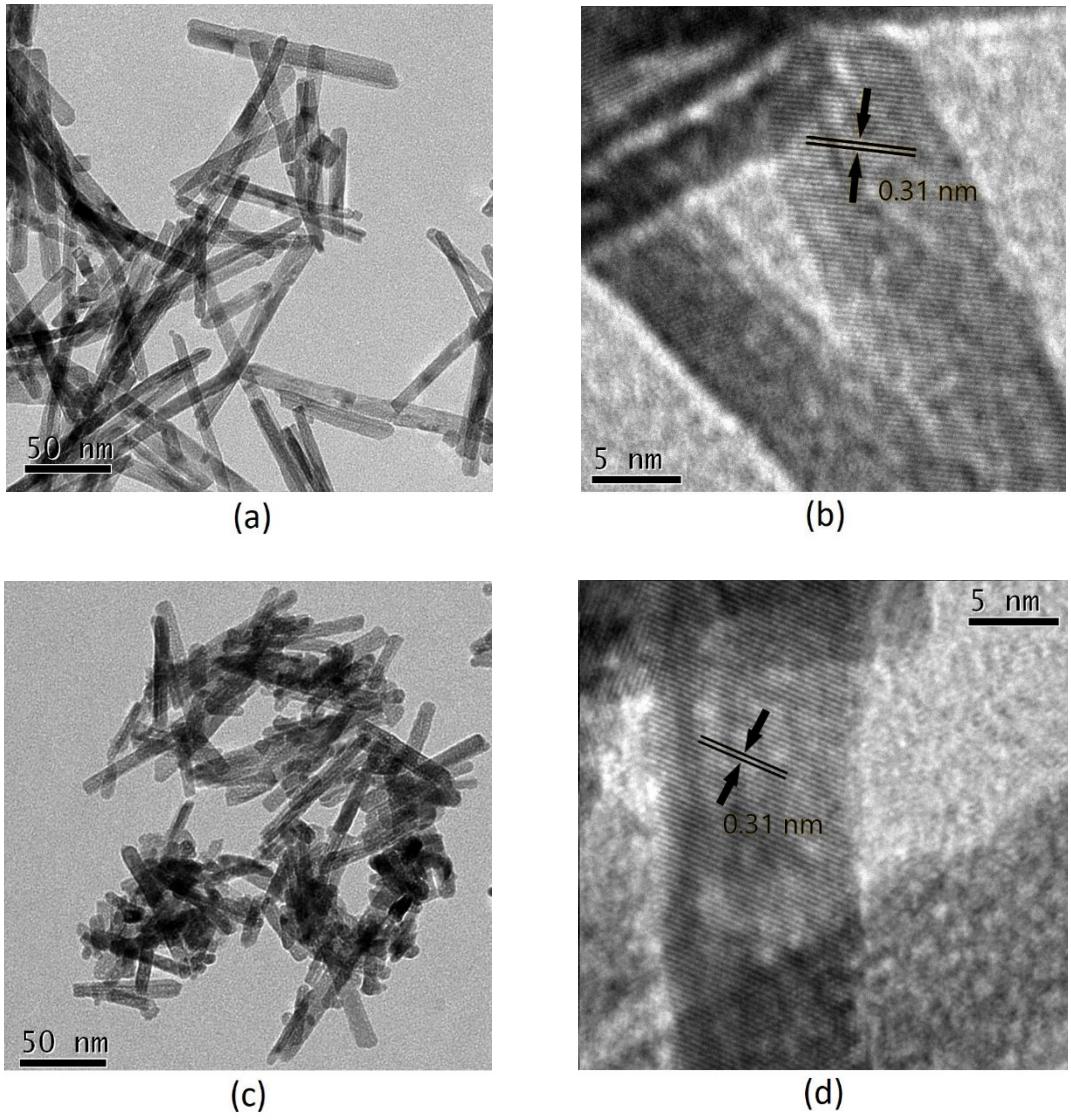

Figure 3.3. TEM and HRTEM images of: (**a**) and (**b**) CeO_2-NR; (**c**) and (**d**) PdO_x/CeO_2-NR.

3.1.1.4. Nitrogen Adsorption-desorption Analysis

Nitrogen adsorption-desorption measurements was utilized to estimate the Brunauer–Emmett–Teller (**BET**) surface areas of pure support CeO_2-NR, PdO_x/CeO_2-NR, and PdO_x/CeO_2-NR-Red catalysts (*Figure 3.4* and *Table 3.1*). The BET surface area of pure ceria nanorod was 116 m^2g^{-1}, comparable to the 106 m^2g^{-1} reported by Wang et al. [125] for ceria nanorod prepared by the same method. The surface area of PdO_x/CeO_2-NR was 88 m^2g^{-1}, in agreement with analogous Pd/CeO_2 system [128]. As expected, the palladium deposition caused a decrease of support surface area. The BET surface area of PdO_x/CeO_2-NR-Red was 93 m^2g^{-1}, slightly higher than the surface area of PdO_x/CeO_2-NR. This might be attributable to the decrease of the amount of palladium on the surface or to the change of Pd particle size.

Pure CeO_2-NR and PdO_x/CeO_2-NR catalysts showed N_2 adsorption–desorption curves V-Type, with H1-Type hysteresis loop for ceria-NR and H2-Type hysteresis loop for PdO_x/CeO_2-NR catalyst (International Union of Pure and Applied Chemistry (**IUPAC**) classification). All these features are characteristic of well-developed and uniform mesoporous morphology (*Figure 3.4a*) but denote that the palladium oxide addition changed the sample porosimetry. Barrett–Joyner–Halenda (**BJH**) pore-size distribution profiles (**PSD**), reported on *Figure 3.4b*, showed a pore distribution in the range 0–100 nm, centered at 40 nm for pure ceria, and narrower PSD profiles centered at about 15–20 nm for PdO_x/CeO_2-NR, due to mesopores with very uniform dimension. The average pore dimension was 19 nm for pure CeO_2-NR and 16 nm for the PdO_x/CeO_2-NR sample (*Table 3.1*), suggesting that the addition of palladium caused a decrease of both pore volume and pore size of the support. The hysteresis of the PdO_x/CeO_2-NR-Red sample is at a lower relative pressure P/P^0. After the reduction of the catalyst, a further pore size decrease was observed.

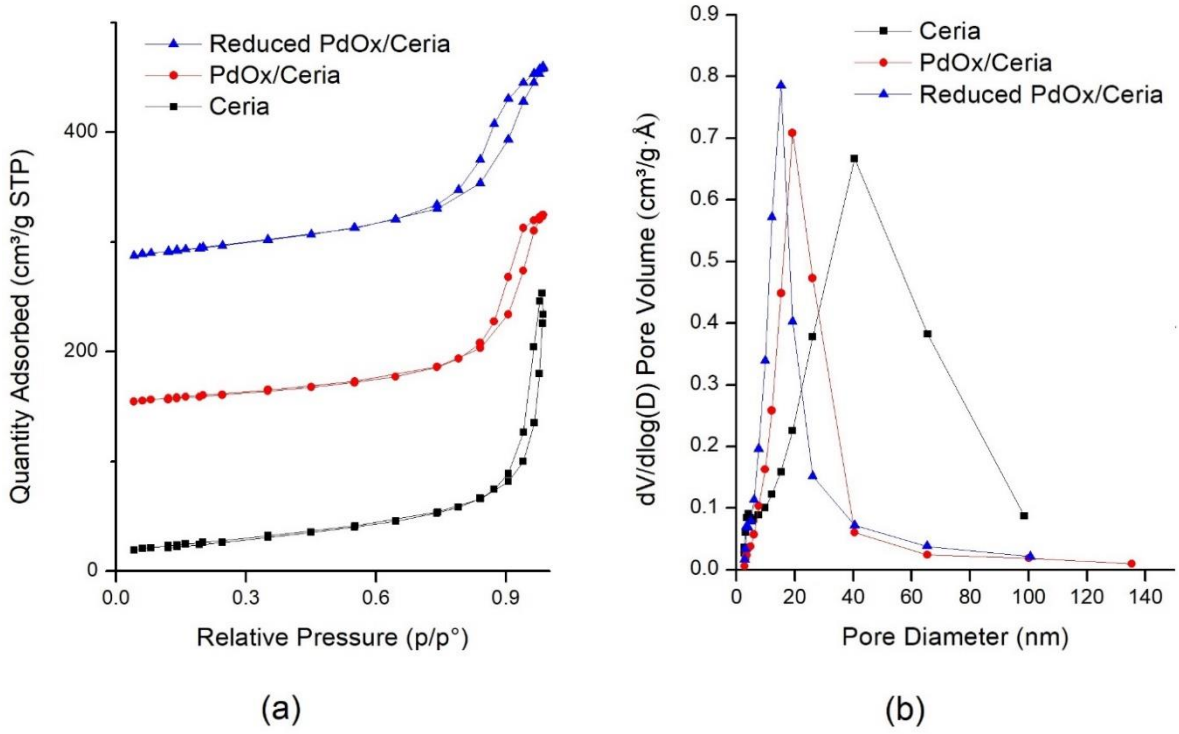

Figure 3.4. Nitrogen adsorption-desorption analysis: (**a**) Nitrogen adsorption and desorption isotherms as a function of P/P°; (**b**) pore-size distributions (PSD).

3.1.1.5. XPS

To have a deeper insight of the electronic and chemical properties at the surface of the Pd/Ce-based catalysts, X-ray photoelectron spectroscopy (**XPS**) studies have been performed (Elettra synchrotron radiation source Trieste, Italy). Ce 3d spectra of CeO_2-NR, PdO_x/CeO_2-NR, and PdO_x/CeO_2-NR-Red are reported in *Figure 3.5*. By following a peak-fitting procedure, five spin orbit pairs related to Ce 3d were individuated, and the resulting components were associated with Ce^{3+} and Ce^{4+} ions by comparison with literature data [158,159]. The amount of oxygen vacancy of ceria is correlated to the amount of Ce^{3+} [120]. From the peak areas, Ce^{3+}/Ce^{4+} ratios were calculated, and the results are reported in *Table 3.2*. The Ce^{3+}/Ce^{4+} ratio for PdO_x/CeO_2-NR is

0.24, equal to that of CeO_2-NR, and in good agreement with the literature data about calcined CeO_2-NR [122], indicating no effect of Pd loading on the surface Ce^{3+} concentration. Unexpectedly, the Ce^{3+}/Ce^{4+} ratio of the reduced catalyst was 0.22, slightly lower than those of pure ceria and PdO_x/CeO_2-NR, but in agreement with literature related to reduced CeO_2-NR catalysts [19].

Photoelectron profiles of PdO_x/CeO_2-NR and PdO_x/CeO_2-NR-Red are shown in *Figure 3.6*, and the detailed atomic percent values of observed Pd species are reported in *Table 3.2*. The most intense signal in Pd 3d spectrum of PdO_x/CeO_2-NR has the Pd $3d_{5/2}$ component at 337.76 eV BE, a binding energy value indicative for oxidized palladium (PdO_x, $x > 1$); the less intense component at lower BE values (Pd $3d_{5/2}$ BE = 335.58 eV) is associated with 10% of PdO [159].

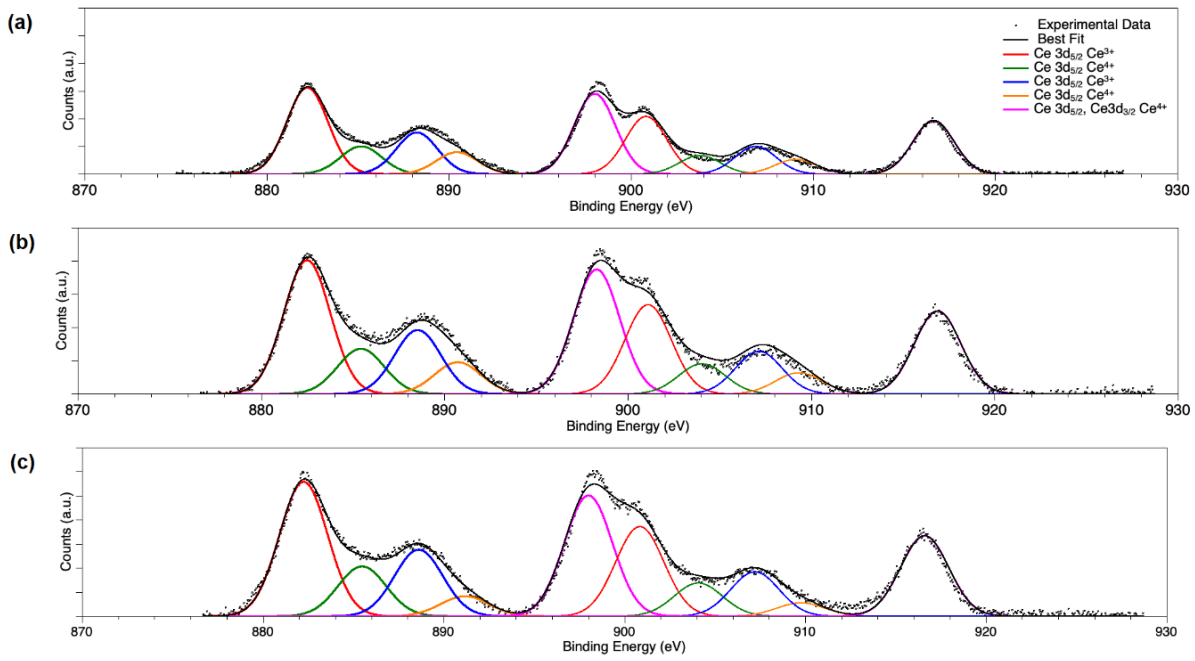

Figure 3.5. XPS spectra of Ce 3d region for the samples: (**a**) CeO_2-NR, (**b**) PdO_x/CeO_2-NR, and (**c**) PdO_x/CeO_2-NR-Red. All Ce $3d_{5/2}$ spin-orbit components, as well as the Ce $3d_{3/2}$ peaks at higher BE values (diagnostic for the presence of Ce^{4+} ions), appear as bold lines in the spectra.

In PdO_x/CeO_2-NR-Red XPS spectra, a Pd 3d component at low BE (Pd $3d_{5/2}$ BE = 334.67 eV) is indicative of metallic palladium (Pd^0) [159], whereas the signal around 337.76 eV BE is still observed. According to *Table 3.2*, 63.5% of Pd in the reduced catalyst contributes to this component. This large amount of oxidized palladium can be interpreted as the result of re-oxidation of surface Pd when exposed to air after H_2-TPR. An alternative interpretation of the high-BE Pd 3d signal is the formation of a Pd – O − Ce structure, similar to the $Pd_xCe_{1-x}O_{2-\delta}$ solid-solution phase [160,161]; in this structure, Pd would act as an electron-donor toward CeO_2.

Furthermore, it is observed in *Table 3.2* that the atomic percentage of Pd decreased from 0.13% to 0.06% after reduction. This might be due to Pd diffusion into the bulk of the ceria support or to Pd sintering during the reduction process. This result is also in agreement with the higher BET surface area of PdO_x/CeO_2-NR-Red in comparison with the PdO_x/CeO_2-NR.

Table 3.2. Atomic percent values of palladium species in PdO_x/CeO_2-NR and PdO_x/CeO_2-NR-Red, collected from XPS study.

Catalyst	Pd^0 %	PdO %	PdO_x (x > 1) %	Pd %/(Pd + Ce)	Ce^{3+}/Ce^{4+}
CeO_2-NR	-	-	-	-	0.24
PdO_x/CeO_2-NR	0	10	90	0.13	0.24
PdO_x/CeO_2-NR-Red	36.5	0	63.5	0.06	0.22

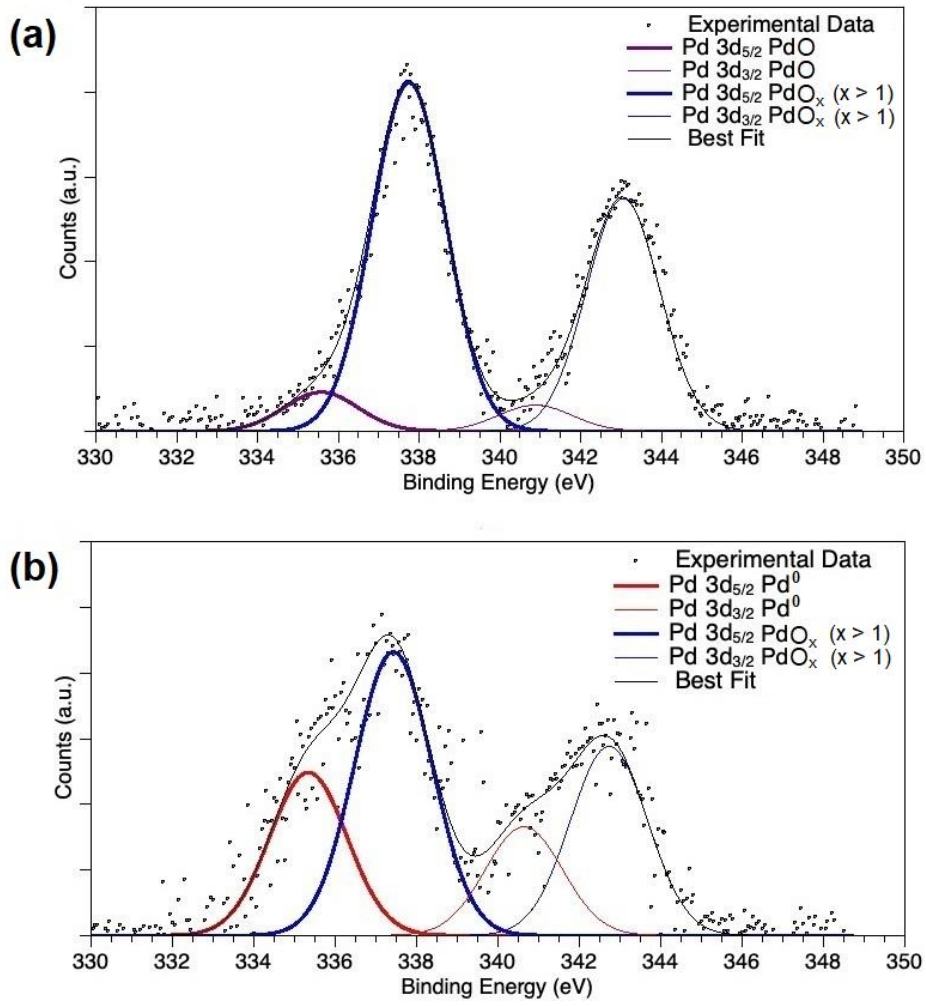

Figure 3.6. XPS spectra of Pd 3d region for (**a**) PdO_x/CeO_2-NR and (**b**) PdO_x/CeO_2-NR-Red.

3.1.2. Catalytic Activity

The catalytic activity in BnOH oxidation was investigated using either PdO_x/CeO_2-NR or PdO_x/CeO_2-NR-Red catalyst. Oxidation of BnOH was performed using a round-bottom three-neck flask equipped with reflux condenser, gas inlet, and thermometer. *Table 3.3* shows the reaction conditions of BnOH oxidation as well as the BnOH conversions and PhCHO selectivities measured by gas chromatography-mass spectrometry (**GC-MS**) using cyclooctanone as internal standard. Air or oxygen was used as oxidant.

Table 3.3. Aerobic oxidation of BnOH to PhCHO: reaction parameters and results.

Exp.	Catalyst	Catalyst Mass (mg)	Solvent	T (°C)	BnOH Conversion (%) [1]	PhCHO Selectivity (%) [1]
1	CeO_2-NR	32	toluene	111	0	-
2	CeO_2-NR	32	EtOH	78	0	-
3	PdO_x/CeO_2-NR	32	toluene	50	9	100
4	PdO_x/CeO_2-NR	32	toluene	65	15	100
5	PdO_x/CeO_2-NR	32	toluene	100	29	100
6	PdO_x/CeO_2-NR	32	toluene	111	35	100
7	PdO_x/CeO_2-NR	32	AcCN	65	6	100
8	PdO_x/CeO_2-NR	32	AcCN	82	14	100
9	PdO_x/CeO_2-NR	32	EtOH	65	50	>97
10	PdO_x/CeO_2-NR	32	EtOH	78	93	96
10(II) [2]	PdO_x/CeO_2-NR	32	EtOH	78	73	96
10(III) [3]	PdO_x/CeO_2-NR	32	EtOH	78	54	97
11	PdO_x/CeO_2-NR	32	MeOH	65	41	>97
12	PdO_x/CeO_2-NR	32	THF	66	<3	-
13	PdO_x/CeO_2-NR-Red	32	toluene	111	25	100
14	PdO_x/CeO_2-NR-Red	32	EtOH	78	13	100
15 [4]	PdO_x/CeO_2-NR	16	EtOH	78	28	>97

[1] Measured by GC-MS after 5 h of oxidation with 20 mL min^{-1} air flow; [2] second round of recyclability test; [3] third round of recyclability test; [4] leaching test: The catalyst was removed after 45 min.

In preliminary catalytic tests using oxygen as oxidant, the BnOH conversions were similar to those obtained using air. Therefore, all the subsequent reactions were performed in air. The effects of temperature, solvent nature, and Pd oxidation state were studied. CeO_2-NR showed no catalytic activity for BnOH oxidation when either toluene or ethanol (**EtOH**) were utilized as solvent (*Table 3.3*, experiments 1 and 2, respectively), proving that the ceria support was not active, similar to the observation by Xin et al., for the aerobic BnOH oxidation catalyzed by pure ceria [127]. In all experiments, PhCHO was the only major product and the selectivity of PhCHO was 96% or more.

3.1.2.1. Effect of Temperature and Solvent

The BnOH oxidation was first performed using PdO_x/CeO_2-NR in toluene at 50 °C and air at a flow of 20 mL/min. The conversion was very low, reaching 9.4% after five hours of reaction, even with a reaction selectivity of 100%. To obtain better conversions, the reaction was tested at higher temperatures (65 and 100 °C) and up to the boiling point of toluene (111 °C). As expected, the conversion increased up to 35% (*Table 3.3*, experiment 6), maintaining 100% selectivity.

Due to the low BnOH conversion in toluene (9%–35%), other solvents were utilized, namely acetonitrile (**AcCN**), EtOH, methanol (**MeOH**), and tetrahydrofuran (**THF**). The oxidation of BnOH, using different solvents at nearly 65 °C after 5 h, is presented in *Table 3.3*. The highest conversions were achieved using EtOH and MeOH as solvents (50% and 41%, respectively). In the same conditions, the BnOH conversions using either toluene or AcCN were 14% and 6%, respectively.

The best result in BnOH oxidation by PdO_x/CeO_2-NR was achieved utilizing the protic EtOH at boiling point (78 °C). In this condition, 93% conversion and 96% selectivity were achieved (*Table 3.3*, experiment 10). This was significantly larger than the results achieved using toluene at 111 °C (35%) or AcCN at 82 °C (14%) (*Table 3.3*, experiments 6 and 8, respectively). In the experiments with EtOH, benzyl ester is detected as a secondary product, probably derived from benzoic acid due to the presence of alcoholic solvent.

The 93% BnOH conversion and 96% PhCHO selectivity achieved by utilizing PdO_x/CeO_2-NR (with (111) exposed plane of CeO_2-NR) in EtOH are slightly higher than those acquired by Wang et al. (84.6% BnOH conversion, 92.8% PhCHO selectivity) [121], in the reaction catalyzed by

palladium oxide supported on truncated octahedral ceria with (111) and (100) exposed plane, at almost the same temperature and higher catalyst/substrate ratio. Wang et al. also prepared and used cubic CeO_2 with (100) exposed plane as support for palladium oxide, which led to significantly lower BnOH conversion (34.0%), suggesting the important role of the ceria morphology and the synergy between palladium and the CeO_2 (111) plane in the catalytic activity. On the other hand, the result achieved by PdO_x/CeO_2-NR-Red (*Table 3.3*, experiment 13) is almost similar to that obtained by Xin et al. (26.60% BnOH conversion) using reduced palladium supported on CeO_2-NR [127].

Looking at the proticity, polarity, and boiling point of the utilized solvents (*Table 3.4*), the collected data might suggest that the polarity of the solvent has a negative effect on the catalytic performance of PdO_x/CeO_2-NR for BnOH oxidation, given the different conversions obtained using toluene, a non-polar solvent, and AcCN, a polar one. This hypothesis can be strengthened by the observation that substrate conversion using EtOH is higher than the more polar MeOH solvent, in the same conditions.

Table 3.4. Properties of solvents used in BnOH oxidation reactions.

Solvent	Proticity	Dielectric Constant	Boiling Point (°C)
toluene	aprotic	2.4	111
THF	aprotic	7.52	66
AcCN	aprotic	37.5	82
EtOH	protic	24.5	78
MeOH	protic	32.7	65

On the other hand, it seems that the proticity of the solvent plays an important role in increasing the BnOH conversion, since the best results at 65 °C were achieved by using the protic and polar EtOH and MeOH solvents. Thus, it can be hypothesized that solvent properties may

have an influence on the reaction mechanism and, if the solvent is both polar and protic, the effect of proticity is dominating. In similar experiments of BnOH oxidation, when Al-Saeedi et al. used Cu oxide nanoparticles as catalyst [100], the more polar dimethyl sulfoxide (**DMSO**) solvent gave the better conversion. However, only aprotic solvents (acetone, AcCN, dimethylformamide (**DMF**), and DMSO) were utilized in that research work.

3.1.2.2. Effect of Pd Oxidation State

To study the effect of the oxidation state of Pd on the aerobic BnOH oxidation, the catalyst reduced by H_2-TPR was utilized, with toluene or EtOH as solvent at their boiling points (*Table 3.3*, experiments 13 and 14, respectively). To compare the catalytic activity of PdO_x/CeO_2-NR and PdO_x/CeO_2-NR-Red, in toluene and EtOH, the conversions of BnOH are reported in *Figure 3.7*. When toluene solvent was used, the catalytic activity of PdO_x/CeO_2-NR-Red was lower than that of PdO_x/CeO_2-NR (25% versus 35%). This result might be attributable to a decrease of Pd amount on the surface after reduction process, in agreement with XPS results. On the other hand, when EtOH solvent was used, the PdO_x/CeO_2-NR-Red showed a BnOH conversion of 13%, considerably less than that of the PdO_x/CeO_2-NR (93%). Consequently, using reduced palladium, the polarity and/or proticity of the solvent look detrimental to the catalytic activity. This is in line with literature data, in which these kinds of reactions are generally performed with aprotic apolar solvents such as toluene or xylene [101].

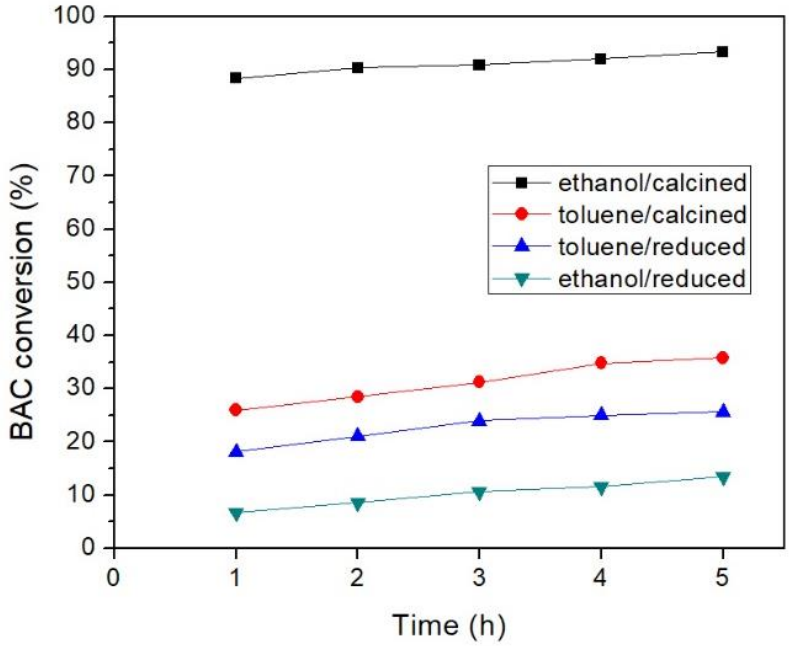

Figure 3.7. BnOH conversion using PdO_x/CeO_2-NR or PdO_x/CeO_2-NR-Red catalysts, as a function of time. Reaction conditions: BnOH 0.16 mmol, catalyst mass 32 mg, reaction temperature 78 °C for ethanol and 111 °C for toluene.

3.1.3. Mechanistic Aspects of BnOH Aerobic Oxidation, Catalyzed with PdO_x/CeO_2-NR

The mechanism of the alcohols oxidation over Pd^0 has been extensively studied [3,99-101] (reported in *Section 1.3.1* and depicted in *Scheme 1.10*). It foresees oxygen chemisorption on palladium surface, assisted homolytic cleavage of the O — H bond of BnOH, and formation of an alkoxide-palladium bond. The subsequent hydrogen abstraction by a near Pd^0 [3] (*Scheme 1.10*), permits the release of the PhCHO and of a molecule of water.

The different behavior of PdO_x/CeO_2-NR, when used in toluene or EtOH, strengthens the hypothesis that the mechanism of BnOH oxidation with this catalyst, might be different from that described by Chan-Thaw et al.[3]. A model is proposed for BnOH oxidation by PdO_x/CeO_2-NR,

in protic solvents (*Scheme 3.1*). XPS data stated that no Pd^0 is present on the surface (*Table 3.2* and *Figure 3.6*); thus, it cannot catalyze the displacement of the hydrogen from the alkoxide intermediate. Furthermore, after the oxidation reaction, XPS analysis of used PdO_x/CeO_2-NR showed a change in the PdO/PdO_x ratio in favor of the less oxidized species (*Table 3.5* and *Figure 3.8*; performed at IPSE Laboratory of DTE, ENEA Casaccia, Rome, Italy). All these evidences, together with the high BnOH conversion obtained with the polar protic EtOH as solvent (*Table 3.3* experiment 10), may be explained with an heterolytic mechanism in which PdO_x/CeO_2-NR participates in a redox cycle [162]. Since the reaction in the highly polar AcCN gave low conversion (*Table 3.3*, experiment 8), the protonation of PdO_x by a protic solvent seems kinetically crucial (*Scheme 3.1*). The more electrophilic protonated metal oxide (II in *Scheme 3.1*) may react with BnOH, producing the addition product III which, after proton release, should give the alkoxide–palladium IV. The reaction may then proceed by a proton abstraction assisted either by another PdO_x, or by the ceria surface oxygen [127], and finally, the elimination of water and PhCHO by redox participation of the metal catalyst. The reduced catalyst V is then re-oxidized by molecular oxygen. Further study should be done to confirm this hypothesis.

Table 3.5. Binding Energy, Full Width Half Maximum and atomic percent values of $Pd3d_{5/2}$ components for the fresh and used PdO_x/CeO_2-NR samples.

Sample	BE (eV)	FWHM (eV)	Assignment	Atomic %
PdO_x/CeO_2-NR	335.79	2.51	PdO	20.1
	337.76	2.51	PdO_x (x>1)	79.9
Used PdO_x/CeO_2-NR	335.82	2.57	PdO	42.7
	337.77	2.57	PdO_x(x>1)	57.3

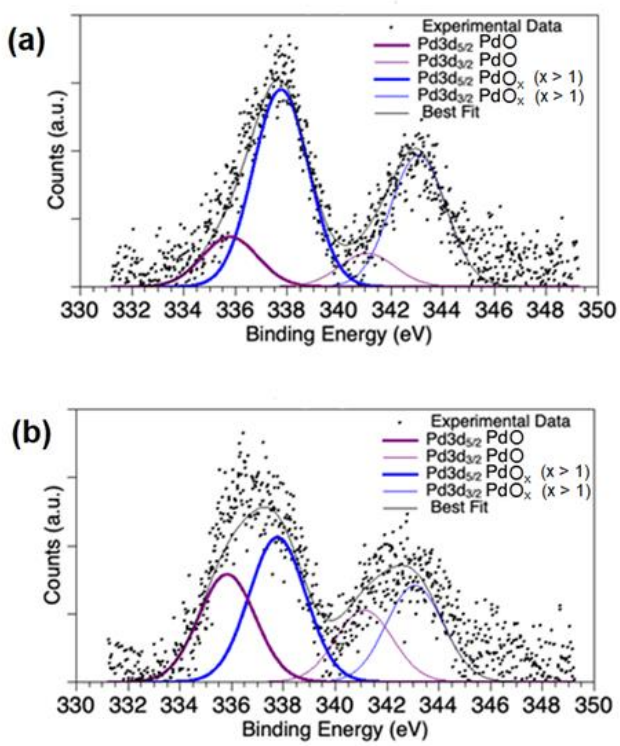

Figure 3.8. XPS spectra of Pd 3d region for (**a**) fresh PdO_x/CeO_2-NR, and (**b**) used PdO_x/CeO_2-NR. BnOH oxidation conditions: 0.16 mmol BnOH, 32 mg catalyst, 20 mL/min air flow, using EtOH as solvent at boiling point, under reflux.

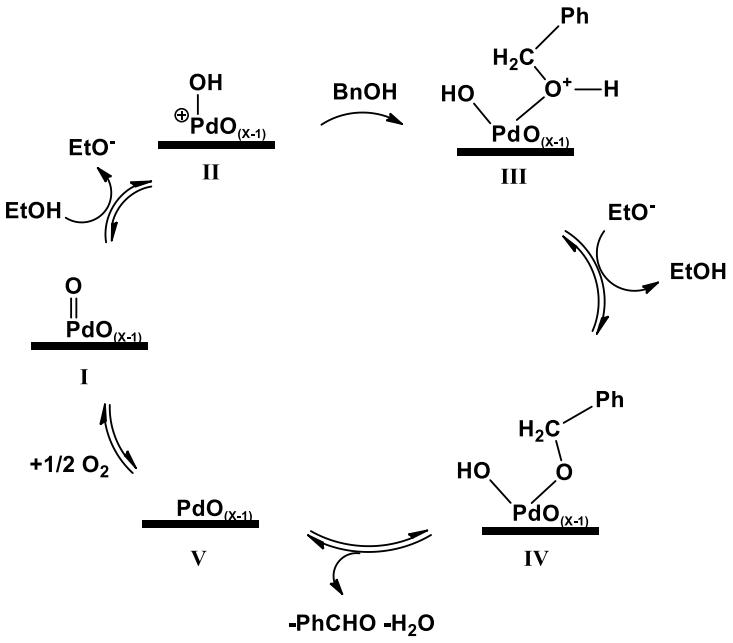

Scheme 3.1. Suggested mechanism of BnOH oxidation catalyzed by PdO_x supported on CeO_2-NR in EtOH solvent. The thick lines represent the CeO_2-NR support.

3.1.4. Recyclability Tests

The recyclability of PdO_x/CeO_2-NR was studied by recovering and reusing the catalyst used in experiment 10 of *Table 3.3*, for two more rounds of reaction, without any pre-treatment. BnOH conversion decreased in the second and third round to 73% and 54%, respectively, but the selectivity of PhCHO remained almost constant (*Figure 3.9* and *Table 3.3* experiments 10(II) and 10(III) respectively). Calcining the catalyst after each catalytic round in EtOH might fully recover the catalytic performances.

3.1.5. Leaching Test

To assess any possible leaching of palladium from the CeO_2-NR support during the BnOH oxidation, a leaching test was conducted (*Table 3.3*, experiment 15). The catalyst was removed after 45 min by centrifugation and the reaction was carried on with the remaining ethanolic solution. After the catalyst was removed, no progress was observed in oxidation reaction because the BnOH conversion and PhCHO selectivity values remained constant afterward. Thus, no considerable palladium leaching occurred during the reaction.

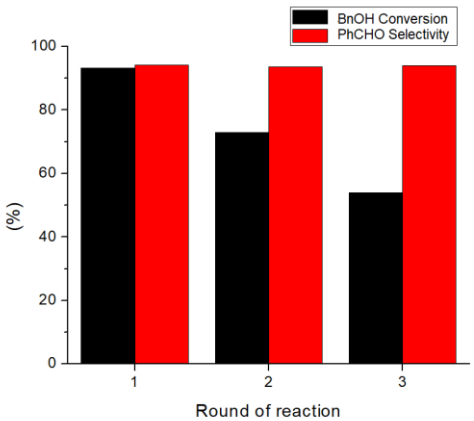

Figure 3.9. Recyclability test of PdO_x/CeO_2-NR. BnOH oxidation conditions: 0.16 mmol BnOH, 32 mg catalyst, 20 mL/min air flow, using EtOH as solvent at boiling point, under reflux

3.2. BnOH oxidation with Pd/CeO_2-NR-Me-Red

The catalytic oxidation of BnOH in toluene or EtOH was performed using Pd/CeO_2-NR-Me-Red. The reaction conditions and results are reported in *Table 3.6*. XPS analysis of Pd/CeO_2-NR-Me-Red showed the presence of Pd^0, PdO and PdO_x on the catalyst surface (*Figure 3.10* and *Table 3.7*). According to the results of XPS, the Pd reduction with TPR was more efficient than Pd reduction with MeOH during palladium wet impregnation, given that 36.5% Pd^0 is present in Pd/CeO_2-NR-Red (*Table 3.5*), while only 4.6% Pd^0 in Pd/CeO_2-NR-Me-Red. The results of BnOH oxidation with Pd/CeO_2-NR-Me-Red showed that this catalyst, similar to Pd/CeO_2-NR-Red, works better in toluene than in EtOH, suggesting that reaction mechanism with Pd/CeO_2-NR-Me-Red is similar to that with Pd/CeO_2-NR-Red. Considering that the conversion of BnOH to PhCHO grows in parallel with the presence of PdO_x, the higher conversion in comparison with Pd/CeO_2-NR-Red might suppose that here PdO_x could be important in enhancing the yield of the reaction while the presence of the Pd^0, even in low concentration, directs the mechanism of the oxidation.

It is noteworthy that according to XPS spectra, there were probably calcium compounds impurity in the Pd/CeO_2-NR-Me-Red sample. This was unexpected since the catalyst was washed with plenty of water after the preparation. The source of this impurity is unknown to the author.

Table 3.6. BnOH oxidation catalyzed by Pd/CeO_2-NR-Me-Red; conditions: 32 mg catalyst, 0.16 mmol BnOH, 20 mL min^{-1} O_2.

solvent	Temperature	Conversion	Selectivity
Toluene	111	43%	~100%
EtOH	78	3%	~100%

Table 3.7. Atomic percentage values of palladium species on Pd/CeO_2-NR-Me-Red, collected from XPS data.

BE	Assignment	Atomic Percentage
334.01	Pd^0	4.6
335.78	PdO	21.5
337.82	PdO_x	73.9

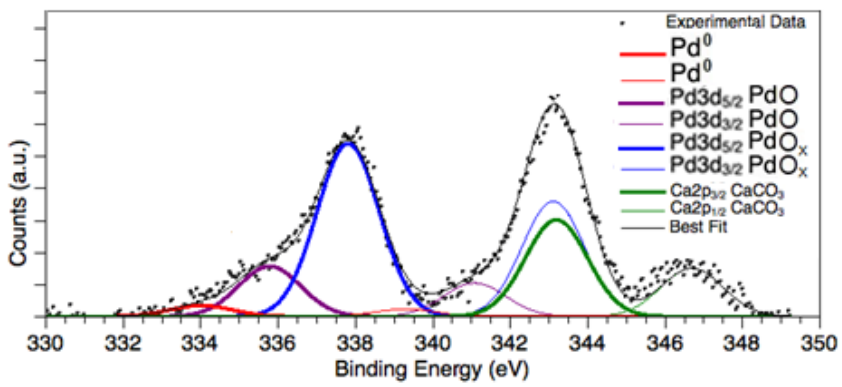

Figure 3.10. XPS spectra of Pd 3d region for Pd/CeO_2-NR-Me-Red.

3.3. BnOH Oxidation with Pd/CeO_2-NR-Hz-Red

Palladium/ceria catalysts prepared by reducing the palladium with hydrazine after wet impregnation was tested for BnOH oxidation in toluene, since we observed that the reduced samples' activity in EtOH was poor. The reaction conditions and results are summarized in *Table 3.8*. Increasing the weight of catalyst from 16 mg to 32 mg and 48 mg resulted in higher BnOH conversion, maintaining ~100% selectivity towards PhCHO. Among all reduced Pd/ceria catalysts, Pd/CeO_2-NR-Hz-Red offered the highest BnOH conversion. Further investigation is

required to justify the reason of the superior catalytic activity of Pd/CeO_2-NR-Hz-Red compared to Pd/CeO_2-NR-Red and Pd/CeO_2-NR-Me-Red.

Table 3.8. Oxidation of BnOH catalyzed by Pd/CeO_2-NR-Hz-Red; conditions: 0.16 mmol BnOH in toluene (10 mL), at 111 °C, 20 mL min^{-1} air

Catalyst Amount	Conversion	Selectivity
16 mg	30	~100%
32 mg	78	~100%
48 mg	86	~100%

3.4. BnOH oxidation catalyzed by Palladium Oxide Supported on CeO_2-NR by Palladium Nitrate Commercial Solution

Utilizing palladium nitrate commercial solutions from Alfa Aesar (**AA**) or Sigma Aldrich (**SA**), four catalysts were prepared (*Table 2.1*) and tested in BnOH aerobic selective oxidation. *Table 3.9* shows the results of the oxidation reactions. Unexpectedly, these samples showed low activity in EtOH, and good activity in toluene. These outcomes were opposite to the results achieved by PdO_x/CeO_2-NR (*Table 3*.3), showing that the mechanism hypothesized for BnOH oxidation in EtOH by PdO_x/CeO_2-NR, cannot be entitled to the reactions catalyzed by the samples prepared with commercial palladium nitrate solutions. To better understand the reason of this contradiction, two of the samples were subjected to XPS analysis and the results are shown in *Figure 3*.11. The XPS analysis of PdO_x/CeO_2-NR-AA5.2 and PdO_x/CeO_2-NR-SA2 showed that there was only one Pd species on the surface of ceria, with Pd $3d_{5/2}$ component at almost 338 eV BE, similar

to the PdO_x component observed in PdO_x/CeO_2-NR (*Figure 3.6)*. Unlike PdO_x/CeO_2-NR, no PdO was detected in the samples prepared by commercial palladium nitrate solutions. This might suggest that the presence of PdO is necessary for the mechanism described in *Scheme 3.1* for BnOH oxidation in EtOH by PdO_x/CeO_2-NR. The XPS of PdO_x/CeO_2-NR-AA5.2 and PdO_x/CeO_2-NR-SA2 showed also the presence of Na or Ca impurities in both samples (not reported in the *Figure 3.11*). These impurities might affect the catalyst preparation and the final oxidation state of the palladium.

Among the samples prepared by commercial solutions, the best result was achieved using PdO_x/CeO_2-NR-SA2 in toluene (95% BnOH conversion with almost 100% PhCHO selectivity). This was also the best result acquired in toluene among all the prepared catalysts in this study.

Table 3.9. BnOH oxidation by palladium oxide supported on CeO_2-NR, prepared with palladium nitrate commercial solution; conditions: 0.16 mmol BnOH, 32 mg catalyst, 20 mL min^{-1} air.

Catalysts	Solvent	Temperature °C	BnOH Conversion	PhCHO Selectivity
PdO_x/CeO_2-NR-AA2	MeOH	64	7	~100
	EtOH	78	8	~100
	toluene	111	46	~100
PdO_x/CeO_2-NR-AA4	EtOH	78	37	92
	toluene	111	96	60
PdO_x/CeO_2-NR-AA5.2	toluene	111	67	80
PdO_x/CeO_2-NR-SA2	EtOH	78	6	81
	toluene	111	95	~100

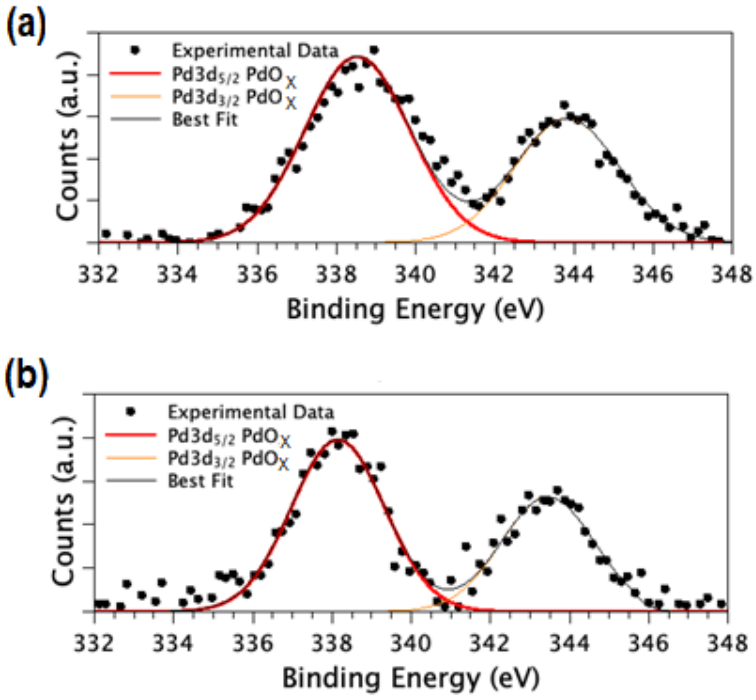

Figure 3.11. XPS spectra of PdO_x/CeO_2-NR-AA5.2 (**a**), and PdO_x/CeO_2-NR-SA2 (**b**).

3.5. Solvent-Free Aerobic Oxidation of Benzylic alcohols

Omitting the usage of solvent can be an attractive idea due to cost and toxicity of many solvents. Aerobic solvent free oxidation of BnOH and substituted benzylic alcohols has been the subject of many research works. For instance, as discussed in *Section 1.3.2.5*, Xin et al., observed that in similar conditions, benzylic alcohols with electron-donating groups (**EDG**) on the aromatic ring were oxidized less than BnOH as well as the benzylic alcohol with electron-withdrawing groups (**EWG**) substituted on the aromatic ring (*Table 1.7*) [127]. Specifically speaking, substitution of methyl (**Me**) and methoxy (**MeO**) on BnOH led to less conversion (18.63% for 4-MeBnOH, 11.12% for 4-MeOBnOH, and 26.60% for BnOH), but addition of nitro NO_2 group resulted in slightly higher conversion, (27.13% of 4-NO_2BnOH was oxidized). This result was

contradictory to that observed in the work of Xu et al., for the oxidation of similar substrates catalyzed by Pd supported on mesoporous carbon, using toluene as solvent [90] (see *Section 3.1.3.2*). Xu et al., observed that addition of EWG (nitro group) decreased the alcohol conversion, while EDG resulted in higher conversion of alcohol compared to BnOH (*Table 1.3*). These opposite results in the literature were a further motive to study the oxidation of substituted benzylic alcohols by the Pd/ceria system prepared by the author.

Oxidation of BnOH and four of its derivatives was performed in solvent-free condition, catalyzed by PdO_x/CeO_2-NR-SA2. Results are reported in *Table 3.10*. BnOH conversion after 5 h was 33% with 99% PhCHO as product. Presence of EDG on BnOH resulted in a general increase in the conversion of the substrates, but decreased the selectivity towards the aldehyde products. In case of 4-MeBnOH and 4-MeOBnOH, the conversion raised to 52% and 54% respectively, with 88% and 83% selectivity towards the corresponding aldehyde, i.e., 4-methylbenzaldehyde and 4-methoxybenzaldehyde respectively. On the contrary, in the oxidation of 4-PhOBnOH a decrease to 13% conversion and 99% selectivity towards 4-phenoxybenzaldehyde, was obtained. This last result could be attributable to the presence of a second PhO- group that could interfere with the interaction of the benzylic alcohol with the catalyst. Testing the BnOH derivatives with EWG placed on benzylic ring led to no conversion of substrates, as observed for 4-NO_2BnOH and 4-MeOCOBnOH compared to BnOH. These results were in-line with the reports of Xu et al., [90], but opposite to the results of Xin et al., [127] research work. This can be explained by the reaction mechanism.

In the mechanism proposed by Xin et al., after the cleavage of O — H bond, the cleavage of C — H bond occurs, passing through a transition state in which, H atom of C — H bond will

migrate to O atom of C — O bond [127]. In this step, which is the rate-determining step, there will be a partial negative charge on the benzylic carbon that can be stabilized if the benzylic ring contains an EWG. In contrast, EDG destabilize the aforementioned partially charged transition state. This can explain the lower conversion of EDG-containing substrates compared to BnOH and the EWG-containing substrate, achieved by Xin et al., [127]. On the other hand, Xu et al., suggest another mechanism in which, first the alcohol is activated on Pd, leading to formation of an alkoxide, and then the dehydrogenation of alkoxide occurs through a carbocation-type transition state (the rate-determining step), following by transformation to aldehyde [90]. Xu et al. explained the high conversion of EDG-containing substrates stating that EDG facilitate the formation of the carbocation in the rate determining transition state; whereas, they attributed the lower conversion of 4-NO_2BnOH to the hindering effect of EWG [90].

Table 3.10. Solvent-free oxidation of BnOH derivatives by PdO_x/CeO_2-NR-SA2; conditions: 10 mmol substrate, 10 mg catalyst, at 100 °C, 10 mL min^{-1} air.

Substrate	Conversion	Aldehyde Selectivity	Aldehyde Yield
BnOH	33%	~100%	34%
4-MeBnOH	52%	88%	46%
4-MeOBnOH	54%	83%	45%
4-PhOBnOH	13%	~100	13%
4-NO_2BnOH	0	N/A	N/A
4-COOMeBnOH	0	N/A	N/A

Considering the opposite behavior of catalysts prepared by Xin et al., [127], and Xu et al., [90], and the similar behavior of PdO_x/CeO_2-NR-SA2 to the catalyst of Xu et al., a mechanism is proposed (*Scheme 3.2.*) for the solvent-free oxidation of BnOH catalyzed by PdO_x/CeO_2-NR-SA2, including a primary cleavage of O — H bond on the metal followed by the cleavage of C — H bond through the carbocation-type transition state which can be boosted if the aromatic ring of the alcohol substrate is substituted by EDG.

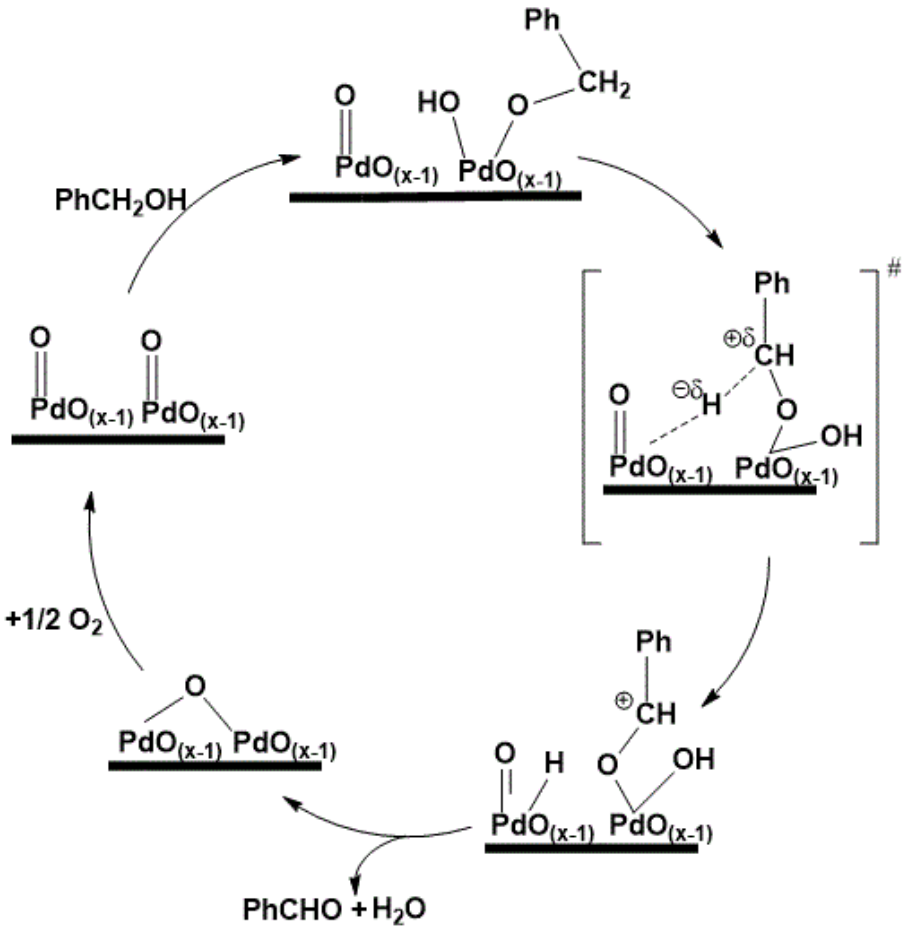

Scheme 3.2. Proposed mechanism for BnOH solvent-free oxidation catalyzed by PdO_x/CeO_2-NR-SA2 using air as oxidant. # represents the transition state.

3.6. BnOH Oxidation with Pd/Silica catalysts

Palladium was deposited on commercial mesoporous silica functionalized by adding amine groups (**NH_2-SiO_2**), and tested for BnOH oxidation in organic solvents. Either palladium metal or Pd-P alloy supported on NH_2-SiO_2 were utilized in oxidation tests. The reaction conditions and results are reported in *Table 3.11*.

Pd^0 supported on NH_2-SiO_2 was not active for BnOH oxidation neither in EtOH nor in toluene. On the other hand, Pd-P alloy supported on NH_2-SiO_2 showed catalytic activity in toluene and AcCN, but it was barely active in EtOH (*Figure 3.12*). Since the best results was achieved in toluene, the rest of the reactions with Pd/silica catalysts were performed using toluene solvent. *Figure 3.13* shows the results of BnOH oxidation in toluene, corresponding to reactions 6, 7, 8 and 9 of *Table 3.11*. Increasing the reaction temperature from 50 to 80 and further to 111 °C improved the BnOH conversion considerably (*Figure 3.13a*). However, the selectivity towards PhCHO decreased when the reaction temperature was increased from 80 to 111 °C (*Figure 3.13b*). Decrease in PhCHO selectivity at temperatures above 100 °C is in line with the heterolytic mechanism model suggested by Chan-Thaw et.al [3] for metallic palladium catalyst. The XPS analysis of Pd-P/ NH_2-SiO_2 (*Figure 3.14*) showed there was only one Pd species on the surface of silica, with Pd $3d_{5/2}$ component at 335.46 eV assigned to Pd^0 [159]. This may strengthen the possibility that the reaction mechanism is similar to that explained by Chan-Thaw [3].

Furthermore, when air was replaced by O_2, BnOH conversion increased significantly for the reactions performed at 111 °C (*Figure 3.13c*). The best yield of PhCHO was achieved at 111 °C, using 20 mL min^{-1} O_2, at the second hour of the reaction (*Figure 3.13d*).

Table 3.11. Oxidation of BnOH catalyzed by Pd/silica catalysts.

Entry	Catalyst	Solvent	Temperature (°C)	BnOH Concentration (M)	Catalyst/BnOH Pd Molar ratio	Oxidant 20 ($mLmin^{-1}$)
1	Pd^0/NH_2SiO_2	Toluene	111	0.016	1:26.7	Air
2	Pd^0/NH_2SiO_2	EtOH	78	0.016	1:26.7	Air
3	Pd-P/ NH_2SiO_2	Toluene	111	0.016	1:26.7	Air
4	Pd-P/ NH_2SiO_2	EtOH	78	0.016	1:26.7	Air
5	Pd-P/ NH_2SiO_2	AcCN	80	0.016	1:26.7	Air
6	Pd-P/ NH_2SiO_2	Toluene	50	0.1	1:100	Air
7	Pd-P/ NH_2SiO_2	Toluene	80	0.1	1:100	Air
8	Pd-P/ NH_2SiO_2	Toluene	111	0.1	1:100	Air
9	Pd-P/ NH_2SiO_2	Toluene	111	0.1	1:100	O_2

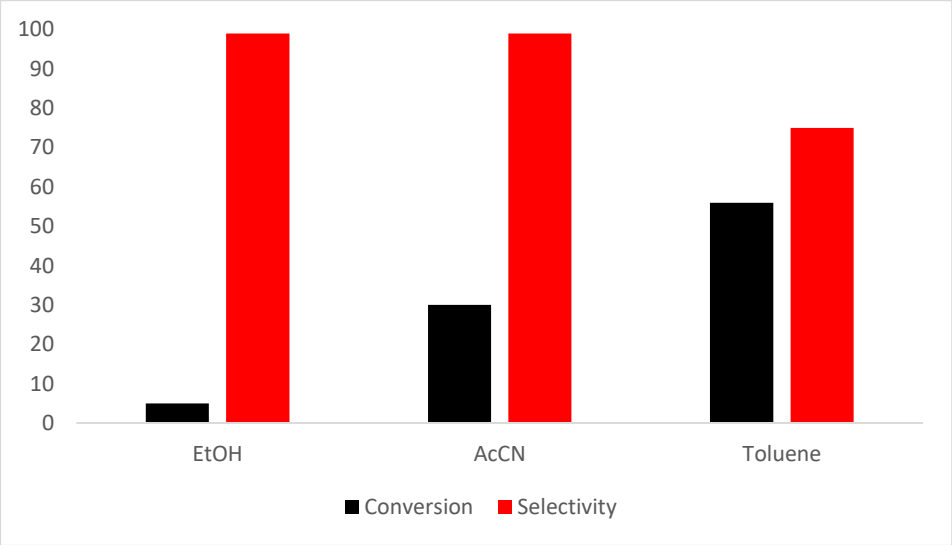

Figure 3.12. BnOH to PhCHO aerobic oxidation catalyzed by Pd-P/NH_2-SiO_2; conditions: 20 mL min^{-1} air, 32 mg catalyst, 0.16 mmol BnOH, reaction temperature of 78 °C for EtOH and AcCN, and 111 °C for toluene solvents.

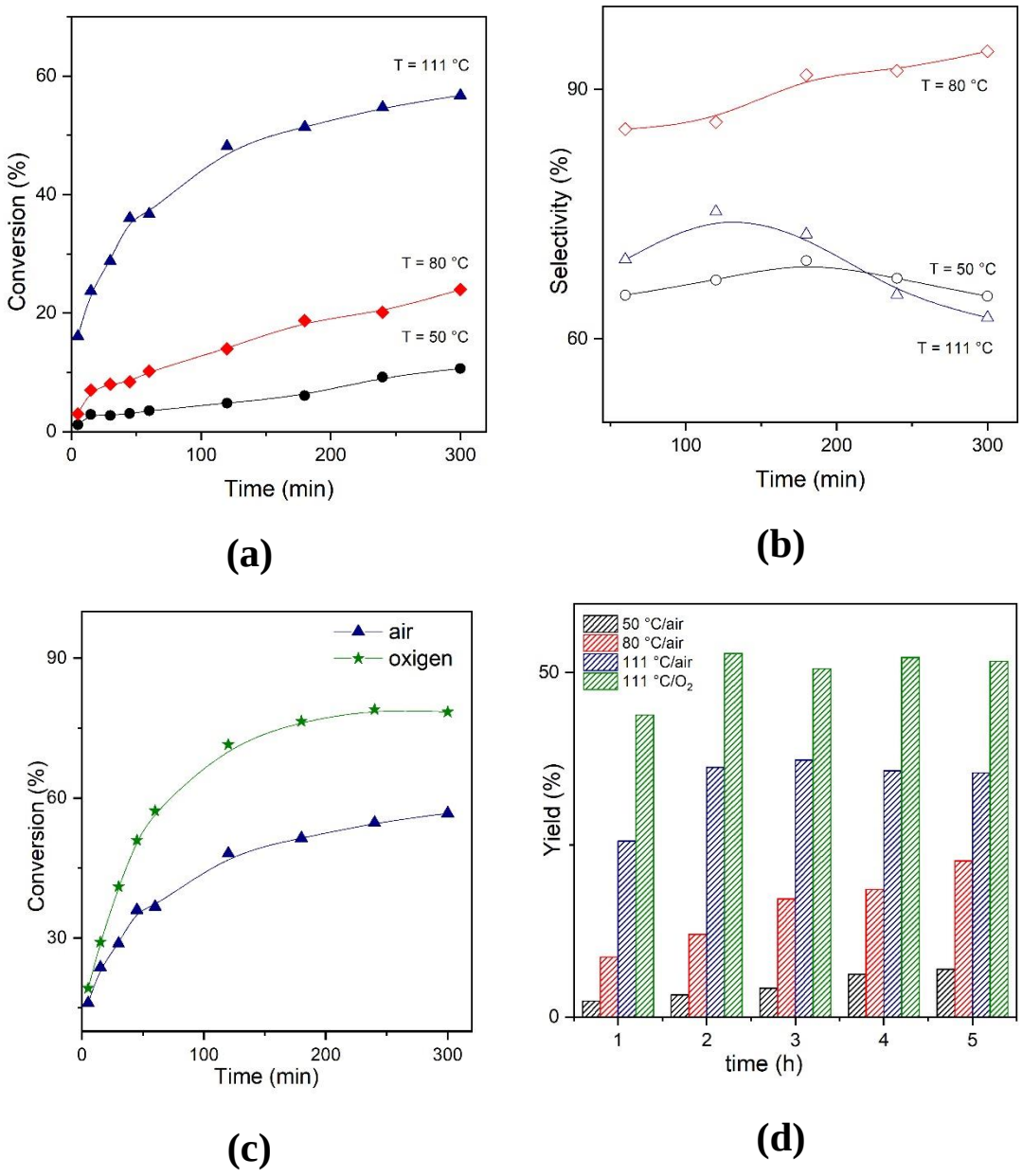

Figure 3.13. Results of BnOH oxidation in toluene, catalyzed by Pd-P/NH_2-SiO_2, using 20 mL min^{-1} air or O_2. Reaction conditions: BnOH 1 mmol, catalyst mass 53.2 mg.

According to XPS analysis of the Pd-P/NH_2-SiO_2 catalyst, a P 2p component at 129.74 eV is observed, assigned to elemental state of phosphorus P^0. This peak was negatively shifted from that of pure phosphorous (130.4 eV), which might be due to acceptance of electron by P from metal elements, suggesting the formation of Pd-P NPs [126,159]. Positive effect of incorporation

of P into supported Pd catalysts are reported for hydrogenation of alkylanthraquinones catalyzed by Pd-P supported on carbon [163], oxidation of formic acid catalyzed by Pd-P supported on carbon nanotubes [164], and oxidation of BnOH catalyzed by Pd-P supported on porous carbon frame [126]. Guo et al., claims that P can enhance the hydrophobicity of the catalyst support which may facilitate the adsorption of the BnOH reactant and the subsequent desorption of the produced PhCHO [126].

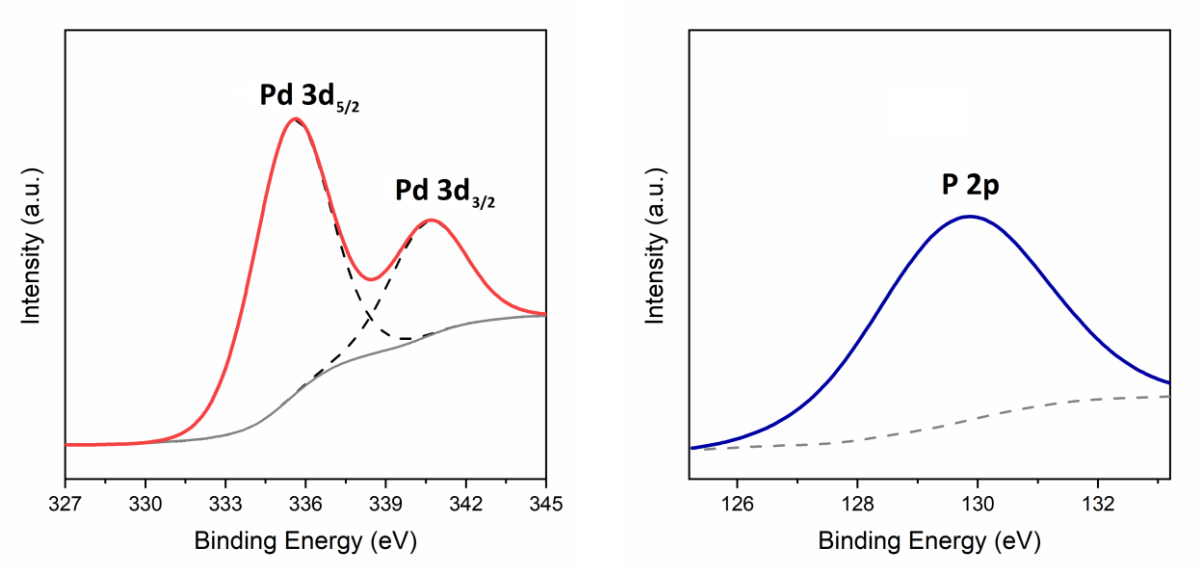

Figure 3.14. Pd 3d and P 2p XPS spectra of Pd-P/NH_2-SiO_2 sample.

3.7. Oxidation of 4-Benzyloxyphenol

All of catalysts prepared during the project (*Table 2.1*), and other catalysts reported in *Section 2.5*, were tested in oxidation of 4-benzyloxyphenol as a lignin model compound containing α — O — 4. In neither of the chromatograms of the reactions, any product peak was observed, nor any change in peak of the substrate. Compared to α — O — 4 and β — O — 4 bonds, the benzylic C

— H and C — OH bonds in lignin model compounds are easier to attack and oxidized, therefore; in many research works aiming at oxidative breakage of C — O bond in lignin and lignin model compounds, high temperature and pressure, expensive and toxic stoichiometric oxidant, and basic or acidic conditions were applied [8,165]. For instance, Elkurtehi et al., reported that while vanadium compounds supported by tetradentate amino-bis(phenolate) ligands were successful as homogeneous catalyst for aerobic oxidation of 4-methoxybenzyl alcohol and 1,2-diphenyl-2-methoxyethanol, the same system showed limited reactivity in oxidation of diphenyl ether and benzyl phenyl ether by H_2O_2 [166]. In another example, Gao et al., testing nitrogen-containing graphene materials as catalyst for breakage of α — O — 4 bond of lignin model compounds, observed that using H_2O_2 as oxidant and mild temperature led to poor results (very low amount of α — O — 4 breakage products), but replacing the hydrogen peroxide with tert-butyl hydroperoxide (**TBHP**) and increasing the temperature significantly boosted the breakage of α — O — 4 bond [167].

Regarding the economic and environmental aspects of utilizing oxidants such as TBHP, and acids or bases, increasing the pressure might be the first suggestion aiming at a successful breakage of C — O in the lignin model compounds by the Pd/ceria and Pd/silica catalytic systems tested in this project.

Chapter 4.

Conclusions

4.1. Pd/Ceria Catalysts

Ceria has been used as support for designing catalytic systems mainly because of its enhanced surface area and high amount of surface-active sites (oxygen vacancies) in comparison with other common supports. In this study, several Pd/ceria catalysts were prepared and tested for environmentally friendly aerobic and selective oxidation of benzyl alcohol (**BnOH**) to benzaldehyde (**PhCHO**). Palladium oxide supported on ceria nanorod was prepared by wet impregnation deposition on the hydrothermally synthesized CeO_2-NR, and a final calcination at 500 °C. XPS data showed that after final calcination, there was 90% PdO_x, ($x > 1$) and 10% PdO on the surface of the support. The activity of this catalyst was higher in protic solvents. The best result was achieved using boiling ethanol (**EtOH**) as a green solvent, leading to 93% BnOH conversion and 96% PhCHO selectivity. On the contrary, the reduced sample worked better in aprotic toluene (25% conversion) than in protic EtOH (13% conversion). The different behavior of calcined and reduced catalysts suggests the possibility of dissimilar reaction mechanisms. With calcined catalyst, a heterolytic and/or solvent proton donation mechanism might explain the higher conversion in protic solvent.

Changing the method of reduction led to change in palladium species on the support, and subsequently different catalytic activity. For the Pd/ceria catalyst reduced by hydrazine following the palladium deposition, a high activity in toluene solvent was observed (86% substrate conversion and ~100% PhCHO selectivity. While reducing the palladium with methanol (**MeOH**) during the wet impregnation process led to a catalyst that was inactive in EtOH and mildly active in toluene (43% conversion, ~100% selectivity). These all show the critical role of electronic

properties of Pd in determination of the reaction mechanism, and the catalytic activity of Pd/ceria system.

Preparing palladium oxide supported on ceria nanorod using palladium(II) nitrate commercial solutions led to production of a catalyst with the activity different than that observed for the similar catalyst prepared by palladium(II) nitrate dehydrate precursor. Similar to reduced catalysts, the catalysts prepared from commercial solutions worked better in toluene, indicating that the reaction mechanism with this catalyst is different than the catalyst prepared by solid palladium precursor. The reason might be the absence of PdO on the surface of ceria in the samples prepared by commercial palladium nitrate solution, as observed in the XPS spectra of the samples. The results for the reactions in toluene were not always reproducible, and the catalytic activity of some samples changed over the time, probably due to change in Pd oxidation state resulted from presence of cerium(III) on the ceria support.

Solvent-free oxidation of BnOH derivatives by palladium oxide supported on ceria nanorod showed the crucial effect of substituted groups on the catalytic activity. The conversion of substrate increased considerably by substituting electron-donating groups (**EDG**) such as methyl or methoxy on BnOH; whereas, electron-withdrawing groups (**EWG**) such as nitro, completely diminished the catalytic activity. Selectivity of the corresponding aldehyde was decreased when the conversion increased due to electron releasing groups, but never less than 83% of aldehyde selectivity was achieved. These observations might be indicative of an ionic reaction mechanism, including a carbocation-type rate-determining transition state that can be boosted by EDG substituents, and hindered by EWG ones.

4.2. Pd/Silica catalysts

Silica has been extensively utilized as support for designation of catalytic systems, especially because of high surface area of silica compared to many other oxides, including ceria. Our preliminary results showed that palladium was not absorbed on non-functionalized silica. But when the commercial mesoporous silica was functionalized with amine groups, both Pd^0 and Pd-P alloy was deposited on the surface of the support. The catalytic testing showed that Pd^0/NH_2-SiO_2 was not active for BnOH oxidation neither in toluene nor in EtOH. However, Pd-P/ NH_2-SiO_2 showed activity in toluene and AcCN, but not in EtOH. The results in toluene was comparable with the results achieved by some of Pd/ceria catalysts, however, since the surface area of silica was almost 5 times more than ceria, important role of ceria support can be understood. For Pd/silica catalyst, changing the oxidant from air to O_2 led to higher reaction efficiency. This was in contrary with Pd/ceria catalysts for which, same results were achieved using air or oxygen. In addition, increasing the temperature to boiling point of toluene led to decrease in selectivity of PhCHO. This phenomenon, although has been observed in previous studies, was contradictory to the results achieved by prepared Pd/ceria systems, suggesting different reaction mechanism when utilizing these two catalytic systems. This observation along with the XPS analysis of the Pd-P/silica sample (Pd^0 was the only palladium species on the surface of silica) might suggest that the reaction mechanism with this catalyst is similar to the mechanism described in *Section 1.3.1*, which is not boosted by proton-donating ability of the protic solvents.

4.3. Future perspectives

During this project, several questions have been raised that can be a motivation for further continuing this research line. Deeper studies on oxidation states of palladium in calcined or reduced samples can improve the insight into the reaction mechanism, considering the significantly different reaction efficiencies achieved by the catalysts that were reduced by different methods, as well as the response of catalysts to organic solvents of different natures regarding the polarity and proticity. Studying the micro-kinetics of the reactions with regard to different secondary products especially in solvent-free reactions, can be another research line that might shed more light on the reaction mechanism. In addition, regarding the economic aspects of utilizing noble metals as catalyst, optimizing the metal loading to achieve the best efficiency can be of utmost importance.

Finally, since neither of the tested catalysts were successful in oxidizing 4-benzyloxyphenol at atmospheric pressure, testing the reaction at higher pressure might lead to breakage of C — O linkage. If performed successfully, further testing the catalysts for depolymerization of lignin can open up a way through a wide field of improving and optimizing the lignin valorization.

Bibliography

1. Davis, S.E.; Ide, M.S.; Davis, R.J. Selective oxidation of alcohols and aldehydes over supported metal nanoparticles. *Green Chem.* **2013**, *15*, 17-45, doi:10.1039/c2gc36441g.
2. Vinod, C.P.; Wilson, K.; Lee, A.F. Recent advances in the heterogeneously catalysed aerobic selective oxidation of alcohols. *Journal of Chemical Technology & Biotechnology* **2011**, *86*, 161-171, doi:10.1002/jctb.2504.
3. Chan-Thaw, C.; Savara, A.; Villa, A. Selective Benzyl Alcohol Oxidation over Pd Catalysts. *Catalysts* **2018**, *8*, 431, doi:10.3390/catal8100431.
4. Jia, A.; Lou, L.-L.; Zhang, C.; Zhang, Y.; Liu, S. Selective oxidation of benzyl alcohol to benzaldehyde with hydrogen peroxide over alkali-treated ZSM-5 zeolite catalysts. *Journal of Molecular Catalysis A: Chemical* **2009**, *306*, 123-129, doi:10.1016/j.molcata.2009.02.035.
5. Choudhary, V.R.; Chaudhari, P.A.; Narkhede, V.S. Solvent-free liquid phase oxidation of benzyl alcohol to benzaldehyde by molecular oxygen using non-noble transition metal containing hydrotalcite-like solid catalysts. *Catalysis Communications* **2003**, *4*, 171-175, doi:10.1016/s1566-7367(03)00027-x.
6. Lingaiah, N.; Reddy, K.M.; Babu, N.S.; Rao, K.N.; Suryanarayana, I.; Prasad, P.S.S. Aerobic selective oxidation of benzyl alcohol over vanadium substituted ammonium salt of 12-molybdophosphoric acid. *Catalysis Communications* **2006**, *7*, 245-250, doi:10.1016/j.catcom.2005.10.013.
7. Rothenberg, G. *Catalysis: Concepts and Green Applications*; WILEY-VCH Verlag GmbH & Co. KGaA: Weinheim, Germany, 2008.
8. Cheng, C.; Wang, J.; Shen, D.; Xue, J.; Guan, S.; Gu, S.; Luo, K.H. Catalytic Oxidation of Lignin in Solvent Systems for Production of Renewable Chemicals: A Review. *Polymers* **2017**, *9*, doi:10.3390/polym9060240.
9. Karkas, M.D.; Matsuura, B.S.; Monos, T.M.; Magallanes, G.; Stephenson, C.R. Transition-metal catalyzed valorization of lignin: the key to a sustainable carbon-neutral future. *Organic & biomolecular chemistry* **2016**, *14*, 1853-1914, doi:10.1039/c5ob02212f.
10. Gómez-Monedero, B.; Ruiz, M.P.; Bimbela, F.; Faria, J. Selective hydrogenolysis of α-O-4, β-O-4, 4-O-5 C-O bonds of lignin-model compounds and lignin-containing stillage derived from cellulosic bioethanol processing. *Applied Catalysis A: General* **2017**, *541*, 60-76, doi:10.1016/j.apcata.2017.04.022.
11. Pandey, M.P.; Kim, C.S. Lignin Depolymerization and Conversion: A Review of Thermochemical Methods. *Chemical Engineering & Technology* **2011**, *34*, 29-41, doi:10.1002/ceat.201000270.
12. Xu, C.; Ferdosian, F. *Conversion of Lignin into Bio-Based Chemicals and Materials*; Springer-Verlag GmbH Germany: Berlin, Germany, 2017.
13. Zakzeski, J.; Bruijnincx, P.C.A.; Jongerius, A.L.; Weckhuysen, B.M. The Catalytic Valorization of Lignin for the Production of Renewable Chemicals. *Chemical reviews* **2010**, *10*, 3552–3599, doi:10.1021/cr900354u.
14. Wang, J.; Gu, H. Novel Metal Nanomaterials and Their Catalytic Applications. *Molecules* **2015**, *20*, 17070-17092, doi:10.3390/molecules200917070.

15. Sharifzadeh, M.; Wang, L.; Shah, N. Decarbonisation of olefin processes using biomass pyrolysis oil. *Applied Energy* **2015**, *149*, 404-414, doi:10.1016/j.apenergy.2015.03.081.
16. Sheldon, R.A. Atom efficiency and catalysis in organic synthesis. *Pure Appl. Chem.* **2000**, *72*, 1233–1246.
17. Trost, B. The atom economy-a search for synthetic efficiency. *Science* **1991**, *254*, 1471-1477, doi:10.1126/science.1962206.
18. Gutmann, B.; Elsner, P.; Roberge, D.; Kappe, C.O. Homogeneous Liquid-Phase Oxidation of Ethylbenzene to Acetophenone in Continuous Flow Mode. *ACS Catalysis* **2013**, *3*, 2669-2676, doi:10.1021/cs400571y.
19. Marconi, E.; Tuti, S.; Luisetto, I. Structure-Sensitivity of CO_2 Methanation over Nanostructured Ni Supported on CeO_2 Nanorods. *Catalysts* **2019**, *9*, 375, doi:10.3390/catal9040375.
20. Moeini, S.S.; Dadashian, F.; Vahabzadeh, F. Recycling of Calotropisgigantea Waste Fiber by Enzymatic Hydrolysis to Produce Bioethanol. *Indian Journal of Science and Technology* **2016**, *9*, doi:10.17485/ijst/2016/v9i9/79662.
21. Urgoitia, G.; Galdón, G.; Churruca, F.; SanMartin, R.; Herrero, M.T.; Domínguez, E. Aerobic oxidation of secondary benzyl alcohols catalyzed by phosphinite-based palladium pincer complexes. *Environmental Chemistry Letters* **2018**, *16*, 1101-1108, doi:10.1007/s10311-018-0730-y.
22. Klaewkla, R.; Arend, M.; Hoelderich, W.F. *A Review of Mass Transfer Controlling the Reaction Rate in Heterogeneous Catalytic Systems, Mass Transfer - Advanced Aspects*; InTech,: 2011.
23. Somorjai, G.A.; Tao, F.; Park, J.Y. The Nanoscience Revolution: Merging of Colloid Science, Catalysis and Nanoelectronics. *Topics in Catalysis* **2008**, *47*, 1-14, doi:10.1007/s11244-007-9028-1.
24. Isaifan, R.J.; Ntais, S.; Baranova, E.A. Particle size effect on catalytic activity of carbon-supported Pt nanoparticles for complete ethylene oxidation. *Applied Catalysis A: General* **2013**, *464-465*, 87-94, doi:10.1016/j.apcata.2013.05.027.
25. Kesavan, J.K.; Luisetto, I.; Tuti, S.; Meneghini, C.; Battocchio, C.; Iucci, G. Ni supported on YSZ: XAS and XPS characterization and catalytic activity for CO_2 methanation. *Journal of Materials Science* **2017**, *52*, 10331-10340, doi:10.1007/s10853-017-1179-2.
26. Wyrwalski, F.; Giraudon, J.-M.; Lamonier, J.-F. Synergistic Coupling of the Redox Properties of Supports and Cobalt Oxide Co_3O_4 for the Complete Oxidation of Volatile Organic Compounds. *Catalysis Letters* **2010**, *137*, 141-149, doi:10.1007/s10562-010-0356-6.
27. Rojluechaia, S.; Chavadeja, S.; Schwankb, J.W.; Meeyoo, V. Catalytic activity of ethylene oxidation over Au, Ag and Au–Ag catalysts: Support effect. *Catalysis Communications* **2007**, *8*, 57-64, doi:10.1016/j.catcom.2006.05.029.
28. Comotti, M.; Li, W.C.; Spliethoff, B.; Schüth, F. Support Effect in High Activity Gold Catalysts for CO Oxidation. *J. Am. Chem. Soc.* **2006**, *128*, 917-924, doi:10.1021/ja0561441.
29. Liu, Y.; Chen, H.; Xu, C.; Sun, Y.; Li, S.; Jiang, M.; Qin, G. Control of Catalytic Activity of Nano-Au through Tailoring the Fermi Level of Support. *Small* **2019**, *15*, e1901789, doi:10.1002/smll.201901789.
30. Ampawa, S.; Krittametaporn, N.; Ungpittagul, T.; Phomphrai, K.; Sangtrirutnugul, P. Triazole-based ligands functionalized silica: Effects of ligand denticity and donors on

catalytic oxidation activity of Pd nanoparticles. *Applied Organometallic Chemistry* **2019**, *33*, 1-12, doi:10.1002/aoc.5238.

31. Chen, Y.Z.; Gu, B.; Uchida, T.; Liu, J.; Liu, X.; Ye, B.J.; Xu, Q.; Jiang, H.L. Location determination of metal nanoparticles relative to a metal-organic framework. *Nature communications* **2019**, *10*, 3462, doi:10.1038/s41467-019-11449-6.
32. Yuan, S.; Lv, X.; Zhang, Y.; Wu, Y.; Chunfeng, M.; Zhou, Y.; Chen, W.; Wang, Y. Fabrication of mesoporous SiO_2/Au/Co_3O_4 hollow spheres catalysts with core-shell structure for liquid phase oxidation of benzyl alcohol to benzaldehyde. *Journal of the Taiwan Institute of Chemical Engineers* **2019**, *103*, 138–148, doi:10.1016/j.jtice.2019.06.021.
33. Zhang, D.; Tang, D.; Yamamoto, T.; Kato, Y.; Horiuchi, S.; Ogawa, S.; Yoshimura, E.; Suzuki, M. Improving biosynthesis of AuPd core-shell nanoparticles through Escherichia coli with the assistance of phytochelatin for catalytic enhanced chemiluminescence and benzyl alcohol oxidation. *Journal of inorganic biochemistry* **2019**, *199*, 110795, doi:10.1016/j.jinorgbio.2019.110795.
34. Mohammadi, M.; Rezaei, A.; Khazaei, A.; Xuwei, S.; Huajun, Z. Targeted Development of Sustainable Green Catalysts for Oxidation of Alcohols via Tungstate-Decorated Multifunctional Amphiphilic Carbon Quantum Dots. *ACS applied materials & interfaces* **2019**, *11*, 33194-33206, doi:10.1021/acsami.9b07961.
35. Nicolau, G.; Tarantino, G.; Hammond, C. Acceptorless Alcohol Dehydrogenation Catalysed by Pd/C. *ChemSusChem* **2019**, *12*, 4953-4961, doi:10.1002/cssc.201901313.
36. Wang, J.; Liang, H.; Zhang, C.; Jin, B.; Men, Y. Bi_2WO_{6-x} nanosheets with tunable Bi quantum dots and oxygen vacancies for photocatalytic selective oxidation of alcohols. *Applied Catalysis B: Environmental* **2019**, *256*, 117874, doi:10.1016/j.apcatb.2019.117874.
37. Zhao, Y.; Li, Y.; Shen, Z.; Hu, X.; Hu, B.; Jin, L.; Sun, N.; Li, M. 3-BocNH-ABNO-catalyzed aerobic oxidation of alcohol at room temperature and atmospheric pressure. *Tetrahedron Letters* **2019**, *60*, 150994, doi:10.1016/j.tetlet.2019.150994.
38. Karimi, B.; Zamani, A. Recent Advances in the Homogeneous Palladium-Catalyzed Aerobic Oxidation of Alcohols. *J. Iran. Chern. Soc* **2008**, *5*, S1-S20.
39. Chakraborty, A.; Chakraborty, T.; Menendez, M.I.; Chattopadhyay, T. Surfactant-Mediated Solubilization of Magnetically Separable Nanocatalysts for the Oxidation of Alcohols. *ACS omega* **2019**, *4*, 11558-11565, doi:10.1021/acsomega.9b01143.
40. Chern, C.-Y.; Tseng, C.-C.; Hsiao, R.-H.; Wong, F.F.; Kuo, Y.-H. Cyclopentadienyl Ruthenium(II) Complex-Mediated Oxidation of Benzylic and Allylic Alcohols to Corresponding Aldehydes. *Heteroatom Chemistry* **2019**, *2019*, 1-8, doi:10.1155/2019/5053702.
41. Ghorbanloo, M.; Nazari, P. A soft anionic hydrogel reactor for silver nanoparticle preparation and use in H_2 production, 4-nitrophenol reduction and alcohol oxidation. *Journal of Porous Materials* **2019**, *27*, 37-47, doi:10.1007/s10934-019-00794-y.
42. Song, H.; Liu, Z.; Gai, H.; Wang, Y.; Qiao, L.; Zhong, C.; Yin, X.; Xiao, M. Nitrogen-Dopped Ordered Mesoporous Carbon Anchored Pd Nanoparticles for Solvent Free Selective Oxidation of Benzyl Alcohol to Benzaldehyde by Using O_2. *Frontiers in chemistry* **2019**, *7*, 458, doi:10.3389/fchem.2019.00458.

43. Mori, T.; Ishii, C.; Kimura, M. Pd-Catalyzed Dehydrogenative Oxidation of Alcohols to Functionalized Molecules. *Organic Process Research & Development* **2019**, *23*, 1709-1717, doi:10.1021/acs.oprd.9b00207.
44. Lu, G.; Huang, X.; Wu, Z.; Li, Y.; Xing, L.; Gao, H.; Dong, W.; Wang, G. Construction of covalently integrated core-shell TiO_2 nanobelts@COF hybrids for highly selective oxidation of alcohols under visible light. *Applied Surface Science* **2019**, *493*, 551-560, doi:10.1016/j.apsusc.2019.06.265.
45. Blackburn, T.F.; Schwartz, J. Homogeneous catalytic oxidation of secondary alcohols to ketones by molecular oxygen under mild conditions. *Journal of the Chemical Society, Chemical Communications* **1977**, *0*, 157-158, doi:10.1039/C39770000157.
46. Nishimura, T.; Onoue, T.; Onoue, K.; Uemura, S. Palladium(II)-Catalyzed Oxidation of Alcohols to Aldehydes and Ketones by Molecular Oxygen. *Journal of Organic Chemistry* **1999**, *64*, 6750-6755, doi:10.1021/jo9906734.
47. Peterson, K.P.; Larock, R.C. Palladium-Catalyzed Oxidation of Primary and Secondary Allylic and Benzylic Alcohols. *Journal of Organic Chemistry* **1998**, *63*, 3185-3189, doi:S0022-3263(97)01268-1.
48. Brink, G.-J.t.; Arends, I.W.C.E.; Sheldon, R.A. Green, Catalytic Oxidation of Alcohols in Water. *Science* **2000**, *287*.
49. Brink, G.-J.t.; Arends, I.W.C.E.; Sheldon, R.A. Catalytic conversions in water. Part 21: mechanistic investigations on the palladiumcatalysed aerobic oxidation of alcohols in water. *Advance Synthesis and Catalysis* **2002**, *344*, 355-369, doi:https://doi.org/10.1002/1615-4169(200206)344:3/4<355::AID-ADSC355>3.0.CO;2-S.
50. Schultz, M.J.; Hamilton, S.S.; Jensen, D.R.; Sigman, M.S. Development and Comparison of the Substrate Scope of Pd-Catalysts for the Aerobic Oxidation of Alcohols. *Journal of Organic Chemistry* **2005**, *70*, 3343-3352.
51. Schultz, M.J.; Park, C.C.; Sigman, M.S. A convenient palladium-catalyzed aerobic oxidation of alcohols at room temperature. *Chemical Communications* **2002**, 10.1039/B209344H, 3034-3035, doi:10.1039/B209344H.
52. Jensen, D.R.; Schultz, M.J.; Mueller, J.A.; Sigman, M.S. A Well-Defined Complex for Palladium-Catalyzed Aerobic Oxidation of Alcohols: Design, Synthesis, and Mechanistic Considerations. *Angewandte Chemie International Edition* **2003**, *42*, 3810-3813, doi:10.1002/anie.200351997.
53. Besson, M.; Gallezot, P. Selective oxidation of alcohols and aldehydes on metal catalysts. *Catalysis Today* **2000**, *57*.
54. Mallat, T.; Baiker, A. Oxidation of Alcohols with Molecular Oxygen on Solid Catalysts. *Chemical reviews* **2004**, *104*, doi:10.1021/cr0200116.
55. Hackett, S.F.J.; Brydson, R.M.; Gass, M.H.; Harvey, I.; Newman, A.D.; Wilson, K.; Lee, A.F. High-Activity, Single-Site Mesoporous Pd/Al_2O_3 Catalysts for Selective Aerobic Oxidation of Allylic Alcohols. *Angewandte Chemie* **2007**, *119*, 8747-8750, doi:10.1002/ange.200702534.
56. Lee, A.F.; Hackett, S.F.J.; Hargreaves, J.S.J.; Wilson, K. On the active site in heterogeneous palladium selox catalysts. *Green Chemistry* **2006**, *8*, 549-555, doi:10.1039/B601984F.

57. Wada, K.; Yano, K.; Kondo, T.; Mitsudo, T. Preparation of palladium oxide nanoparticles-encapsulating porous oxide catalysts for oxidation utilizing a silsesquioxane ligand. *Catalysis Today* **2006**, *117*, 242-247, doi:10.1016/j.cattod.2006.05.024.
58. Yang, G.; Zhu, W.; Zhang, P.; Xue, H.; Wang, W.; Tian, J.; Song, M. Recyclable Carbon Supported Copper-Manganese Oxide for Selective Aerobic Oxidation of Alcohols in Combination with 2,2,6,6-Tetramethylpiperidyl-1-oxyl under Neutral Condition. *Advance Synthesis and Catalysis* **2008**, *350*, 542-546, doi:10.1002/adsc.200700513.
59. Anderson, R.; Griffin, K.; Johnston, P.; Alsters, P.L. Selective Oxidation of Alcohols to Carbonyl Compounds and Carboxylic Acids with Platinum Group Metal Catalysts. *Advanced Synthesis & Catalysis* **2003**, *345*, 517-523.
60. Yamaguchi, K.; Mizuno, N. Supported Ruthenium Catalyst for the Heterogeneous Oxidation of Alcohols with Molecular Oxygen. *Angewandte Chemie International Edition* **2002**, *41*, 4538-4542.
61. Yamaguchi, K.; Mizuno, N. Scope, kinetics, and mechanistic aspects of aerobic oxidations catalyzed by ruthenium supported on alumina. *Chemistry* **2003**, *9*, 4353-4361, doi:10.1002/chem.200304916.
62. Abad, A.; Corma, A.; García, H. Supported gold nanoparticles for aerobic, solventless oxidation of allylic alcohols. *Pure and Applied Chemistry* **2007**, *79*, 1847-1854, doi:10.1351/pac200779111847.
63. JamJam, N.M.; Taufiq Yap, Y.H.; Muhamad, E.N.; Izham Saiman, M.; Saleh, T.A. Free solvent oxidation of molecular benzyl alcohol by newly synthesized AuPd/titania catalysts. *Inorganic Chemistry Communications* **2019**, *107*, 107471, doi:10.1016/j.inoche.2019.107471.
64. Mao, D.; Qiu, J.; Jia, M.; Zhang, X.-F.; Yao, J. Platinum supported cellulose-based carbon with oxygen-containing functional groups for benzyl alcohol oxidation. *Journal of Physics and Chemistry of Solids* **2019**, *135*, 109095, doi:10.1016/j.jpcs.2019.109095.
65. Reddy, V.G.; Jampaiah, D.; Chalkidis, A.; Sabri, Y.M.; Mayes, E.L.H.; Bhargava, S.K. Highly dispersed cobalt oxide nanoparticles on manganese oxide nanotubes for aerobic oxidation of benzyl alcohol. *Catalysis Communications* **2019**, *130*, 105763, doi:10.1016/j.catcom.2019.105763.
66. Tan, J.; Liu, X.B.; Chen, W.F.; Hu, Y.L. Synthesis of Magnetically Separable Nanocatalyst $CoFe_2O_4$@SiO_2@MIL-53(Fe) for Highly Efficient and Selective Oxidation of Alcohols and Benzylic Compounds with Hydrogen Peroxide. *ChemistrySelect* **2019**, *4*, 8477-8481, doi:10.1002/slct.201901690.
67. Joice, E.K.; Rison, S.; Akshaya, K.B.; Varghese, A. Platinum decorated polythiophene modified stainless steel for electrocatalytic oxidation of benzyl alcohol. *Journal of Applied Electrochemistry* **2019**, *49*, 937-947, doi:10.1007/s10800-019-01336-9.
68. Liu, L.; Zhou, X.; Liu, L.; Jiang, S.; Li, Y.; Guo, L.; Yan, S.; Tai, X. Heterogeneous Bimetallic Cu–Ni Nanoparticle-Supported Catalysts in the Selective Oxidation of Benzyl Alcohol to Benzaldehyde. *Catalysts* **2019**, *9*, 538, doi:10.3390/catal9060538.
69. Venezia, B.; Douthwaite, M.; Wu, G.; Sankar, M.; Ellis, P.; Hutchings, G.J.; Gavriilidis, A. Slurry loop tubular membrane reactor for the catalysed aerobic oxidation of benzyl alcohol. *Chemical Engineering Journal* **2019**, *378*, 122250, doi:10.1016/j.cej.2019.122250.
70. Alshammari, H.M.; Humaidi, J.R.; Alhumaimess, M.S.; Aldosari, O.F.; Alotaibi, M.H.; Hassan, H.M.A.; Wawata, I. Bimetallic Au:Pd nanoparticle supported on MgO for the

oxidation of benzyl alcohol. *Reaction Kinetics, Mechanisms and Catalysis* **2019**, *128*, 97-108, doi:10.1007/s11144-019-01639-0.
71. Lv, X.; Yuan, S.; Zhang, Y.; Fu, Y.; Wu, Y.; Zhou, Y.; Huang, R.; Huang, Z. Preparation of cyclonic Co_3O_4/Au/mesoporous SiO_2 catalysts with core–shell structure for solvent-free oxidation of benzyl alcohol. *Journal of the Taiwan Institute of Chemical Engineers* **2019**, *102*, 448-455, doi:10.1016/j.jtice.2019.06.013.
72. Olmos, C.M.; Chinchilla, L.E.; Villa, A.; Delgado, J.J.; Hungría, A.B.; Blanco, G.; Prati, L.; Calvino, J.J.; Chen, X. Size, nanostructure, and composition dependence of bimetallic Au–Pd supported on ceria–zirconia mixed oxide catalysts for selective oxidation of benzyl alcohol. *Journal of Catalysis* **2019**, *375*, 44-55, doi:10.1016/j.jcat.2019.05.002.
73. Diez, A.S.; Piqueras, C.M.; Araiza, D.G.; Díaz, G.; Volpe, M.A. Preparation andCharacterization of Cu-CeO_2catalytic materials forthe oxidation of benzyl alcohol to benzaldehyde in water. *Materials Chemistry and Physics* **2019**, *232*, 265-271, doi:10.1016/j.matchemphys.2019.04.053.
74. Opeida, I.A.; Sheparovych, R.B.; Hrynda, Y.M.; Khavunko, O.Y.; Kompanets, M.O.; Shendryk, A.N. Kinetics of oxidation of benzyl alcohols with molecular oxygen catalyzed by N-hydroxyphthalimide: Role of hydroperoxyl radicals. *International Journal of Chemical Kinetics* **2019**, *51*, 679-688, doi:10.1002/kin.21287.
75. Yu, Y.; Lu, B.; Wang, X.; Zhao, J.; Wang, X.; Cai, Q. Highly selective oxidation of benzyl alcohol to benzaldehyde with hydrogen peroxide by biphasic catalysis. *Chemical Engineering Journal* **2010**, *162*, 738-742, doi:10.1016/j.cej.2010.05.057.
76. Nasrollahzadeh, M.; Bagherzadeh, M.; Karimi, H. Preparation, characterization and catalytic activity of $CoFe_2O_4$ nanoparticles as a magnetically recoverable catalyst for selective oxidation of benzyl alcohol to benzaldehyde and reduction of organic dyes. *Journal of colloid and interface science* **2016**, *465*, 271-278, doi:10.1016/j.jcis.2015.11.074.
77. Choudhary, V.R.; Dumbre, D.K.; Narkhede, V.S.; Jana, S.K. Solvent-free selective oxidation of benzyl alcohol and benzaldehyde by tert-butyl hydroperoxide using MnO^{-4} -exchanged Mg–Al–hydrotalcite catalysts. *Catalysis Letters* **2003**, *86*, 229-233, doi:1011-372X/03/0300-0229/0.
78. Behera, G.C.; Parida, K.M. Liquid phase catalytic oxidation of benzyl alcohol to benzaldehyde over vanadium phosphate catalyst. *Applied Catalysis A: General* **2012**, *413-414*, 245-253, doi:10.1016/j.apcata.2011.11.016.
79. Marko, I.n.E.; Giles, P.R.; Tsukazaki, M.; Chelle´-RegnautIsabelle; Urch, C.J.; Brown, S.M. Efficient, Aerobic, Ruthenium-Catalyzed Oxidation of Alcohols into Aldehydes and Ketones. *Journal of the American Chemical Society* **1997**, *119*, 12661-12662, doi:S0002-7863(97)03227-7.
80. Dijksman, A.; Marino-Gonza´lez, A.; Mairata i Payeras, A.; Arends, I.W.C.E.; Sheldon, R.A. Efficient and Selective Aerobic Oxidation of Alcohols into Aldehydes and Ketones Using Ruthenium/TEMPO as the Catalytic System. *Journal of the American Chemical Society* **2001**, *123*, 6826-6833, doi:10.1021/ja0103804.
81. Han, D.; Xu, T.; Su, J.; Xu, X.; Ding, Y. Gas-Phase Selective Oxidation of Benzyl Alcohol to Benzaldehyde with Molecular Oxygen over Unsupported Nanoporous Gold. *ChemCatChem* **2010**, *2*, 383-386, doi:10.1002/cctc.201000001.
82. Zhan, G.; Huang, J.; Du, M.; Sun, D.; Abdul-Rauf, I.; Lin, W.; Hong, Y.; Li, Q. Liquid phase oxidation of benzyl alcohol to benzaldehyde with novel uncalcined bioreduction Au

catalysts: High activity and durability. *Chemical Engineering Journal* **2012**, *187*, 232-238, doi:10.1016/j.cej.2012.01.051.
83. Liu, H.; Liu, Y.; Li, Y.; Tang, Z.; Jiang, H. Metal-Organic Framework Supported Gold Nanoparticles as a Highly Active Heterogeneous Catalyst for Aerobic Oxidation of Alcohols. *Journal of Physical Chemisry C* **2010**, *114*, 13362–13369, doi:10.1021/jp105666f.
84. Ma, C.Y.; Cheng, J.; Wang, H.L.; Hu, Q.; Tian, H.; He, C.; Hao, Z.P. Characteristics of Au/HMS catalysts for selective oxidation of benzyl alcohol to benzaldehyde. *Catalysis Today* **2010**, *158*, 246-251, doi:10.1016/j.cattod.2010.03.080.
85. Li, H.; Qin, F.; Yang, Z.; Cui, X.; Wang, J.; Zhang, L. New Reaction Pathway Induced by Plasmon for Selective Benzyl Alcohol Oxidation on BiOCl Possessing Oxygen Vacancies. *Journal of the American Chemical Society* **2017**, *139*, 3513-3521, doi:10.1021/jacs.6b12850.
86. Liotta, L.F.; Venezia, A.M.; Deganello, G.; Longo, A.; Martorana, A.; Schay, Z.; Guczi, L. Liquid phase selective oxidation of benzyl alcohol over Pd–Ag catalysts supported on pumice. *Catalysis Today* **2001**, *66*, 271–276, doi:10.1016/S0920-5861(00)00650-7.
87. Mori, K.; Hara, T.; Mizugaki, T.; Ebitani, K.; Kaneda, K. Hydroxyapatite-Supported Palladium Nanoclusters: A Highly Active Heterogeneous Catalyst for Selective Oxidation of Alcohols by Use of Molecular Oxygen. *Journal of the American Chemical Society* **2004**, *126*, 10657-10666, doi:10.1021/ja0488683.
88. Karimi, B.; Abedi, S.; Clark, J.H.; Budarin, V. Highly Efficient Aerobic Oxidation of Alcohols Using a Recoverable Catalyst: The Role of Mesoporous Channels of SBA-15 in Stabilizing Palladium Nanoparticles. *Angewandte Chemie* **2006**, *118*, 4894-4897, doi:10.1002/ange.200504359.
89. Zhou, Y.; Xiang, Z.; Cao, D.; Liu, C.-j. Preparation and Characterization of Covalent Organic Polymer Supported Palladium Catalysts for Oxidation of CO and Benzyl Alcohol. *Industrial & Engineering Chemistry Research* **2014**, *53*, 1359-1367, doi:10.1021/ie403279y.
90. Xu, J.; Shang, J.-K.; Chen, Y.; Wang, Y.; Li, Y.-X. Palladium nanoparticles supported on mesoporous carbon nitride for efficiently selective oxidation of benzyl alcohol with molecular oxygen. *Applied Catalysis A: General* **2017**, *542*, 380-388, doi:10.1016/j.apcata.2017.05.036.
91. Sharma, M.; Das, B.; Deka, B.K.; Park, Y.B.; Bhargava, S.K.; Bania, K.K. Pd/Cu-Oxide Nanoconjugate at Zeolite-Y Crystallite Crafting the Mesoporous Channels for Selective Oxidation of Benzyl-Alcohols. *ACS applied materials & interfaces* **2017**, *9*, 35453-35462, doi:10.1021/acsami.7b11086.
92. Akbari, S.; Mokhtari, J.; Mirjafari, Z. Solvent-free and melt aerobic oxidation of benzyl alcohols using Pd/Cu_2(BDC)$_2$DABCO–MOF prepared by one-step and through reduction by dimethylformamide. *The Royal Society of Chemistry* **2017**, *7*, 40881–40886, doi:10.1039/c7ra07209k.
93. Enache, D.I.; Barker, D.; Edwards, J.K.; Taylor, S.H.; Knight, D.W.; Carley, A.F.; Hutchings, G.J. Solvent-free oxidation of benzyl alcohol using titania-supported gold–palladium catalysts: Effect of Au–Pd ratio on catalytic performance. *Catalysis Today* **2007**, *122*, 407-411, doi:10.1016/j.cattod.2007.01.003.

94. Miedziak, P.J.; He, Q.; Edwards, J.K.; Taylor, S.H.; Knight, D.W.; Tarbit, B.; Kiely, C.J.; Hutchings, G.J. Oxidation of benzyl alcohol using supported gold–palladium nanoparticles. *Catalysis Today* **2011**, *163*, 47-54, doi:10.1016/j.cattod.2010.02.051.
95. Marx, S.; Baiker, A. Beneficial Interaction of Gold and Palladium in Bimetallic Catalysts for the Selective Oxidation of Benzyl Alcohol. *The Journal of Physical Chemistry C* **2009**, *113*, 6191–6201, doi:10.1021/jp808362m.
96. Ma, C.Y.; Dou, B.J.; Li, J.J.; Cheng, J.; Hu, Q.; Hao, Z.P.; Qiao, S.Z. Catalytic oxidation of benzyl alcohol on Au or Au–Pd nanoparticles confined in mesoporous silica. *Applied Catalysis B: Environmental* **2009**, *92*, 202-208, doi:10.1016/j.apcatb.2009.07.007.
97. Chen, Y.; Lim, H.; Tang, Q.; Gao, Y.; Sun, T.; Yan, Q.; Yang, Y. Solvent-free aerobic oxidation of benzyl alcohol over Pd monometallic and Au–Pd bimetallic catalysts supported on SBA-16 mesoporous molecular sieves. *Applied Catalysis A: General* **2010**, *380*, 55-65, doi:10.1016/j.apcata.2010.03.026.
98. Khawaji, M.; Chadwick, D. Au-Pd Bimetallic Nanoparticles Immobilised on Titanate Nanotubes: A Highly Active Catalyst for Selective Oxidation. *ChemCatChem* **2017**, *9*, 4353-4363, doi:10.1002/cctc.201700851.
99. Zope, B.N.; Hibbitts, D.D.; Neurock, M.; Davis, R.J. Reactivity of the Gold/Water Interface During Selective Oxidation Catalysis. *Science* **2010**, *330*, 74-78, doi:10.1126/science.1195055.
100. Al-Saeedi, S.; Abdel-Rahman, L.; Abu-Dief, A.; Abdel-Fatah, S.; Alotaibi, T.; Alsalme, A.; Nafady, A. Catalytic Oxidation of Benzyl Alcohol Using Nanosized Cu/Ni Schiff-Base Complexes and Their Metal Oxide Nanoparticles. *Catalysts* **2018**, *8*, 452, doi:10.3390/catal8100452.
101. Savara, A.; Chan-Thaw, C.E.; Rossetti, I.; Villa, A.; Prati, L. Benzyl Alcohol Oxidation on Carbon-Supported Pd Nanoparticles: Elucidating the Reaction Mechanism. *ChemCatChem* **2014**, *6*, 3464-3473, doi:10.1002/cctc.201402552.
102. Savara, A.; Rossetti, I.; Chan-Thaw, C.E.; Prati, L.; Villa, A. Microkinetic Modeling of Benzyl Alcohol Oxidation on Carbon-Supported Palladium Nanoparticles. *ChemCatChem* **2016**, *8*, 2482–2491, doi:10.1002/cctc.201600368.
103. Dell'Anna, M.M.; Mali, M.; Mastrorilli, P.; Cotugno, P.; Monopoli, A. Oxidation of benzyl alcohols to aldehydes and ketones under air in water using a polymer supported palladium catalyst. *Journal of Molecular Catalysis A: Chemical* **2014**, *386*, 114-119, doi:10.1016/j.molcata.2014.02.001.
104. Rostamnia, S.; Doustkhah, E.; Karimi, Z.; Amini, S.; Luque, R. Surfactant-Exfoliated Highly Dispersive Pd-Supported Graphene Oxide Nanocomposite as a Catalyst for Aerobic Aqueous Oxidations of Alcohols. *ChemCatChem* **2015**, *7*, 1678-1683, doi:10.1002/cctc.201500126.
105. Moreno, I.; Dummer, N.F.; Edwards, J.K.; Alhumaimess, M.; Sankar, M.; Sanz, R.; Pizarro, P.; Serrano, D.P.; Hutchings, G.J. Selective oxidation of benzyl alcohol using in situ generated H2O2 over hierarchical Au–Pd titanium silicalite catalysts. *Catalysis Science & Technology* **2013**, *3*, 2425, doi:10.1039/c3cy00493g.
106. Kong, L.; Wang, C.; Gong, F.; Zhu, W.; Zhong, Y.; Ye, X.; Li, F. Magnetic Core–Shell Nanostructured Palladium Catalysts for Green Oxidation of Benzyl Alcohol. *Catalysis Letters* **2016**, *146*, 1321-1330, doi:10.1007/s10562-016-1756-z.
107. Yan, Y.; Chen, Y.; Jia, X.; Yang, Y. Palladium nanoparticles supported on organosilane-functionalized carbon nanotube for solvent-free aerobic oxidation of benzyl alcohol.

Applied Catalysis B: Environmental **2014**, *156-157*, 385-397, doi:10.1016/j.apcatb.2014.03.043.
108. Cao, E.; Sankar, M.; Firth, S.; Lam, K.F.; Bethell, D.; Knight, D.K.; Hutchings, G.J.; McMillan, P.F.; Gavriilidis, A. Reaction and Raman spectroscopic studies of alcohol oxidation on gold–palladium catalysts in microstructured reactors. *Chemical Engineering Journal* **2011**, *167*, 734-743, doi:10.1016/j.cej.2010.08.082.
109. Qi, B.; Wang, Y.; Lou, L.-L.; Yang, Y.; Liu, S. Solvent-free aerobic oxidation of benzyl alcohol over palladium catalysts supported on MnO x prepared using an adsorption method. *Reaction Kinetics, Mechanisms and Catalysis* **2012**, *108*, 519-529, doi:10.1007/s11144-012-0529-y.
110. Riemer, D.; Mandaviya, B.; Schilling, W.; Götz, A.C.; Kühl, T.; Finger, M.; Das, S. CO_2-Catalyzed Oxidation of Benzylic and Allylic Alcohols with DMSO. *ACS Catalysis* **2018**, *8*, 3030-3034, doi:10.1021/acscatal.7b04390.
111. Sheikhi, E.; AdibMorteza; Morteza, A.; Gohari, S.J.A. Sulfuric Acid-Promoted Oxidation of Benzylic Alcohols to Aromatic Aldehydes in Dimethyl Sulfoxide: An Efficient Metal-Free Oxidation Approach. *Syn lett* **2018**, *29*, doi:10.1055/s-0037-1609149.
112. Yang, Z.-W.; Zhao, X.; Li, T.-J.; Chen, W.-L.; Kang, Q.-X.; Xu, X.-Q.; Liang, X.-X.; Feng, Y.; Duan, H.-H.; Lei, Z.-q. Catalytic properties of palygorskite supported Ru and Pd for efficient oxidation of alcohols. *Catalysis Communications* **2015**, *65*, 34-40, doi:10.1016/j.catcom.2015.02.021.
113. Dimitratos, N.; Villa, A.; Wang, D.; Porta, F.; Su, D.; Prati, L. Pd and Pt catalysts modified by alloying with Au in the selective oxidation of alcohols. *Journal of Catalysis* **2006**, *244*, 113-121, doi:10.1016/j.jcat.2006.08.019.
114. Ferri, D.; Mondelli, C.; Krumeich, F.; Baiker, A. Discrimination of Active Palladium Sites in Catalytic Liquid-Phase Oxidation of Benzyl Alcohol. *J Phys Chem B* **2006**, *110*, doi:10.1021/jp065779z.
115. Yan, Z.; Tomer, A.; Perrussel, G.; Ousmane, M.; Katryniok, B.; Dumeignil, F.; Ponchel, A.; Liebens, A.; Pera-Titus, M. A Pd/CeO_2"H_2Pump" for the Direct Amination of Alcohols. *ChemCatChem* **2016**, *8*, 3347-3352, doi:10.1002/cctc.201600855.
116. Meng, L.; Jia, A.-P.; Lu, J.-Q.; Luo, L.-F.; Huang, W.-X.; Luo, M.-F. Synergetic Effects of PdO Species on CO Oxidation over PdO–CeO_2 Catalysts. *The Journal of Physical Chemistry C* **2011**, *115*, 19789-19796, doi:10.1021/jp2056688.
117. Liu, J.; Wang, F.; Dewil, R. CeO_2 Nanocrystalline-Supported Palladium Chloride: An Effective Catalyst for Selective Oxidation of Alcohols by Oxygen. *Catalysis Letters* **2009**, *130*, 448-454, doi:10.1007/s10562-009-9962-6.
118. Alhumaimess, M.; Lin, Z.; Weng, W.; Dimitratos, N.; Dummer, N.F.; Taylor, S.H.; Bartley, J.K.; Kiely, C.J.; Hutchings, G.J. Oxidation of benzyl alcohol by using gold nanoparticles supported on ceria foam. *ChemSusChem* **2012**, *5*, 125-131, doi:10.1002/cssc.201100374.
119. Zhang, H.; Xie, Y.; Sun, Z.; Tao, R.; Huang, C.; Zhao, Y.; Liu, Z. In-situ loading ultrafine AuPd particles on ceria: highly active catalyst for solvent-free selective oxidation of benzyl alcohol. *Langmuir : the ACS journal of surfaces and colloids* **2011**, *27*, 1152-1157, doi:10.1021/la1034728.
120. Lei, Y.; Li, W.; Liu, Q.; Lin, Q.; Zheng, X.; Huang, Q.; Guan, S.; Wang, X.; Wang, C.; Li, F. Typical crystal face effects of different morphology ceria on the activity of Pd/CeO_2

catalysts for lean methane combustion. *Fuel* **2018**, *233*, 10-20, doi:10.1016/j.fuel.2018.06.035.
121. Wang, X.; Chen, J.; Jianxin, Z.; Wang, Q.; Li, Z.; Qin, R.; Wu, C.; Xie, Z.; Zheng, L. The synergy between atomically dispersed Pd and cerium oxide for enhanced catalytic properties. *Nanoscale* **2017**, *9*, 6643-6648 doi:10.1039/C6NR09707C.
122. Lykaki, M.; Pachatouridou, E.; Carabineiro, S.A.C.; Iliopoulou, E.; Andriopoulou, C.; Kallithrakas-Kontos, N.; Boghosian, S.; Konsolakis, M. Ceria nanoparticles shape effects on the structural defects and surface chemistry: Implications in CO oxidation by Cu/CeO_2 catalysts. *Applied Catalysis B: Environmental* **2018**, *230*, 18-28, doi:10.1016/j.apcatb.2018.02.035.
123. Du, X.; Zhang, D.; Shi, L.; Gao, R.; Zhang, J. Morphology Dependence of Catalytic Properties of Ni/CeO_2 Nanostructures for Carbon Dioxide Reforming of Methane. *The Journal of Physical Chemistry C* **2012**, *116*, 10009-10016, doi:10.1021/jp300543r.
124. Wang, S.; Zhao, L.; Wang, W.; Zhao, Y.; Zhang, G.; Ma, X.; Gong, J. Morphology control of ceria nanocrystals for catalytic conversion of CO_2 with methanol. *Nanoscale* **2013**, *5*, 5582-5588, doi:10.1039/c3nr00831b.
125. Wang, W.-W.; Yu, W.-Z.; Du, P.-P.; Xu, H.; Jin, Z.; Si, R.; Ma, C.; Shi, S.; Jia, C.-J.; Yan, C.-H. Crystal Plane Effect of Ceria on Supported Copper Oxide Cluster Catalyst for CO Oxidation: Importance of Metal–Support Interaction. *ACS Catalysis* **2017**, *7*, 1313-1329, doi:10.1021/acscatal.6b03234.
126. Guo, W.; Niu, S.; Shi, W.; Zhang, B.; Yu, W.; Xie, Y.; Ji, X.; Wu, Y.; Su, D.; Shao, L. Pd–P nanoalloys supported on a porous carbon frame as an efficient catalyst for benzyl alcohol oxidation. *Catal. Sci. Technol.* **2018**, *8*, 2333-2339, doi:10.1039/C8CY00554K.
127. Xin, P.; Li, J.; Xiong, Y.; Wu, X.; Dong, J.; Chen, W.; Wang, Y.; Gu, L.; Luo, J.; Rong, H., et al. Revealing the Active Species for Aerobic Alcohol Oxidation by Using Uniform Supported Palladium Catalysts. *Angew Chem Int Ed Engl* **2018**, *57*, 4642-4646, doi:10.1002/anie.201801103.
128. Tan, H.; Wang, J.; Yu, S.; Zhou, K. Support Morphology-Dependent Catalytic Activity of Pd/CeO_2 for Formaldehyde Oxidation. *Environmental science & technology* **2015**, *49*, 8675-8682, doi:10.1021/acs.est.5b01264.
129. Kumar, A.K.; Sharma, S. Recent updates on different methods of pretreatment of lignocellulosic feedstocks: a review. *Bioresources and bioprocessing* **2017**, *4*, 7, doi:10.1186/s40643-017-0137-9.
130. Deng, H.; Lin, L.; Sun, Y.; Pang, C.; Zhuang, J.; Ouyang, P.; Li, Z.; Liu, S. Perovskite-type Oxide $LaMnO_3$: An Efficient and Recyclable Heterogeneous Catalyst for the Wet Aerobic Oxidation of Lignin to Aromatic Aldehydes. *Catalysis Letters* **2008**, *126*, 106-111, doi:10.1007/s10562-008-9588-0.
131. Ouyang, X.; Ruan, T.; Qiu, X. Effect of solvent on hydrothermal oxidation depolymerization of lignin for the production of monophenolic compounds. *Fuel Processing Technology* **2016**, *144*, 181-185, doi:10.1016/j.fuproc.2015.12.019.
132. Isikgor, F.H.; Becer, C.R. Lignocellulosic biomass: a sustainable platform for the production of bio-based chemicals and polymers. *Polymer Chemistry* **2015**, *6*, 4497-4559, doi:10.1039/c5py00263j.
133. Vassilev, S.V.; Baxter, D.; Andersen, L.K.; Vassileva, C.G. An overview of the chemical composition of biomass. *Fuel* **2010**, *89*, 913-933, doi:10.1016/j.fuel.2009.10.022.

134. Chen, Z.; Wan, C. Biological valorization strategies for converting lignin into fuels and chemicals. *Renewable and Sustainable Energy Reviews* **2017**, *73*, 610-621, doi:10.1016/j.rser.2017.01.166.
135. DeLucia, N.A.; Jystad, A.; Laan, K.V.; Tengco, J.M.M.; Caricato, M.; Vannucci, A.K. Silica Supported Molecular Palladium Catalyst for Selective Hydrodeoxygenation of Aromatic Compounds under Mild Conditions. *ACS Catalysis* **2019**, *9*, 9060-9071, doi:10.1021/acscatal.9b02460.
136. Calvaruso, G.; Clough, M.T.; Rechulski, M.D.K.; Rinaldi, R. On the Meaning and Origins of Lignin Recalcitrance: A Critical Analysis of the Catalytic Upgrading of Lignins Obtained from Mechanocatalytic Biorefining and Organosolv Pulping. *ChemCatChem* **2017**, *9*, 2691 – 2700, doi:10.1002/.
137. Rensel, D.J.; Rouvimov, S.; Gin, M.E.; Hicks, J.C. Highly selective bimetallic FeMoP catalyst for C–O bond cleavage of aryl ethers. *Journal of Catalysis* **2013**, *305*, 256-263, doi:10.1016/j.jcat.2013.05.026.
138. Zhou, X.-F.; Lu, X.-J. Co(salen) supported on graphene oxide for oxidation of lignin. *Journal of Applyed Polymer Science* **2016**, *133*, 44133, doi:10.1002/app.44133.
139. Rahimi, A.; Azarpira, A.; Kim, H.; Ralph, J.; Stahl, S.S. Chemoselective metal-free aerobic alcohol oxidation in lignin. *Journal of the American Chemical Society* **2013**, *135*, 6415-6418, doi:10.1021/ja401793n.
140. Kriz, G.S.; Lampman, G.M.; Pavia, D.L.; Engel, R.G. *Introduction to Organic Laboratory Techniques: A Microscale Approach*, 4th ed.; Brooks Cole: Belmont, California, 2006.
141. Edmond, d.H.; Srtroobant, V. *Mass Spectrometry: Principles and Applications*, 3rd ed.; Wiley-Interscience: Toronto, 2013.
142. Brown, K.L.; Tautfest, G.W. Faraday-Cup Monitors for High-Energy Electron Beams. *Review of Scientific Instruments* **1956**, *27*, 696-702, doi:10.1063/1.1715674.
143. Allen, J.S. An Improved Electron Multiplier Particle Counter. *Review of Scientific Instruments* **1947**, *18*, 739-749, doi:10.1063/1.1740838.
144. Brunauer, S.; Emmett, P.H.; Teller, E. Adsorption of Gases in Multimolecular Layers *Journal of the American Chemical Society* **1938**, *60*, 309-319.
145. SING, K.S.W.; EVERETT, D.H.; HAUL , R.A.W.; MOSCOU, L.; PIEROTTI, R.A.; ROUQUEROL, J.; SIEMIENIEWSKA, T. REPORTING PHYSISORPTION DATA FOR GAS/SOLID SYSTEMS with Special Reference to the Determination of Surface Area and Porosity. *Pure & Appl. Chem.* **1985**, *57*, 603—619, doi:10.1351/pac198557040603.
146. Moulder, J.F.; Stickle, W.F.; 'Sobol, P.E.; Bomben, K.D. *Handbook of X-ray Photoelectron Spectroscopy*; Physical Electronics Inc: Eden Prairie, Minnesota, 1996.
147. Shirley, D.A. High-Resolution X-Ray Photoemission Spectrum of the Valence Bands of Gold. *Physical Review B* **1972**, *5*, 4709-4714, doi:10.1103/PhysRevB.5.4709.
148. Liu, B.; Liu, R.; Li, Q.-J.; Yao, M.-G.; Zou, B.; Cui, T.; Liu, B.-B.; Liu, J. Study of high pressure structural stability of CeO_2 nanoparticles. *Chinese Physics C* **2013**, *37*, 098003, doi:10.1088/1674-1137/37/9/098003.
149. Feng, T.; Tang, R.; Shang, N.; Feng, C.; Gao, S.; Wang, C. Pd nanoparticles supported on CeO_2 as efficient catalyst for hydrogen generation from formaldehyde solution at room temperature. *Applied Organometallic Chemistry* **2017**, *31*, e3889, doi:10.1002/aoc.3889.
150. Luo, J.-Y.; Meng, M.; Xian, H.; Tu, Y.-B.; Li, X.-G.; Ding, T. The Nanomorphology-Controlled Palladium-Support Interaction and the Catalytic Performance of Pd/CeO_2 Catalysts. *Catalysis Letters* **2009**, *133*, 328-333, doi:10.1007/s10562-009-0194-6.

151. Luisetto, I.; Tuti, S.; Romano, C.; Boaro, M.; Di Bartolomeo, E. Dry reforming of methane over Ni supported on doped CeO_2: New insight on the role of dopants for CO_2 activation. *Journal of CO_2 Utilization* **2019**, *30*, 63-78, doi:10.1016/j.jcou.2019.01.006.
152. Kurnatowska, M.; Kepinski, L.; Mista, W. Structure evolution of nanocrystalline $Ce_{1-x}Pd_xO_{2-y}$ mixed oxide in oxidizing and reducing atmosphere: Reduction-induced activity in low-temperature CO oxidation. *Applied Catalysis B: Environmental* **2012**, *117-118*, 135-147, doi:10.1016/j.apcatb.2011.12.034.
153. Agostini, G.; Groppo, E.; Piovano, A.; Pellegrini, R.; Leofanti, G.; Lamberti, C. Preparation of supported Pd catalysts: from the Pd precursor solution to the deposited Pd^{2+} phase. *Langmuir : the ACS journal of surfaces and colloids* **2010**, *26*, 11204-11211, doi:10.1021/la1005117.
154. Pinna, F.; Menegazzo, F.; Signoretto, M.; Canton, P.; Fagherazzi, G.; Pernicone, N. Consecutive Hydrogenation of Benzaldehyde Over Pd Catalysts Influence of Supports and Sulfur Poisoning. *Applied Catalysis A: General* **2001**, *219*, 195–200, doi:10.1016/S0926-860X(01)00685-8.
155. Luo, M.F.; Hou, Z.Y.; Yaun, X.X.; Zheng, X.M. Characterization study of CeO_2 supported Pd catalyst for low-temperature carbon monoxide oxidation. *Catalysis Letters* **1998**, *50*, 205-209, doi:10.1023/A:1019023220271.
156. Gopinath, R.; Lingaiah, N.; Sreedhar, B.; Suryanarayana, I.; Sai Prasad, P.S.; Obuchi, A. Highly stable Pd/CeO_2 catalyst for hydrodechlorination of chlorobenzene. *Applied Catalysis B: Environmental* **2003**, *46*, 587-594, doi:10.1016/s0926-3373(03)00321-7.
157. Jiang, D.; Wang, W.; Zhang, L.; Zheng, Y.; Wang, Z. Insights into the Surface-Defect Dependence of Photoreactivity over CeO_2 Nanocrystals with Well-Defined Crystal Facets. *ACS Catalysis* **2015**, *5*, 4851-4858, doi:10.1021/acscatal.5b01128.
158. Shyu, J.Z.; Weber, W.H.; Gandhi, H.S. Surface Characterization of Alumina-Supported Ceria. *The Journal of Physical Chemistry* **1988**, *92*, 4964-4970, doi:10.1021/j100328a029.
159. NIST X-ray Photoelectron Spectroscopy Database, Version 4.1. Availabe online: https://srdata.nist.gov/xps/ (accessed on October 15, 2018).
160. You, R.; Li, Z.; Cao, T.; Nan, B.; Si, R.; Huang, W. Synthesis in Glovebox: Utilizing Surface Oxygen Vacancies to Enhance Atomic Dispersion of Palladium on Ceria for CO Oxidation and Propane Combustion. *ACS Appl. Nano Mater.* **2018**, *1*, 4988-4997, doi:10.1021/acsanm.8b01116.
161. Tang, K.; Ren, Y.; Liu, W.; Wei, J.; Guo, J.; Wang, S.; Yang, Y. Insight Investigation of Active Palladium Surface Sites in Palladium-Ceria Catalysts for NO + CO Reaction. *ACS applied materials & interfaces* **2018**, *10*, 13614-13624, doi:10.1021/acsami.8b02557.
162. Vohs, J.M. Site requirements for the adsorption and reaction of oxygenates on metal oxide surfaces. *Chemical reviews* **2013**, *113*, 4136-4163, doi:10.1021/cr300328u.
163. Belykh, L.B.; Skripov, N.I.; Sterenchuk, T.P.; Akimov, V.V.; Tauson, V.L.; Savanovich, T.A.; Schmidt, F.K. Role of phosphorus in the formation of selective palladium catalysts for hydrogenation of alkylanthraquinones. *Applied Catalysis A: General* **2020**, *589*, 117293, doi:10.1016/j.apcata.2019.117293.
164. Yu, W.; Xin, Z.; Zhang, W.; Xie, Y.; Wang, J.; Niu, S.; Wu, Y.; Shao, L. The role of surface functionalities in fabricating supported Pd-P nanoparticles for efficient formic acid oxidation. *Chemical Physics Letters* **2017**, *686*, 155-160, doi:10.1016/j.cplett.2017.08.020.
165. Lange, H.; Decina, S.; Crestini, C. Oxidative upgrade of lignin – Recent routes reviewed. *European Polymer Journal* **2013**, *49*, 1151-1173, doi:10.1016/j.eurpolymj.2013.03.002.

166. Elkurtehi, A.I.; Walsh, A.G.; Dawe, L.N.; Kerton, F.M. Vanadium Aminophenolate Complexes and Their Catalytic Activity in Aerobic and H_2O_2-Mediated Oxidation Reactions. *European Journal of Inorganic Chemistry* **2016**, *2016*, 3123-3130, doi:10.1002/ejic.201600068.
167. Gao, Y.; Zhang, J.; Chen, X.; Ma, D.; Yan, N. A Metal-Free, Carbon-Based Catalytic System for the Oxidation of Lignin Model Compounds and Lignin. *ChemPlusChem* **2014**, *79*, 825-834, doi:10.1002/cplu.201300439.